ABSTRACT

Title of Thesis: SEISMIC RESILIENCE STUDY OF STEEL CONCENTRICALLY BRACED FRAME STRUCTURE WITH DUAL VISCOUS AND METALLIC HYSTERETIC DAMPER

Jianshu Xu
Master of Science, 2019

Thesis Directed By:

Professor Yunfeng Zhang,

Department of Civil and Environmental Engineering

Steel concentrically braced frames（CBF）are popular seismic resistant structural systems widely used all over the world due to their high elastic stiffness and moderate ductility for many decades. However, conventional CBFs are subject to soft-story damage pattern which may lead to collapse caused by overly large drift concentrated in one story in strong earthquakes; measures to enhance the seismic resilience of CBFs is thus desirable. This study looks into quantifying the seismic resilience of CBFs with and without dual-action damping devices by following the newly released 2018 ed. FEMA P58 procedure. The dual-action damping device include a viscous damper and

metallic hysteretic dampers which are activated at different timing: viscous damper always active and effective in controlling story drift during small and moderate earthquakes, while metallic hysteretic dampers are activated only when the story drift exceeds a pre-specified value during strong earthquakes. A six-story steel CBF building designed by SAC Steel Project research (1999) is adopted as prototype building to demonstrate the effectiveness of dual-action damping device in enhancing the seismic resilience of CBFs. Nonlinear static analyses as well as nonlinear time-history analysis were performed to obtain the Engineering Demand Perimeters (EDP) required for seismic resilience evaluation. Collapse Fragility is developed based on incremental dynamic analysis (IDA) by SPO2IDA Tool. The distribution function of Decision Variables (DV), including Repair cost, Repair time, Casualties etc., is obtained through Monte-Carlo simulation of prior nonlinear time-history analysis EDP by Performance Assessment Calculation Tool (PACT). It is found from this study that the Collapse Risk and the Potential Loss of the prototype structure with dampers have been significantly reduced, suggesting the dual-action damping device provides a beneficial alternative for enhancing the seismic resilience of CBFs.

SEISMIC RESILIENCE STUDY OF STEEL CONCENTRICALLY BRACED FRAME STRUCTURE WITH DUAL VISCOUS AND METALLIC HYSTERETIC DAMPER

by

Jianshu Xu

Thesis submitted to the Faculty of the Graduate School of the
University of Maryland, College Park, in partial fulfillment
Of the requirements for the degree of
Master of Science
2019

Advisory Committee:

Dr. Yunfeng Zhang, Chair

Dr. Amde M. Amde

Dr. Reilly Allison

Acknowledgement

Foremost, I would like to express my sincere gratitude to my advisor Dr. Yunfeng Zhang for his continuous support of my masters' research, his patience, motivation, enthusiasm, and immense knowledge. His advice on both research as well as on my career have been invaluable. His guidance helped me all the time of research and writing of the thesis.

I would like to thank the rest of my thesis committee: Dr. Amde M. Amde and Dr. Reilly Allison. for their enthusiastic supports, insightful comments and questions.

I would like to thank the previous work done by Dr. K. Arshia and H.Liu.

Last but not the least, I would like to thank my parents, Yi Xu and Jian He for their unconditional love, encouragement and support.

Table of Contents

List of Tables

List of Figures

List of Abbreviations

CBF Concentrically Braced Frame

DBE Design Basis Earthquake

DV Decision Variables

EDP Engineering Demand Perimeters

FEMA Federal Emergency Management Agency

IDA Incremental dynamic analysis

MCE Maximum considered earthquake

PACT Performance Assessment Calculation Tool

SP Shear Panel

SBC Shear-Bending combined

TPAD Trapezoidal Plate Added Damping

PBEE Performance-Based Earthquake Engineering

Chapter 1 Introduction

1.1 Background

Steel Concentrically Braced Frame (CBF) has been widely used in seismically active zones throughout the world, typically in mid-rise and low-rise buildings. It proves to be one of the most efficient structure systems to resist seismic lateral force due to its high stiffness and strength. The centerline of beam, column and brace intersect with each other at the same joint to provide a load distribution of truss action. Several types of CBF structures have also been used as retrofit alternative for existing structures. However, CBF's seismic performance is also limited by its unfavorable performance of low inelastic deformation and capacity of energy dissipation. [1] According to the AISC code, columns and beams are required to remain essentially elastic under earthquake loading. Inelastic deformation appears in braces.

Pre-specified damage regions are concentrated in the brace of CBF. The cyclic lateral earthquake force will load the brace on one side under intension and the other side in compression. The tension brace is likely to result in ductile yielding while the compression brace will end up in brittle global buckling. However, since the seismic force acting on the structure is the cyclic excitation, the tension-yielded brace is likely to suffer from subsequent compression buckling. Engineers found both tension yielding and compression buckling failure in a CBF brace after the Hyogoken-Nanbu Earthquake in Kobe, Japan, 1995. Braces with design to resist tension or compression

only has been found go through severe damage during the earthquake. [1] Tension yielding and compression buckling are expected failure mode in CBF system since the structure is likely to remain standing. There will be large inelastic deformation demand in the middle of the brace and plastic hinge is expected to be found at the mid-span of the brace under certain level of earthquake ground motion. Local buckling/yielding, torsional buckling and unintended fracture before inelastic deformation of the brace are strictly restricted in the CBF system. [1]

There is a likelihood of soft story even collapse during large magnitude earthquakes in CBF due to its sensitivity to irregular distribution of mass and strength along the building height. In the 1990s, researchers have found significant economic loss due to unexpected large plastic rotation deformation at the joint of beam, column and brace. Unbalanced internal force has been found as a major problem of connection design. Later design codes (ANSI/AISC 341-16) come up with special treatment and restriction on connection design. [2] All related decision variables (DV) estimation, basically potential repair cost and repair time, are based on the way the connection has been design. Variance in design approach will result in damage state division of the connection directly which will further affect the fragility functions development of each structure performance group.

According to FEMA P-336, the economic annualized earthquake loss (AEL) in the United States is reported as in average of 6.1 billion US dollars per year. It provides an estimation of potential minimum value of direct loss from the earthquake regardless of the life-long performance of the infrastructure. This magnitude represents an average magnitude over a relatively long period, which means it should not be a typical

reference for a specific year. The annualized earthquake loss ratio (AELR) is also reported to compare potential seismic risk with AEL. The report also figures out that California accounts for 61% of the annual earthquake loss of about 3.7 billion US dollars. On the metropolitan level of the AEL estimation, Los Angeles and San Francisco lead up to 80% of the total loss. [3] Based on the information provided, the case study in this research looks into a six floor steel SCBF structural located in downtown area, Los Angeles.

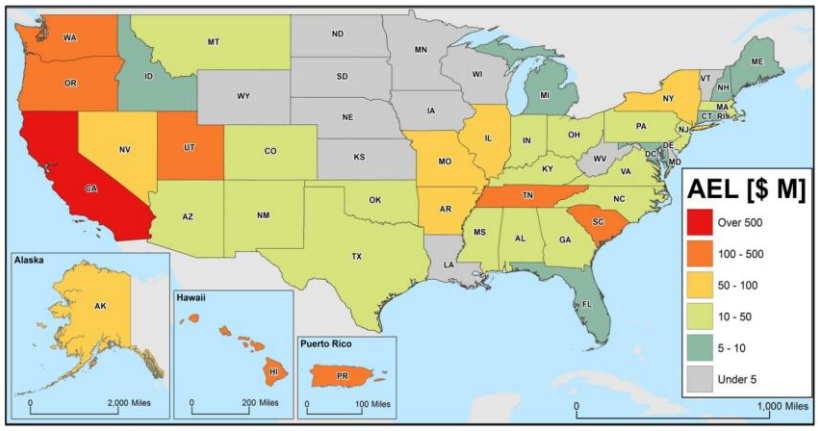

Figure 1.1 Annualized Earthquake Losses by State（FEMA P-366, 2017）

The most favorable way to reduce potential loss from extreme disasters is to take mitigation measures as well as preventive actions before such destructive events take place. Structure resilience can be enhanced by mitigation measures. These mitigation measures can be generally based on either structural level or component level. [4] For Steel CBF systems, rehabilitation on component level mainly related to brace as well as gusset plate connection. Structure level performance can also be improved by better seismic resistance integrity action between beams, columns and braces. In this study,

dual-action viscous and metallic damping devices are employed for seismic rehabilitation.

However, these measures are not always sufficient in terms of unexpected level disasters. There will be significant direct loss of properties and casualties from structure damage. Owners will also suffer from indirect loss including building down time as well as potential environmental impacts. Once the damage occurs, the structure will go through a recovery procedure. The economic and time expense of the retrofit is quantified probability distribution form by Seismic Performance Assessment of Buildings (FEMA P-58). This method has an edge over Performance-based Seismic Design codes in that it allows the stakeholders to assess different kinds of potential loss from a range of level of expected earthquakes. [5]

1.2 Research Objectives

This first objective of this study is to perform nonlinear static analysis as well as nonlinear time-history analysis to determine the seismic response of the CBF structures with and without dual action dampers. Numerical analysis will be performed using general nonlinear structural analysis software – Opensees (for "Open System for Earthquake Engineering Simulation) [6]. A six-story inverted-V (Chevron) steel CBF building and three-story steel CBF building were selected as the prototype building, which were then excited with an ensemble of 20 earthquake ground motion records scaled to the design basis earthquake at the selected location. The ground motion record has been scaled to the design code level of the late 1990s to match the

design date of the prototype building. The ground motion record was also scaled to account for the uncertainty in the response spectrum near the fundamental period of the prototype structure. To mitigate the seismic response of the steel CBF buildings, a dual action damper comprised of a viscous and metallic hysteretic damper was installed at each floor and Engineering Demand Parameters (EDP) are compared with the corresponding prototype structure without such supplemental dampers. This research aims to illustrate how dual viscous and metallic damper can prevent the occurrence of excessive story drift under DBE level earthquake.

The second objective of this research is to employ a software tool called PACT, a recently developed tool accompanying FEMA P-58 (2018) to assess the resilience of rehabilitated CBF structures with dual action dampers under the selected level earthquake. This research aims to demonstrate the basic procedure of PACT, including risk-based Monte Carlo simulation of EDP values and fragility function development. Then the fragility function and the decision variable estimation model for the dual action damper will be developed in order to use PACT for this purpose. Potential casualties will be estimated based on the results of collapse analysis. Since the occurrence of excessive story drift can be prevented by installing the dual damper system, there will be less risk for the collapse of either a single story or the entire CBF structure.

1.3 Thesis Organization

This study investigates the seismic performance and resilience of CBF buildings with and without a newly developed dual viscous and metallic damper under DBE levels of earthquakes. The fragility function of the dual action damper is developed and its economic and environmental impact is assessed in accordance with FEMA-P58 procedure.

Chapter 2 presents a literature review of previous work done in three major fields: first the evolution and seismic performance assessment of CBF structures are presented. Then the development of ADAS & TADAS damper system in structures proposed in the 1990s and the research on its seismic mitigation effect during the early 2000s are reviewed, as well as some modified versions of the original TADAS damping system and newly-developed simulation models. Then the background of the Performance-Based Earthquake Engineering (PBEE) Framework is reviewed as well as case study done in recent years;

Chapter 3 mainly focuses on the numerical model and finite element analysis of the 3-story CBF and the 6-story CBF buildings selected as the prototype structures for this numerical simulation study. In this chapter, the general information of the CBF structure and numerical models for both CBF structure and dual action dampers are presented and verified. Nonlinear static analysis is applied to provide an insight of the structure performance especially useful for potential collapse analysis. Nonlinear time history analysis will be performed to get the EDPs which is necessary for PACT input, under selected earthquake ground motion record scaled to account for uncertainties of different types. The benefits of applying the dual action damper will be demonstrated based on the results of time-history analysis.

Chapter 4 focuses on seismic resilience assessment of CBF buildings using PACT. The assessment results will be presented in terms of five decision variables (DV): repair time, repair cost, casualties, unsafe placard and environmental impact. This chapter introduces general procedure of employing PACT to determine the values of such DVs. The benefits of installing dual action dampers to mitigate the seismic response of the original CBF building are demonstrated by comparing the consequence variables.

Chapter 5 presents the conclusions and summaries of this research and provides suggestions for worthy future research work.

Chapter 2 Literature Review

2.1 Energy Dissipation Device

Energy dissipation devices have been put into practice for earthquake-resistance structures since the 1970s. These energy dissipation systems can be generally divided into three categories: Passive Dissipation systems, Active/Semi-active systems, and Base isolation systems. [7] An active structural control system (Figure 2.1) consists of three major parts: Sensors, Data processing devices and Actuators. Sensors are used to measure the external seismic excitations as well as structure response EDPs. The Data processing devices then will obtain the EDP from sensors and calculate necessary inner control forces. Once the control forces have been carried out, the actuator will produce the required forces acting on the structure. Since the magnitude of the earthquake ground motion is unpredictable and damage is strictly not allowed to appear in all these equipment during the entire event, special protections for the active control system must be built and it might be not useful for regions with high earthquake hazard level. The system needs external power sources supply in case of the power outrage during the event. These suggest less favorable economy benefit and flexibility in construction. [8]

Passive Energy dissipation system (Figure 2.2) is a more widely used approach for earthquake resistance in structures. This system is designed basically to absorb external energy input from seismic excitation in order to mitigate energy transmitted to primary structural elements and damage in these regions can be minimized. It brings more favorable construction flexibility because this type of energy dissipation

device only needs to be installed at the superstructure of the building and only replacement of the damper is needed for retrofit action. It is more economically efficient as it does not require external power supply. It also acts integrally with the structure and is more stable for its less probability of influenced by other factors such as humidity, temperature etc. [7]

Hysteretic systems basically include metallic dampers and friction dampers. The energy dissipation methodology of metal damper is based on the yielding and plastic deformation of metals while friction dampers depend on the energy transformation to heat by dry sliding friction. Added Damping and Stiffness (ADAS) and Triangular Added Damping and Stiffness (TADAS) are two typical metallic dampers in new generations of structures. X-shaped and triangular dampers have been found to be among the most efficient configuration for metallic dampers. Idealized Force-displacement response of Metallic Dampers is shown in Figure 2.3. [8]

At the early researches on the metallic dampers in 1970d, Ozdemir et al. come up with a load-rate independent model to describe the force-displacement relationship of a metallic damper device. Two variables: the damper force F and the internal back force B are employed to describe damper performance with respect to time. Four parameters are selected to indicate the seismic response of the metallic: initial elastic device stiffness k_0, the slope of the force-displacement curve in the inelastic range α, initial yielding force F_0, and the exponent n. Further constitutive relationship model for the metallic material includes uniaxial bilinear steel model as well as Giuffré-Menegotto-Pinto Model with Isotropic Strain Hardening prediction. Future models are more likely to account for describing deterioration behavior of the metallic material. [7]

A series of researches have been done on the seismic resisting performance of the ADAS &TADAS devices in different types of structures. S. Alehashem, A.Keyhani, and H.Pourmohammad et al. looked into ADAS & TADAS installed on the superstructure of a 10-floor steel frame. [9] Four different configuration of the steel frame are studied: CBF with X-shaped brace, CBF with chevron shaped brace, eccentrically braced frame (EBF), steel frame with ADAS & TADAS. (Figure 2.4-2.5) They found that the structures with ADAS & TADAS have respectively higher fundamental period than EBF, CBF and chevron systems which suggests more induced ductility of the system. The induced base shear is relatively smaller compared to all other types of steel frames. The drift ratio and roof acceleration can be reduced significantly by the ADAS & TADAS dampers.

Steel brace has been used as a retrofit method to enhance the stiffness of Reinforced Concrete (RC) Structures. [10] Although the increased stiffness is desirable, it will also introduce extra base shear and increase the original internal force in the primary elements. Destructive soft story effect can also be observed in the RC structures in Mehdi & N. Ali's research. Figure 2.6 visualizes how story drift can be reduced where base shear of the structure can also be reduced.

Recent Studies have been focusing on the modification of the ADAS & TADAS damping systems. R. Mohammadi and A. Nasri looked into the behavior of a 6-floor structure with TADAS dampers under big seismic excitation. (Figure 2.7) They found that when exposed to large deformations, pins in the damper are likely to hit the top of the holes which will result in an abrupt increase in damper stiffness where it can be considered as rigid element. (Figure 2.8) It will result in unfavorable large geometric

deformation in the primary elements like beams, columns, and bracing systems. They suggest avoiding pins hitting the top by calculation of a minimum height for the damper holes. [11]

Z. Li, G. Shu, Z. Huang et al. came up with an innovative shear-bending combined metallic damper, which consists of several shear panel (SP) dampers and a series of K-shaped metal plates dampers. This energy dissipation device functions by shear yielding of the SP damper as well as plastic hinge developed in K-shaped metal plates as Figure 2.9-2.10. It was found that dampers with SP only has poor hysteretic performance due to significant pinching effect which ban be reduced by applying shear-bending combined (SBC) damper. (Figure 2.11) The capability of energy dissipation is enhanced by the combination of individual shearing and bending component. Notable over-strength effect has been observed in the system. They figured out that a smaller gap is beneficial for the SBC system. However, special treatment is needed for these small gaps to prevent potential scratch damage. [12]

A. Ghaffary and R.K.Mohammadi et al. employed combined finite element analysis programs (Virtual Hybrid Simulation system) to study a one story steel frame with TADAS damper. A detailed TADAS model was built in ABAQUS and the model of the remaining structure was developed in Opensees. This study looked into how variance in metallic plate numbers, plate spacing influence the seismic resistance performance of the metallic damper. It was found that the frame's displacement can be reduced by applying more metal plates. (Figure 2.12) However, there would be increase in base shear if more metal plate has been used. The hysteretic curve indicated the energy dissipated by 4 or 6 plates was similar but the 4-plate system

went through a smoother stiffness increase. The plate spacing should be restricted to a medium value. A small spacing is likely to worsen the pinching effect and a large spacing will probably result in a notable stiffness decrease of the device. [13]

H.S Dareini and B.H. Hashemi came up with a modified ADAS&TADAS system. [14] They found that nowadays the damping devices are mainly designed to start energy dissipation when the relative displacement has reached certain level so it might be not effective to consume the energy input of moderate level earthquake. They developed the dual TADAS system with two sets metallic plate. The gaps between the plates in each set are different. The first set of plate start working at an early stage, and the second set of plate will take effect after certain level of inter-story drift. The result indicates increase in stiffness and energy dissipation capability. This thesis also employs dual damping system under different levels of earthquake. The SCBF system works with viscous damper only at initial stage. If the inter-story drift exceeds 1%, a metallic TPAD metallic damper will function as a supplement for the original damping system. The Trapezoidal Added Damping Plate (TPAD) is developed by A. K. Esfahani shows that the plate is connected to a round rod as shown in Figure 2.13. [15] This rod can not only decrease the friction force when the TPAD plate slides inside the fuse holder but can also to reduce the local bearing on TPAD plate from plastic deformation.

2.2 Performance-Based Earthquake Engineering (PBEE) Methodology

During the late 1990s, ATC and FEMA come up with the first generation of PBEE assessment. The general process of the assessment is visualized in Figure 2.14(a). A Base Shear to Displacement curve is developed by static pushover analysis under an induced design level lateral force. Performance-oriented variables include estimated repair cost to a total replacement ratio, potential casualty rate and down time etc. The decision variables are directly related to the structure response parameters from a simplified analysis procedure. The biggest shortcoming of this assessment method is that the overall performance of the system is controlled merely by any component in the worst damage state. Thus the decision variables are likely to be overestimated. [16] Another pioneering PBEE effort example is the *seismic performance objectives for buildings* chart developed by FEMA 356, where the structural designer and owner work together to determine a reasonable combination limit of performance and seismic excitation level as shown in Figure 2.14(b). [17]

The Pacific Earthquake Engineering Research (PEER) center introduced the PBEE framework methodology later which is generally accepted as the most efficient seismic performance assessment approach since then The Performance Assessment Calculation Tool (PACT) employed in this study is based on this fundamental theory. It can be described by equation 2.1 below and Figure 2.15. [17] The flowchart generally consists of 4 sequential steps: hazard analysis, structure response analysis, damage state determination, and loss and impact estimation. Intensity Measures (IM), Engineering Demand Parameters (EDP), and Decision Variables (DV) are four corresponding product of the analysis sequential analysis. Each parameter is given as

conditional probability of the prior parameter from its predecessor analysis. The annual probability of exceedance of each parameter is provided as a representative if the distribution. Direct loss is estimated as the result of EDP simulations. The example of an analysis of transportation systems suggests that both direct and indirect losses can be estimated by the performance assessment network. [17]

$$\lambda(DV) = \iiint G\langle DV|DM\rangle \, dG\langle DM|EDP\rangle \, dG\langle EDP|IM\rangle \, d\lambda(IM) \qquad \text{(Equation 2.1)}$$

Several case studies employing PBEE framework to predict the potential loss and indirect impact has been carried out during the last decade. The FB&C provided a commercial seismic risk assessment report of an 8-Story RC SMF located in San Francisco, CA. [18] The overall performance is assessed by three aspects: Safety, Damage and Recovery, according to U.S. Resiliency Council (USRC) Seismic Rating criteria. The repair loss is presented in a continuous seismic hazard scenario at three probability exceedance level shown in Figure 2.16. G. M. D. Gobbo, M. S. Williams and A. Blakeborough looked into a 16-story X-shaped CBF structure decision variables at both ULS ultimate limit state (ULS) as well as serviceability limit state (SLS) level.[19] They basically paid attention to the repair cost proportion of the structure component and non-structure component as shown in Figure 2.17. They developed the fragility curve for a non-structure partition. They suggested that DVs from the non-structural components based on acceleration EDP is not negligible.

C. Del Vecchio, M. Di Ludovico, S. Pampanin, and A. Prota performed a case study on RC buildings damaged by L'Aquila earthquake to compare the actual repair cost versus predicted repair cost as shown in Figure 2.18.[20] They found that total

predicted repair costs are significantly lower than actual costs, in the range 7-13% of the total replacement cost. The main sources of error come from the estimation on repair cost of nonstructural components like partitions. They also suggested that fragility curve should be modifies according to the quality of construction. Y. Dong and D. M. Frangopol provided an all-round seismic assessment report including environmental impact and resilience as shown in Figure 2.19, which is useful for Life Cycle Assessment of the Building. [21] They also compared building down time based on two different repair schemes: fast track and slow track in Figure 2.20.

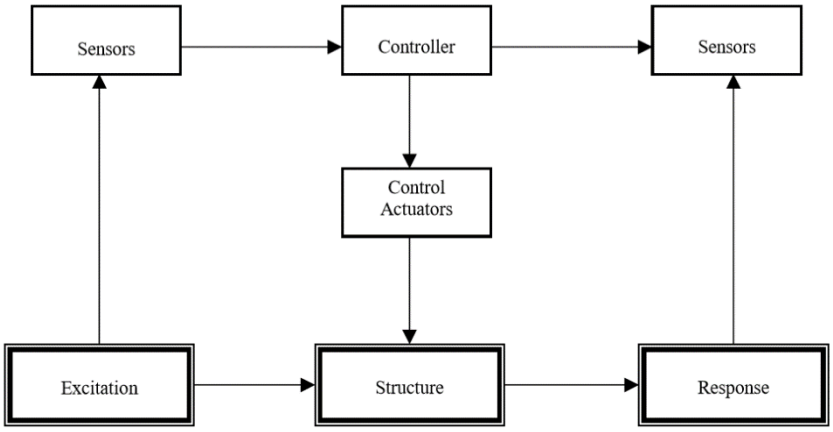

Figure 2.1 Energy dissipation system with active control (Soong and Spencer) [7]

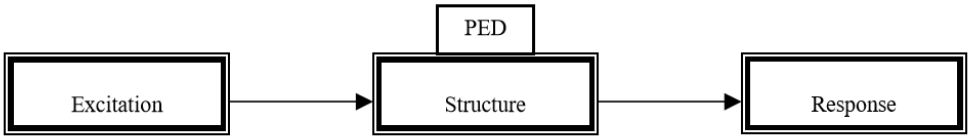

Figure 2.2 Passive energy dissipation system (Soong and Spencer) [7]

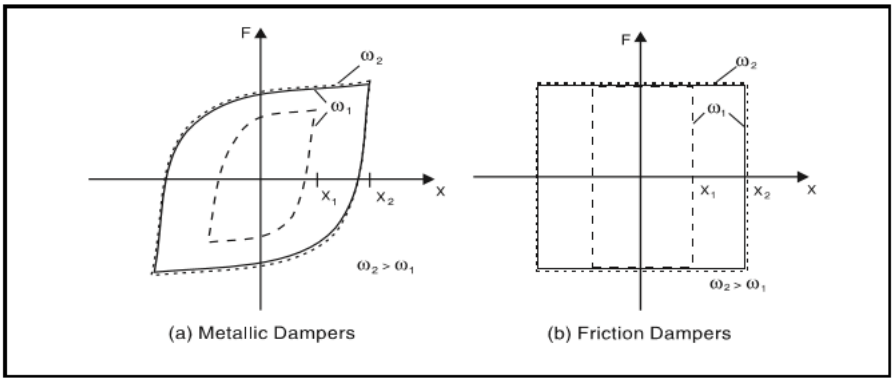

Figure 2.3 Idealized Force-Displacement responses of hysteretic devices (Constantinou, Soong and Spencer) [8]

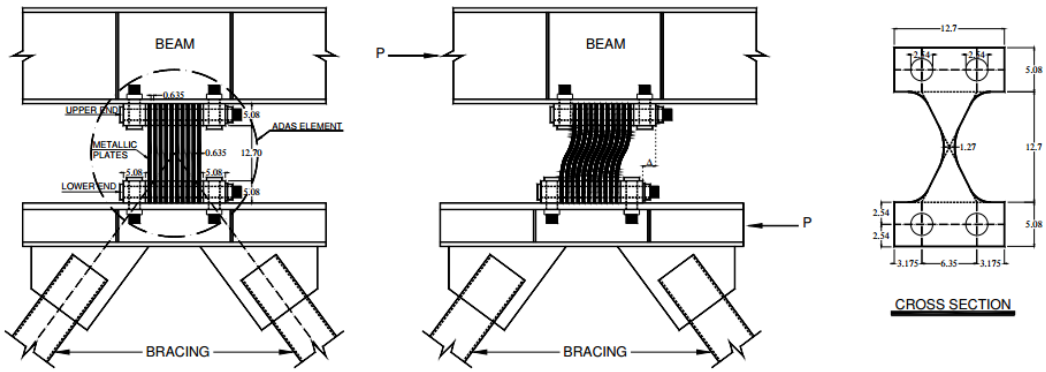

Figure 2.4 Seismic behavior of ADAS damper during earthquake excitation (Alehashem, Keyhani and Pourmohammad) [9]

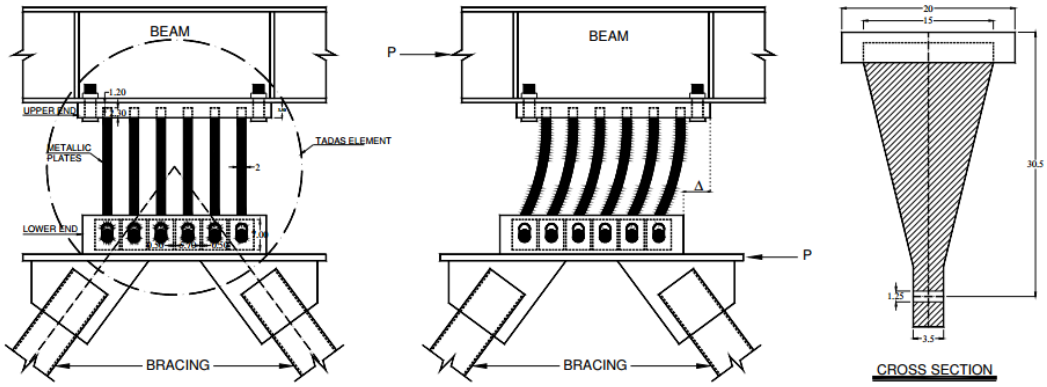

Figure 2.5 Seismic behavior of TADAS damper during earthquake (Alehashem, Keyhani and Pourmohammad) [9]

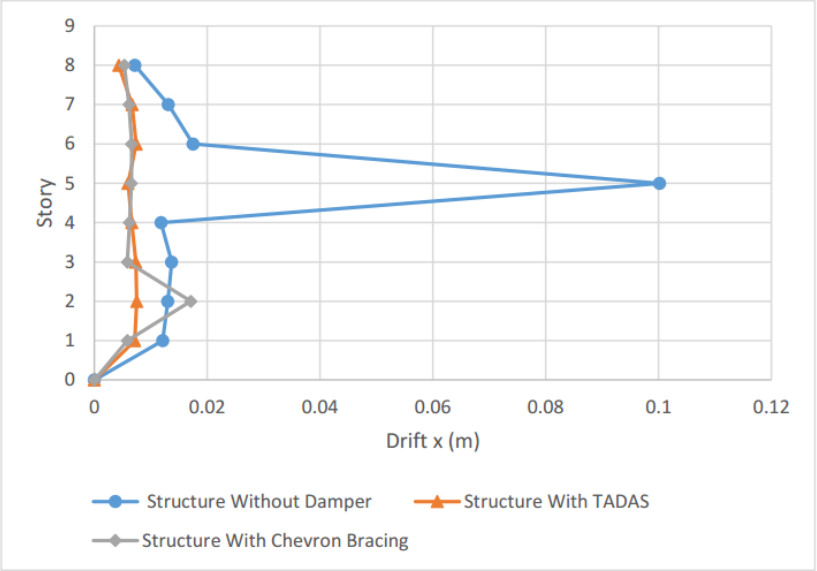

Figure 2.6 Story drift of 8-floor RC frame with different post-earthquake retrofit methods (Mehdi and Ali) [10]

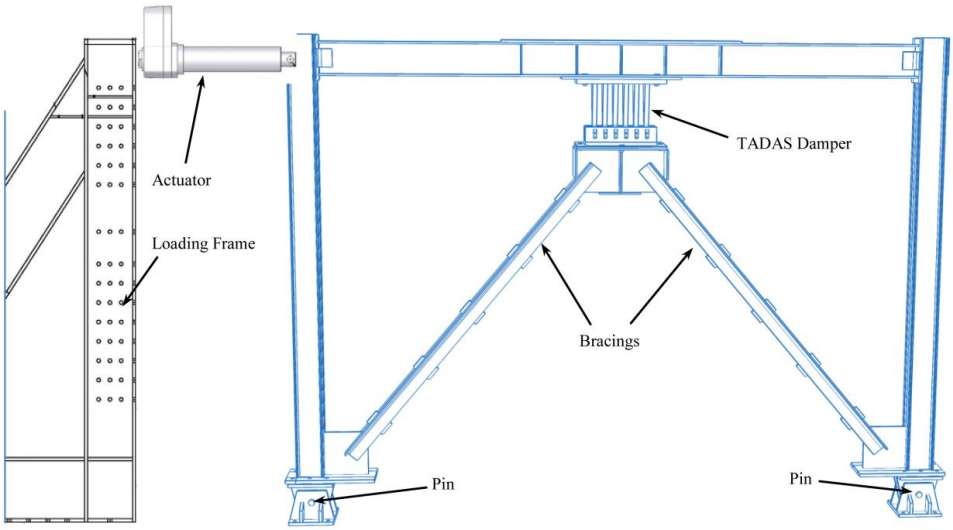

Figure 2.7 Experimental layout of a one-story steel frame with TADAS (Mohammadi, Nasri and Ghaffary) [11]

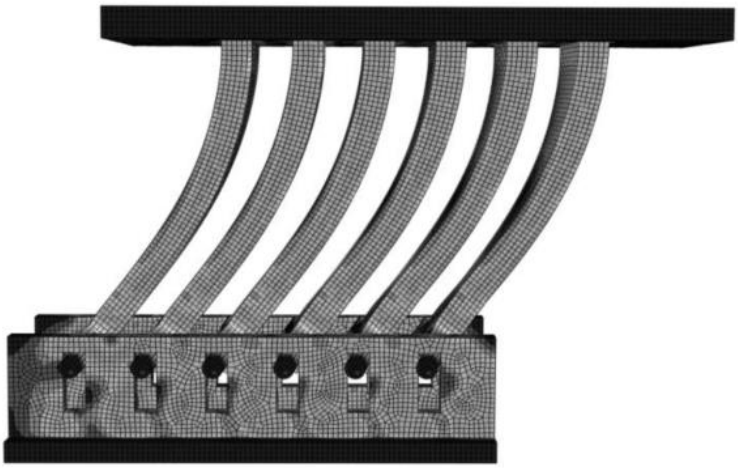

Figure 2.8 Pins hitting the top of the holes in the TADAS under very large deformation in Abaqus (Mohammadi, Nasri and Ghaffary) [11]

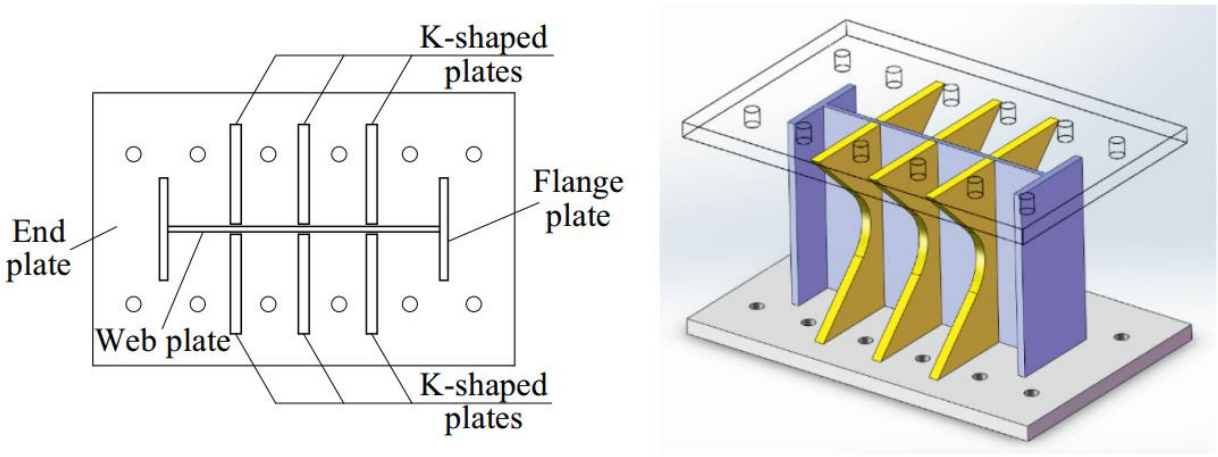

Figure 2.9 Top and 3D views of the shear-bending combined metallic damper (Li, Shu and Huang) [12]

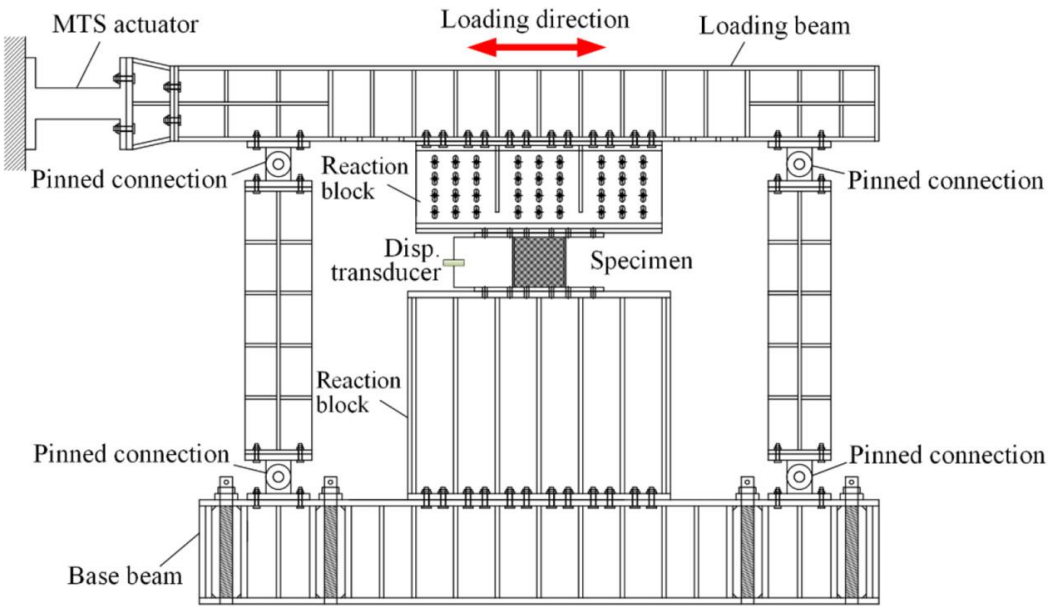

Figure 2.10 Test Setup for the Shear-Bending Combined metallic damper (Li, Shu and Huang) [12]

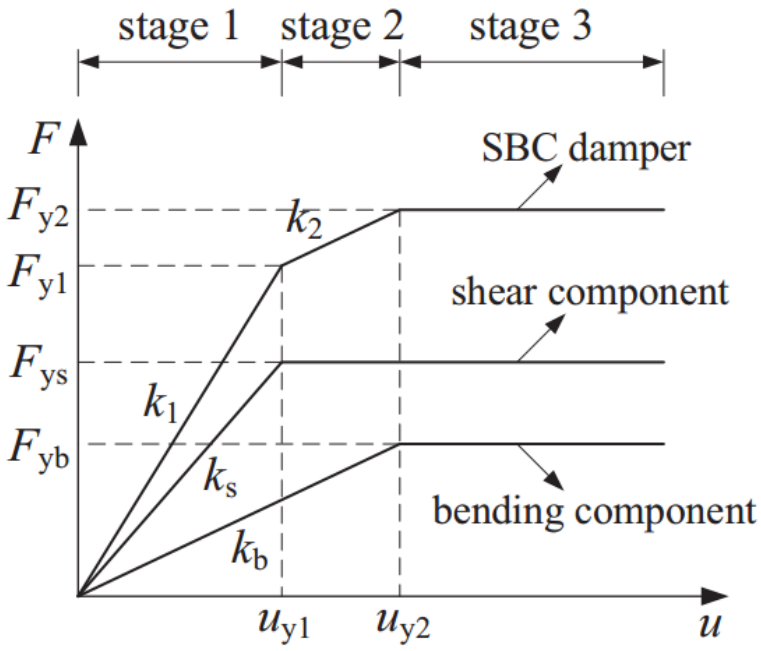

Figure 2.11 Force-displacement relation of the SBC damper (Li, Shu and Huang) [12]

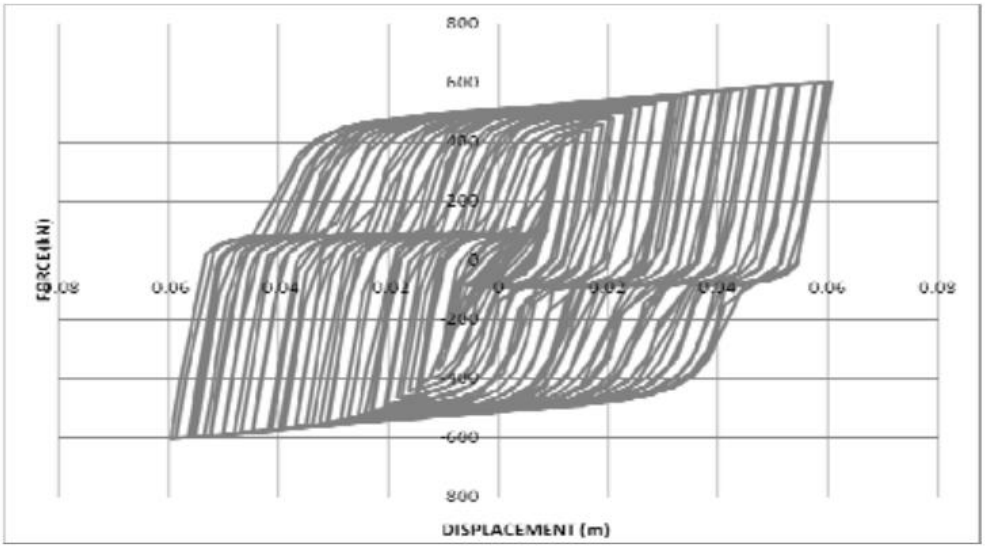

Figure 2.12 Force-displacement hysteretic curve of the modified dual damper system (Li, Shu and Huang) [12]

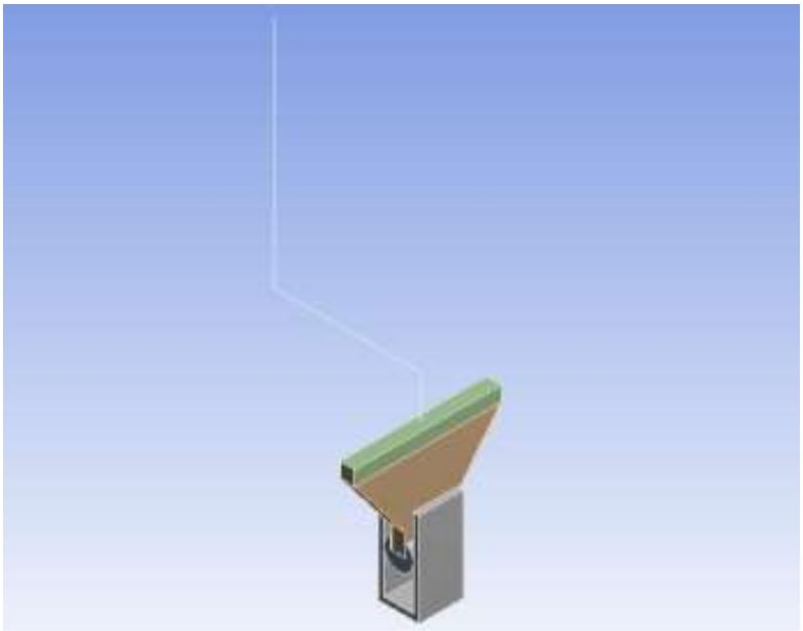

Figure 2.13 ANSYS model of replaceable TPAD hysteric damper (A. K. Esfahani) [15]

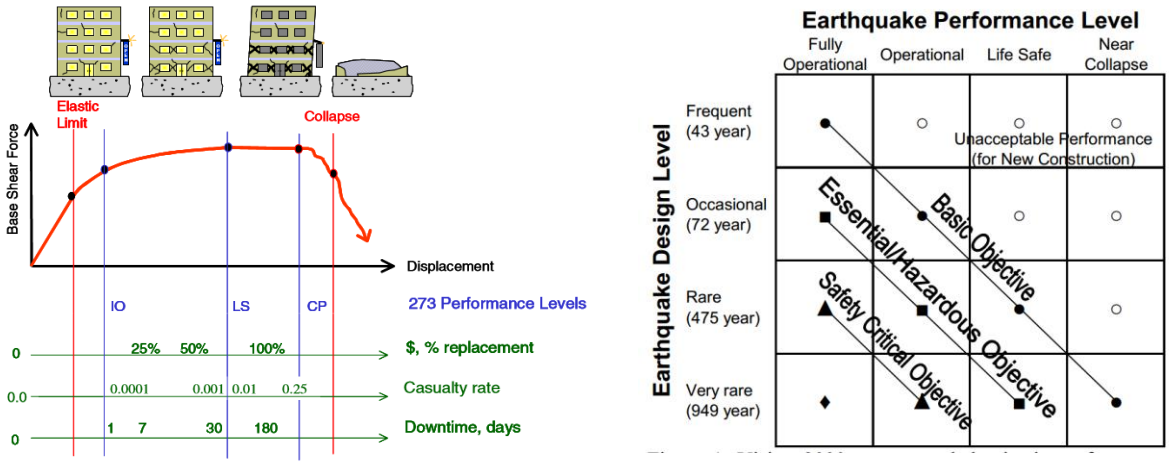

Figure 2.14 (a) Visualization of General Procedure (Holmes)

(b) Vision 2000 recommended seismic performance objectives for buildings

First Generation of PBEE [16,17]

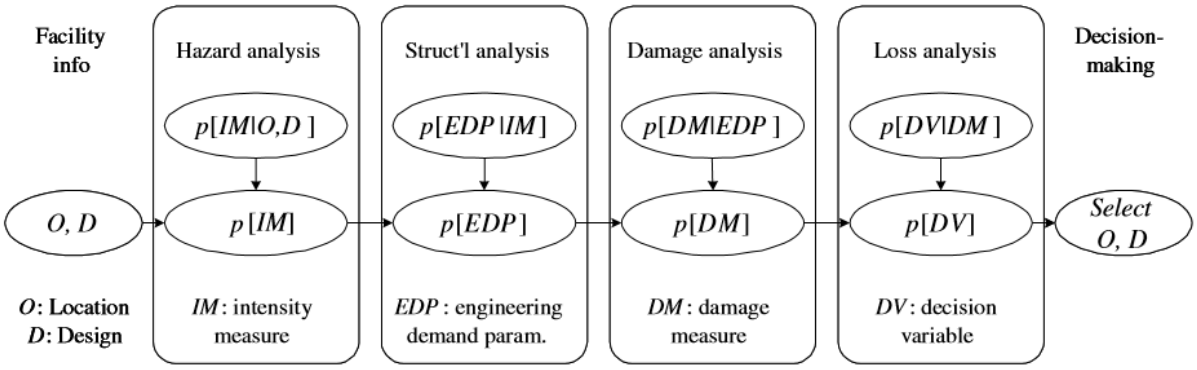

Figure 2.15 PBEE Probabilistic Framework (Cornell, Porter) [17]

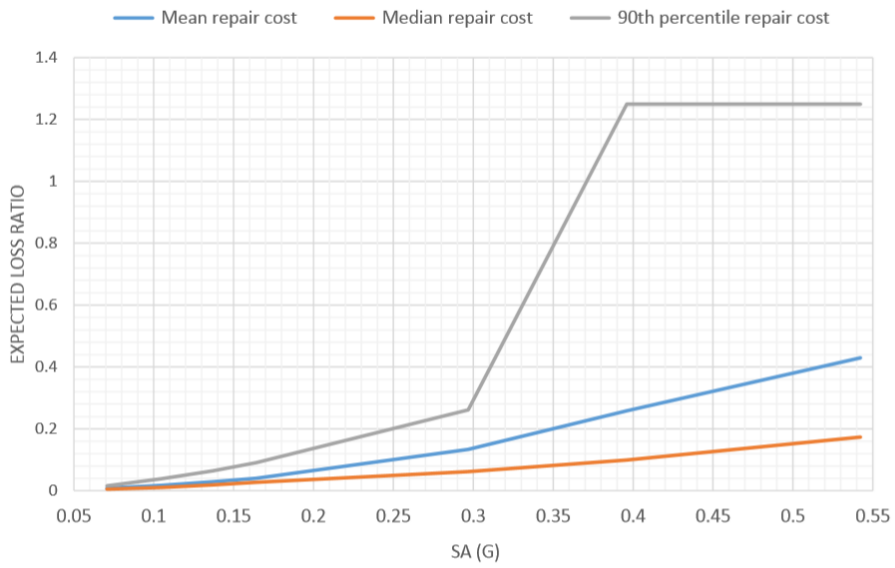

Figure 2.16 continuous seismic hazard scenarios at three probability exceedance level (FB&C Engineers Consulting Group) [18]

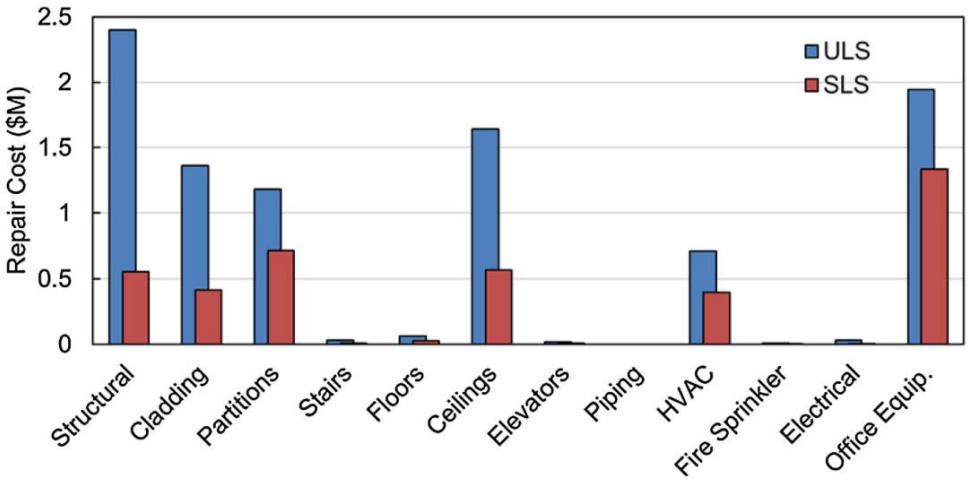

Figure 2.17 Mean repair costs arranged by fragility group for the ultimate limit state (ULS) and serviceability limit state (SLS) (G. M. D. Gobbo, M. S. Williams and A. Blakeborough) [19]

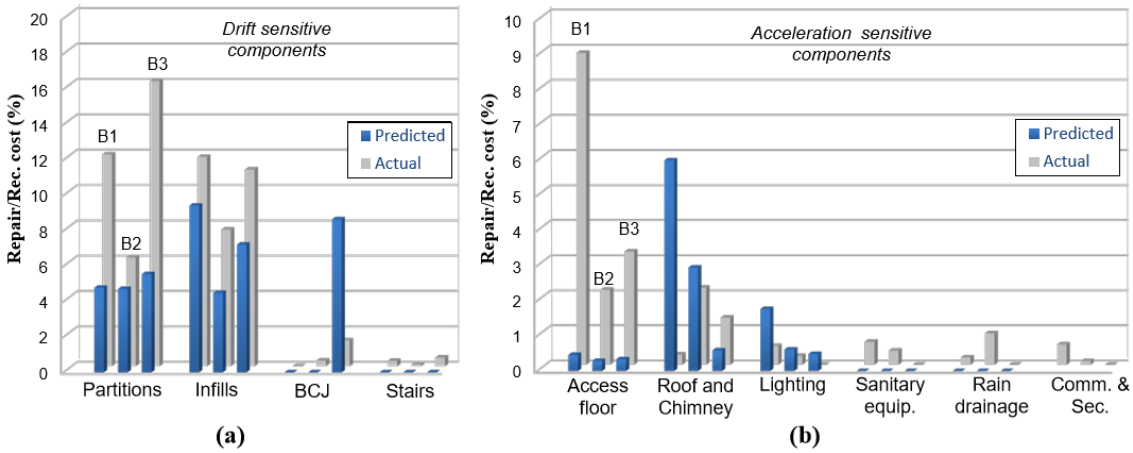

Figure 2.18 Actual and predicted repair costs Comparison: (a) drift sensitive components; (b) acceleration sensitive components (C. Del Vecchio et al.) [20]

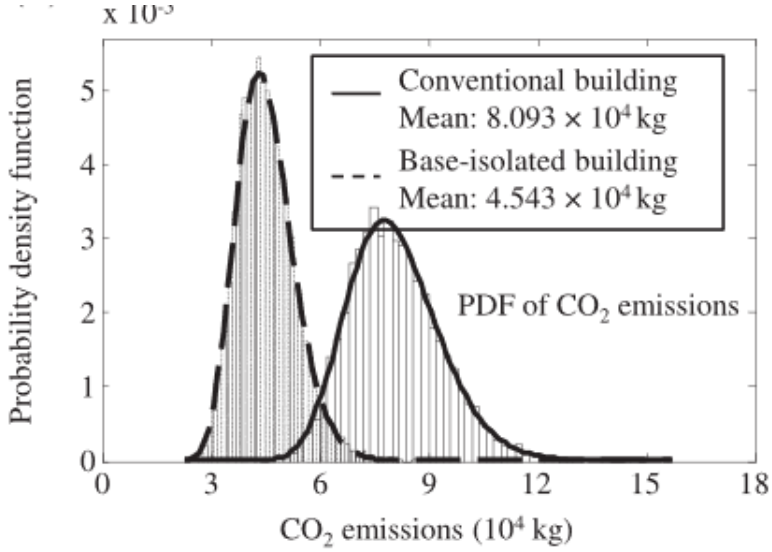

Figure 2.19 CO_2 emission probability density function under 1940 EI Centro Earthquake (Dong and Frangopol) [21]

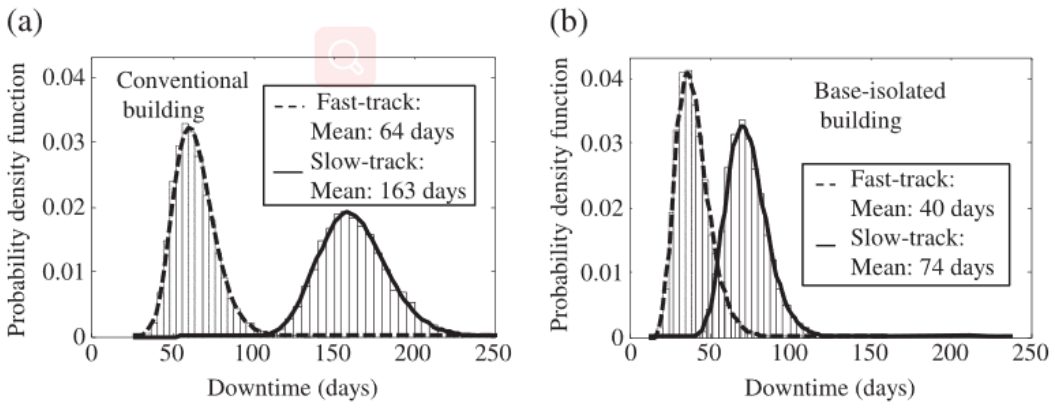

(a) Conventional Building (b) Base-isolated Building

Figure 2.20 Downtime PDF by fast-track and slow-track repair scheme (Dong and Frangopol) [21]

Chapter 3 Numerical Modeling and Analysis of Steel Concentrically Braced Frame (CBF) Buildings under Seismic Loading

3.1 Prototype CBF Building

This study is intended to investigate the vibration mitigation effect of the dual viscous and TPAD dampers on steel CBF structures under seismic ground motion excitation. Two prototypes steel CBF buildings are selected for this purpose: a 3-story CBF structure and a 6-story CBF structure, both with inverted V-shape (or Chevron) bracing configuration. These two prototype CBF structures were originally designed for the SAC Project (1997) [22] according to two design codes: the *1997 NEHRP Recommended Provisions for Seismic Regulations for New Buildings and Other Structures (FEMA, 1997)* and *the Load Resistance Factor Design Specification for Structural Steel Buildings (AISC, 1993).* The prototype structures are both designed for locations in downtown Los Angeles with site Class D. Based on the seismic design code at the design time, the importance factor was taken as one. It is noted that most recent seismic design code - ASCE 7-16 code (2016) recommends an importance factor of 1.25 for commercial office use.

The configurations of these two prototype structures are shown in Figures 3.1-3.3. The 3-story structure has a plan area of 22,816 square feet, measuring 124 ft. in length and 148 ft. in width. Each bay has a bay width of 30 feet. Typical story height is 13 feet. The 6-story structure has a square floor plan, with a dimension of 154 feet in both

directions. Its bay width is also 30 feet. The 6-story CBF building functions as a commercial office building, so the first story height is designed as 18 ft. while other story has the same story height of 13 feet. A total of eight braced bays participate in the seismic force resisting system in the 3-story CBF structure, with four bays in each direction. The 6-story CBF building has 12 braced bays in total, whereas each direction has 6 bays. The plan distribution of the braced bays is shown in Figure 3.1.

The concept of Special Concentrically braced frame (SCBF) first came up after the 1994 Northridge Earthquake near Los Angeles, California. SCBF structures become more ductile and are expected to have reduced seismic base shear by implementing ductile detailing and design provisions of all the components and connections. The braces in the SCBF systems are expected to take several large cycles of compression buckling and tension yielding without pre-mature fracture. Wide-flange sections are used for all the beams and columns while hollow-shaped sections are applied to the braces. The steel material is ASTM A992 Grade 50 steel. Expected post-elastic strength of the braces has been enhanced by construction detailing. Yang and Mahin (2005) proposed the use of yielding strength for the braces with HSS sections to be 60 ksi. Uriz et al. [23] suggested that the yielding strength for beams and columns' material could be increased to 55 ksi, as adopted also for this study. The same design (i.e., member sections) as the original design by Sabili's (2001) [22] is adopted in the current study. The sections of members in a braced bay are listed in Table 3.1 and 3.2.

The seismic mass of each floor in the 6-story CBF structure is listed in Table 3.3. Effective seismic mass includes all dead load. Self-weight of the structure includes steel frames, roofing, ceiling, partitions, and etc. 50 percent of live load is also taken

into consideration for the total seismic mass. The live load is 50 psf. Seismic mass is assigned to each floor node of the lean-on column. Because six braced frames contribute to the seismic resistance in each orthogonal direction of the 6-story building, the seismic mass applied to the corresponding floor node is taken as one-sixths of total mass at each floor. Similarly, the seismic mass of the 3-story structure assigned to the model's lean-on column is proportioned by the ratio of tributary area of each braced bay. Since there are four braced bays in each plane, the lumped mass is one-fourth of that of the entire floor.

Numerical models for both nonlinear static and time history analysis of these two conventional steel CBF structures under seismic ground motion excitation were established in a general nonlinear structural analysis program - Opensees [9]. Beams, columns and braces are all modelled using displacement beam and column element object, which considers plastic hinges spread along the element based on displacement formulation. Each column is divided into 5 segments while beams and braces are divided into 10 segments. Braces are divided into 20 elements to account for large deformation. Corotational geometric transformation type is applied to the elements to account for potentially large displacement in the structure such as buckled brace. A camber equal to 0.1 percent of the brace length is set as the initial imperfection to the middle-length point of the member in order to trigger the buckling of the member similar to the approach by Liu (2018)[24]. The effect of the initial imperfection will be discussed in detail later. Braces are physically connected to beams and columns with gusset plates which can be idealized as pin connection in the numerical model. Lean-on column with lumped mass at the floor nodes is added to account for the global P-

delta effect. Lean-on column is modeled as serial-connected rigid truss elements and no moment appears at joints so that the lateral stiffness is zero.

The first three vibration periods of the two steel CBF frames are listed in Tables 3.4 to 3.5. The fundamental period of the 3-story CBF is 0.304 seconds and the fundamental period of the 6-story CBF is 0.647 sec. The first three mode shapes of these two CBF structures are presented in Figure 3.6 and 3.7.

The CBF structures with dual viscous and metallic damper system are shown in Figure 3.4 and 3.5. The dampers are installed in the auxiliary bay attached to the original CBF bay. Since the auxiliary bay is formed by simple connected beams and columns, it will not contribute the lateral stiffness of the entire structural system before the TPAD is engaged. The dual damper system is connected to V-shaped braces. The braces are modeled using rigid beam element with large section size of much larger stiffness than the adjacent beam. Since the braces are connected to the beam ends, a rigid triangular module is formed to ensure that the displacement at the bottom node of the brace is almost the same as the upper floor node. The viscous damper and the metallic TPAD damper work independent of each other to provide energy dissipation at pre-specified inter-story drift ratios. A two node link element with viscous material is employed to model the viscous damper. The serial-connected beamwith hinge elements are used to simulate the TPAD steel plate in the numerical model. The metallic TPAD damper is modeled with two elastic gap elements connected to the steel plate element in both sides. Details of the TPAD damper will be given in Chapter 3.2. The dual action damper is connected to the lower support floor through a rigid

link element. These connections between the dampers and support members (e.g., braces and beams) are simplified as pin joints in the numerical model.

3.2 Mechanics and Property of the TPAD Damper

In order to mitigate the vibration of steel CBF buildings under severe earthquake ground motion excitation, supplemental damping devices are conceived for this purpose to dissipate more seismic energy. In this study, a metallic hysteric damper called TPAD damper (Keivan 2018) [15] is adopted, which is inspired from the design of TADAS devices. A schematic view of TPAD device in steel frame is shown in Figure 3.9-3.10. TPAD is a trapezoidal plate connected to a round bar. In the TPAD design, its trapezoidal shaped energy dissipation plate is connected to a round rod as shown in the figure. The material steel Q235 with a yielding strength of 235 MPa was used for the trapezoidal shape energy dissipation steel plates, which is equivalent to A36 steel by ASTM standard.

Figure 3.8.a shows the geometry of the trapezoidal plate in TPAD device adopted for this study, each trapezoidal plate measures 125 mm (4.921 in.) at top, 25 mm (0.984 in.) at base, with a total length of 125 mm. The trapezoidal plate of 100 mm (3.937 in.) in length is extended to have a 25-mm wide tongue plate segment near its base. Thickness of each plate is 20 mm (0.7874 in.). In the pilot test, a set of 4 metallic steel plates for each TPAD device is installed in each story. As mentioned earlier, each set of steel plates in the TPAD are connected to the upper floor through V bracing and lower floor by a rigid steel holder device (modeled as elastic gap element in the numerical model). The initial gap of each set is designed to be one percent of the story

height so that the metallic TPAD device will not be engaged until the inter-story drift ratio exceeds 1%. In this study, four set of TPAD devices are installed in each story to increase the energy dissipation and the original numerical model for the TPAD is thus increased to four times the original steel plate width of the pilot study. As shown in Figure 3.8.b, tapered elements are used where the trapezoidal-shaped steel plate is divided into 10 segments in length, and each segment is assumed to be constant section with corresponding width equal to the average width over the segment length. *Beamwithhinge* element is used for the tapered plate in the numerical model built in the Opensees software. The integration method of modified Gauss–Radau quadrature is used for the *Beamwithhinge* element. This method can avoid strain-softening behavior of the conventional force-based beam and column elements by specifying the hinge lengths to confine the nonlinearity of the material at the element ends. [25] The plastic deformation of the steel trapezoidal plates provides the source of energy dissipation, where plastic hinge will form along its length. Thus the properties of the concentrated plastic hinge element in the numerical model is based on half of each segment length while the part lying in-between the plastic hinge elements is considered elastic in each segment (Figure 3.12). Aggregator section model is employed for each segment which combines the axial, shear as well as bending behaviors. However, since the energy dissipation of those trapezoidal plates is primarily from flexural-induced plastic deformation and axial force (from friction) is small, only moment-curvature property is assigned for each aggregator. Axial force-elongation property is also assigned for each segment in the pushover analysis of the single steel plate to avoid compatibility error, but they will not be assigned to the time-

history analysis model. Moment-curvature property is derived based on the Steel01 material. Yielding strength of the rectangular section will be the upper limit of the elastic range of the material and a strain hardening ratio of 0.05 is considered for the plastic deformation range.

The tapered-beam-element numerical model for the trapezoidal TPAD plate is validated by conducting a nonlinear static analysis test of one TPAD plate in which a concentrated load is applied to the free end of the aggregated tapered-beam element in the horizontal direction. The theoretical P-Δ curve of the steel TPAD plate (Figure 3.15) can be derived using the Principal of Virtual Work (PVW) method. The function is integrated along the length of the trapezoidal plate in which the moment inertia of the cross section varies linearly with *x* and the square tongue segment has constant moment of inertia value.

$$\Delta = \int_0^l \frac{Mm}{EI_x} dx$$

The theoretical elastic lateral stiffness (Load to displacement ratio) of each individual metallic plate is determined to be 98.7 kips/in. Each TPAD set contains four steel plates welded to its base plate, so the total lateral stiffness of the TPAD set is 395.0 kips/in. in the elastic range. Yielding strength of the metallic plate aggregator is determined by the maximum force applied when the extreme fibers at the base section first yield. A sample strain contour plot (Figure 3.11) by Keivan (2018) reveals the first occurrence location of the plastic hinges. The displacement of the free tip will be used as the EDP demand to determine the damage state of the TPAD damper when developing fragility functions. The maximum allowable lateral force is calculated

when the yielding stress of the material is distributed over the entire cross section at the base section. The lateral forces at the elastic and plastic strength level are calculated to be 14.88 kips and 22.13 kips respectively. Figure 3.14 shows the P-Δ curve from the nonlinear static pushover analysis of the numerical model (Figure 3.13). The initial lateral stiffness of the taper-beam element in the elastic deformation range is found to be 387.7 kips/in from the numerical analysis. The tapered-beam aggregator model is thus believed to be acceptable since the error of the elastic stiffness compared to the theoretical value is about 1.6%. The lateral force at yielding strength for the numerical model is 12.83 kips, about 10% lower than the analytical value. This error is believed to be caused by the approximation made in the numerical model of TPAD since the surface area of the tapered-beam model is smaller than the actual TPAD plate.

In parallel to the TPAD damper, a viscous damper is also connected to V bracing to introduce viscous damping to the CBF structure. Unlike the TPAD damper, this viscous damper has no gap element connected to it and thus is always activated during the entire seismic excitation. It is modelled by a Two-node-link element with viscous material. The damping coefficient is 7,000 kN/(m/s) and the power factor is taken as 0.5.

3.3 Nonlinear Static Pushover Analysis and IDA Results

This section consists of three parts: Nonlinear static pushover analysis of a single brace in CBF, Nonlinear static pushover analysis of the 3-story and 6-story CBF

structures, and the Incremental Dynamic Analysis for consideration for potential collapse will be used by SPO2IDA tool based on the previous results.

Since seismic performance of steel CBF structures significantly depends on the behavior of bracings, it is critical to develop accurate numerical models to faithfully capture the nonlinear behavior of steel bracings undergoing yielding, buckling, and a combined failure under cyclic loading. The linear perturbation model (Figure 3.16) is used to simulate the initial camber for all braces in this study. Alternatively, this can also be done by using a quadratic perturbation model and test in this study showed that doing so will not result in much difference in the numerical analysis results. Large initial camber would cause substantial decrease in critical load for buckling, as shown in Figure 3.17. Compression members can be classified into long, intermediate or short columns based on their slenderness ratio. Long column usually fails elastically, with an abrupt buckling during elastic range. The Euler formula can fairly accurately predict its critical stress which is usually much lower than its corresponding yielding stress. However, most braces in real life are considered as intermediate compression members which would fail in mixed yielding and buckling condition, and their behavior is said to be inelastic. Unsurprisingly, the critical load of such compression members predicted by nonlinear numerical model comes out to be lower than the Euler formula given critical load. A 45 inches long L-section compression element has been selected in this study to validate the numerical model for intermediate columns with different yielding strength and identical initial camber value. The results are close to those from Johnson Formula for Intermediate column shown below.

$$\sigma_{cr} = \frac{P_{cr}}{A} = S_y - \left(\frac{S_y}{2\pi}\frac{KL}{r}\right)^2 \left(\frac{1}{E}\right)$$

Nonlinear static pushover analysis provides a useful insight of the CBF structure performance under different levels of seismic lateral force. It is also useful to predict potential 'weak story' effect caused by premature brace buckling and associated concentrated story deformation in a particular story. The load pattern mimics the dominating vibration mode shape and in this study an inverted triangular shape along the height of the structure on each story is adopted based on the assumption that first mode shape of structure dominates the response. The lateral loads will increase monotonically until the roof drift ratio reaches 4% in both the 3-story and the 6-story buildings. The base shear vs. roof displacement curves are shown in Figures 3.19 and 3.18.

For the 2D single braced-bay model of the 6-story building, its elastic deformation stage will end when the base shear reaches about 810 kips while the roof drift comes to 4.19 in. Performance of a braced bay from the 3-story structure will remain elastic until base shear reaches 610.86 kips when the roof drift is 1.215 in. There is an abrupt drop in the pushover curve for the 3-story CBF (the base shear drops to 489.67 kips). This would happen when a number of braces in the same story have elastic buckling occur almost at the same time. A partial collapse of the entire building might take place due to soft story effect which should be avoided through careful design or installing supplemental seismic response modification devices such as hysteretic dampers. The same abrupt drop would occur even when the roof mass is reduced to 75 % that of lower story, suggesting that it is more effective to increase the strength of

structural components in the roof story to reduce the abrupt change in lateral stiffness or strength between adjacent stories. The remaining strength after buckling of compression braces will primarily rely on the tension strength of the braces on the opposite side. This sudden decrease in base shear is not observed in the 6-story CBF structure. Similar observations can be made in the nonlinear time-history analysis results later on and the dual action damper has been shown to be effective in reducing the risk of collapse.

The finite element model in this study is limited to model the nonlinear behavior of steel CBF structure system under DBE earthquake loading, therefore the ultimate deflection before collapse is roughly estimated from the full scale experimental results on CBF test specimens by Cameron et al.[26] . Only elastic and non-negative (hardening) range is considered reliable in the CBF model as in Figure 3.20. The fitted Base shear vs. displacement curve for the SPO2IDA tool is shown in Figure 3.21.

The simplified method obtaining the incremental dynamic analysis (IDA) results by SPO2IDA tool is applied and the outcome is shown in Figures 3.22 to 3.23. Figure 3.22 shows the IDA results based on relationship of spectrum acceleration (SA) to roof displacement. The ordinate SA values are obtained by applying variant scale factors on different ground motion records.

The SPO2IDA method simplifies the entire CBF structure into an SDOF system with the same elastic and plastic properties, and use simulation to obtain the seismic response. Therefore the IDA analysis only considers the potential global collapse associated with first vibration mode dominant response. The R-μ curve is shown in

Fig 3.23, where R is the ratio between SA and the yielding acceleration SA_y, where μ refers to the ductility of the structure. The results are shown in the form of expected maximum displacement given SA on three discretized probability level. In this study, the median collapse Sa (T) is taken as 1.9g, whereas the dispersion β is 0.6.

3.4 Nonlinear Time History Analysis

3.4.1 Ground Motion Input and Scaling

As mentioned in Chapter 2, seismic performance of the steel CBF structure can be evaluated within the PBEE framework, which generally consists of four assessment steps as visualized in Figure 2.15.

Earthquake hazard analysis is the first step of PBEE assessment procedure. Most design codes currently in the United States employ Intensity-based assessment to account for risk and uncertainties of earthquake intensity measurements given the location and designs of building. Intensity-based assessments evaluate seismic performance of the structure provided that it is subjected to the given intensity of earthquake shaking, with the damping ratio taken as 5% for the elastic acceleration response spectra. Design criteria in the widely-used building code are based on the response spectrum acceleration from selected Design-basis Earthquake (DBE) ground motion records.

Engineering Demand Parameters in this study mainly refers to the drift ratio and acceleration on each floor by performing nonlinear time-history analysis of steel CBF structures with or without dual action dampers. The uncertainties from the EDP values

given Intensity measurements are considered in two aspects. The 3-story and the 6-story CBF structures will undergo seismic base excitation based on twenty DBE level ground motion records for Los Angeles by Somerville *et al.* (1997) as listed in Table 3.6. These records are originally obtained by a number of global seismographic network stations from different earthquake events, and have been scaled to the metropolitan of Los Angeles thereby introducing uncertainties from other properties of the earthquake (e.g. epicenter distance).

ASCE 7-10/16 provide design response spectrum for use in seismic design. The DBE SA is computed using the parameter values from the USGS seismic design map. However, for some ground motion record, the corresponding SA value at the structure's fundamental period can be quite different from the DBE SA (Figure 3.24) value and as such the ground motion record should be scaled to the design spectrum level. Figure 3.25 presents the corresponding design response spectrum for several versions of seismic codes and also median spectrum of the selected ground motion records. It is seen that the median spectral curve falls in between the two design spectral curves, especially in the constant acceleration range.

Potential change in the natural period of the structure could occur after structural failure such as severe plastic deformation or buckling of key structural components. To avoid scaling only at a specific period value (e.g., initial natural period value), weighted ground motion amplification (α) factor for each ground motion record in this study is obtained by the following equation,

$$\alpha = \sum_{i=1}^{n} P_i \frac{DSA(T_i)}{RSA(T_i)}$$

where, T_i refers to the vibration period of the structure and is assumed to vary over a certain range due to possible damage-induced structural property change. In this study, T_i is taken as discretized points distributed in the neighboring region of the natural period of the structure, where *n* in the equation refers to the total number of these points and *Pi* is the probability that the fundamental period of the structure to be T_i. DSA refers to the design spectrum acceleration at T_i, while RSA is the response spectrum acceleration at T_i for the concerned ground motion record. Four discretized points are selected for both the 3-story and 6-story structures, and are listed in Table 3.7 and Table 3.8. The expected DBE level peak horizontal acceleration of the earthquake ground motion has 10% probability of exceedance in 50 years.

Maximum considered event (MCE) level earthquake ground motion records are also applied to the 3-story CBF structure. This ground motion records are scaled to 1.5 times that of DBE level ground motions and is useful to demonstrate the effectiveness of the dual damper in controlling the seismic response of steel CBF structures. The earthquake ground motion scaled to MCE level earthquake has 2% probability of exceedance in 50 years.

It is noted that the each ground motion record has been linearly interpolated with a refined time interval of 0.001 seconds because of nonlinear time history analysis requirements for numerical accuracy and stability. The numerical model considers 2% Rayleigh damping assigned to the first mode.

3.4.2 EDP results from Time-history analysis

Engineering Demand Parameters (EDP) can be obtained from running nonlinear time history analysis of the structure subjected to earthquake ground motion. EDPs such as inter-story drift ratio and floor acceleration response are closely related to the Decision Variable in the PACT software accompanying FEMA P-58 (2018). For example, Damage states (DM) of the structure components are mostly dependent on the inter-story drift ratio while DMs of certain non-structural components largely affected by floor acceleration. This section focuses on the distribution and mean value of inter-story drift, acceleration and residual drift from nonlinear time history analysis, which will be used as input to the fragility functions in Chapter 4.

Figure 3.26 shows the distribution of peak inter-story drift ratio along the height of 6-story CBF structure. The peak drift here refers to the maximum value of corresponding floor drift during the duration of each ground motion. The “mean” refers to the ensemble average value of the structural response over the twenty ground motion records.

It is seen that larger inter-story drift ratios mainly occurred in the first story and the roof story while the drift ratio is relatively small in the intermediate floor. This is likely caused by significant change in member section sizes (e.g., beams, columns or braces) between adjacent stories and thus abrupt change in story stiffness. Most drift ratios are still below the code drift limit 2% given by ASCE 7-16. However, since most drift ratio has exceeded 1%, there will be damage in the structure. For example, brace buckled and damages in the gusset plate occurred. Figure 3.28 shows the drift

ratio demand of each story of the 6-story CBF structure with dual action dampers (viscous damper + TPAD metallic hysteretic damper) corresponding to the DBE level earthquake. Most of the drifts have been reduced to be less than 1% or even more. Figure 3.29 and 3.30 show the distribution of the floor acceleration response. The acceleration is the absolute acceleration and tends to be greater at upper floors than the lower ones, which suggests non-structural components in upper stories might suffer more acceleration related damage. A comparison of mean acceleration demand on each floor is shown in Figure 3.31. It suggests that dual damping system is effective in lowering the acceleration response of each floor in most cases of time-history analysis so that loss can be reduced respectively. It should be noted that the dual action dampers selected in this numerical study have not been optimized and thus better results might be expected for optimal design of dual action dampers for the 6-story CBF structure. Residual drift is also needed to determine if the repair is worthwhile or complete replacement is justified, together with the repair fragility discussed in Chapter 4. The residual drift demand of each story is calculated as the average drift of the last 30 seconds free vibration response in the time history analysis. It is noted that an additional 30-seconds zero acceleration values are appended to each ground motion to simulate the free vibration response. Figures 3.32 and 3.33 show the distribution of residual drift demand for the structure without and with the dual action dampers. The residual drift on the first floor is larger than other floors, suggesting that structural components around the first floor have sustained larger plastic deformation.

Nonlinear time history analysis of the 3-story CBF structure has also been conducted as well in order to obtain the EDP values required for resilience evaluation. Figures

3.34 to 3.36 show the story drift ratio distribution under selected DBE excitation. As for the CBF structure without dual action dampers, the roof inter-story drift ratio is significantly larger than that of other stories. Thus there is a higher risk of collapse occurrence in the roof, likely due to the abrupt drop in story stiffness. Compared with the original 3-story CBF, the structure with dual dampers significantly reduces the roof story drift, while most of the story drift on each floor is much smaller than 1%. Using the dual action dampers is able to reduce potential collapse risk and corresponding loss and casualties. The acceleration response of the 3-story CBF is also plotted in Figures 3.37 to 3.39. The floor acceleration is generally larger on the upper floor than the lower ones. The dual action damper is effective in reducing the floor acceleration except for the roof by 40% or even more. It is again noted that the dual action dampers selected in this numerical study have not been optimized and thus improved results are very likely to happen if optimal design of dual action dampers for the 6-story CBF structure is adopted. The residual drift results from time-history analysis are also compared in Figure 3.40-3.41. The residual drift on the first and second stories are negligible for both cases where these stories can be expected to have similar post-earthquake performance compared to the intact structure before earthquake. Adding dual dampers can significantly reduce the residual drift of the roof story.

Time-history analysis is also applied to the 3-story CBF under MCE level seismic excitation. The results in Figure 3.42 comparing the DVs indicate that TPAD metallic damper can further reduce the mean drift demand by about 10%.

3.5 Summary and Conclusion

This chapter performs nonlinear static analysis and time-history analysis of both CBF prototype structure with and without dual action dampers (viscous damper + metallic TPAD damper) using finite element models built in a general nonlinear structural analysis software - Opensees. Viscous dampers start to work from the beginning. The metallic TPAD dampers function as a supplement to the viscous damper when story drift exceeds a pre-specified value (1% assumed in this study). For nonlinear time history analysis, an ensemble of twenty earthquake ground motion records are scaled to the design response spectrum of the 1997 version seismic code. Scale factors have also been weighted to average out the fluctuation effect of response spectrum near the fundamental period of the prototype CBF structures which are associated with the uncertainty in seismic excitation. It is found that tapered *BeamwithHinge* element with aggregator section can exactly model the mechanical behavior of steel TPAD damper. Pushover analysis of a single trapezoidal shaped steel energy dissipation plate in TPAD damper was conducted to validate its nonlinear finite element model by comparing with analytical formulation derived mechanical properties.

The nonlinear pushover analysis of the 3-story and 6-story CBF structures provides a useful insight of their performance under large lateral loading. For the 3-story CBF structure, although the brace in tension will provide post-elastic strength, several compression braces in the same floor buckled at the same time which may lead to increased story deformation in this specific story. This phenomenon is consistent with the soft story effect observed in time-history analysis, where large drift only occurred in the roof story. As for the 6-story CBF structure, relatively larger drift happened in

the upper stories and ground story, especially for the stories where significant change in the member section size exists. Dual action dampers are found to effectively reduce the acceleration on all floors (except for roof) by about 40% to 50%, and lower the story drift by about 20% on average. Residual drifts were also reduced which would help to prevent complete structural replacement.

The function of the metallic TPAD dampers can be considered as backup damping device when an unexpected large earthquake takes place. The mean drift ratio of the 3-story CBF under MCE level excitation can be further lowered by about 10%, which is helpful in controlling collapse during extreme events.

Table 3.1 Member section sizes of 3-story prototype CBF structure （from Sabili 2000） [22]

Story	Brace	Braced Frame Column	Braced Frame Beam
3	HSS 6x6x1/2	W12x96	W18x46
2	HSS 8x8x1/2		W27x84
1	HSS 8x8x1/2		W30x90

Note: only members in the braced bays are shown here.

Table 3.2 Member section sizes of 6-story prototype CBF structure （from Sabili 2000） [o]

Story	Brace	Braced Frame Column	Braced Frame Beam
6	HSS 5x5x1/2	W14x132	W27x94
5	HSS 6x6x1/2		W30x99
4	HSS 8x8x1/2		W30x116
3	HSS 8x8x1/2	W14x211	W30x116
2	HSS 8x8x1/2		W30x116
1	HSS 10x10x1/2		W36x150

Note: only members in the braced bays are shown here.

Table 3.3 Seismic mass of 6-story prototype CBF structure

	Roof	**5th floor**	**4th floor**	**3th floor**	**2th floor**	**1th floor**
Steel Framing(psf.)	14.06017059	15.62666667	18.97069294	20.61555406	20.61555406	25.44904838
Floors and Roof(psf.)	34.25	34.25	34.25	34.25	34.25	34.25
Ceilings/Flooring(psf.)	3	3	3	3	3	3
Mechanical/Electrical(psf.)	7	7	7	7	7	7
Partitions(psf.)	0	10	10	10	10	10
Dead Load(psf.)	58.31017059	69.87666667	73.22069294	74.86555406	74.86555406	79.69904838
25%Live Loads(psf.)	12.5	12.5	12.5	12.5	12.5	12.5
Total Load(psf.)	70.81017059	82.37666667	85.72069294	87.36555406	87.36555406	92.19904838
Distributed Area(sf.)	3750	3750	3750	3750	3750	3750
Weight of Exterior Wall(lb.)	8020.833333	16250	16250	16250	16250	16250
Seismic Mass(lb.)	265538.1397	308912.5	321452.5985	327620.8277	327620.8277	345746.4314

	273558.9731	325162.5	337702.5985	343870.8277	343870.8277	361996.4314
Seismic Mass (kips.)	273.5589731	325.1625	337.7025985	343.8708277	343.8708277	361.9964314

Table 3.4 Nature period of first three modes for 6-story prototype CBF structure

	6-Chevron	6-Cheveron with dual damper
1st	0.6468	0.6291
2nd	0.2309	0.2236
3rd	0.1307	0.1245

Note: Unit is in second.

Table 3.5 Nature period of first two modes for 3-story prototype CBF structure

	3-Chevron	3-Cheveron with dual damper
1st	0.3039	0.2975
2nd	0.1249	0.1205

Note: Unit is in second.

Table 3.6 Features of DBE ground motion

	Ground Motion	**Duration**	**PGA (g)**
LA01	Imperial Valley, 1940, El Centro	53.46	0.46
LA02	Imperial Valley, 1940, El Centro	53.46	0.68
LA03	Imperial Valley, 1940, El Centro	39.38	0.39
LA04	Imperial Valley, 1940, El Centro	39.38	0.49
LA05	Imperial Valley, 1940, El Centro	39.08	0.3

LA06	Imperial Valley, 1940, El Centro	39.08	0.23
LA07	Landers 1992, Barstow-Vineyard & H	79.98	0.42
LA08	Landers 1992, Barstow-Vineyard & H	79.98	0.43
LA09	Landers 1992, Yermo Fire Station	79.98	0.52
LA10	Landers 1992, Yermo Fire Station	79.98	0.36
LA11	Loma Prieta 1989, Gilroy	39.98	0.67
LA12	Loma Prieta 1989, Gilroy	39.98	0.97
LA13	Northridge 1994, County Fire Station	59.98	0.68
LA14	Northridge 1994, County Fire Station	59.98	0.66
LA15	Northridge 1994, Rinaldi	14.95	0.53
LA16	Northridge 1994, Rinaldi	14.95	0.58
LA17	Northridge 1994, Sylmar,Olive View	59.98	0.57
LA18	Northridge 1994, Sylmar,Olive View	59.98	0.82
LA19	North Palm Springs 1986	59.98	1.02
LA20	North Palm Springs 1987	59.98	0.99

Note: PGAs are not scaled

Table 3.7 Discretized fundamental period distribution of the 6-story prototype CBF structure

I	1	2	3	4
Ti (s)	0.55	0.65	0.75	0.9
Pi	0.2	0.5	0.2	0.1

Table 3.8 Discretized fundamental period distribution of the 3-story prototype CBF structure

I	1	2	3	4
Ti (s)	0.20	0.30	0.40	0.55
Pi	0.2	0.5	0.2	0.1

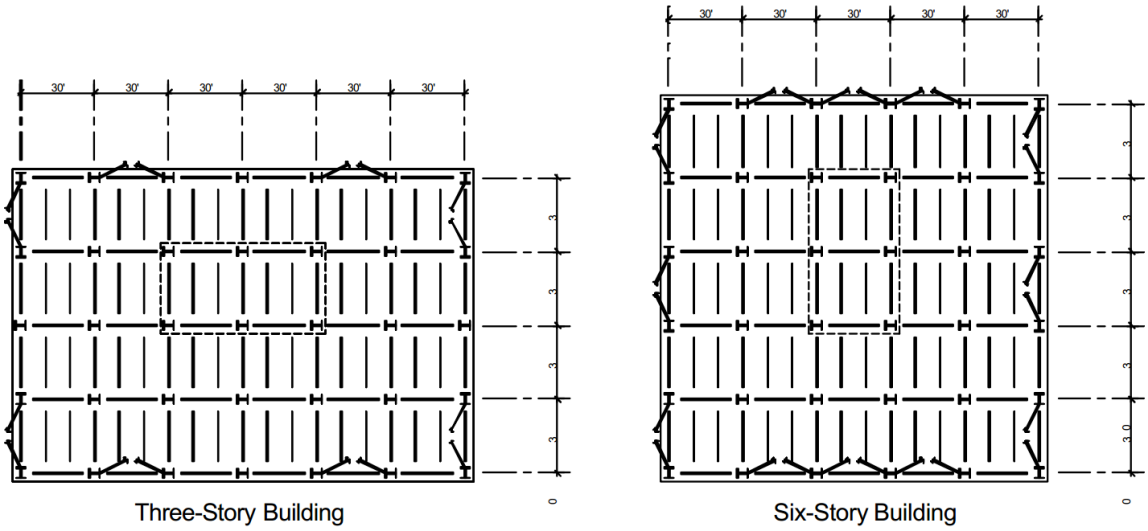

Figure 3.1 Plane views of 3-story and 6-story prototype buildings (from Sabelli (2000)) [22]

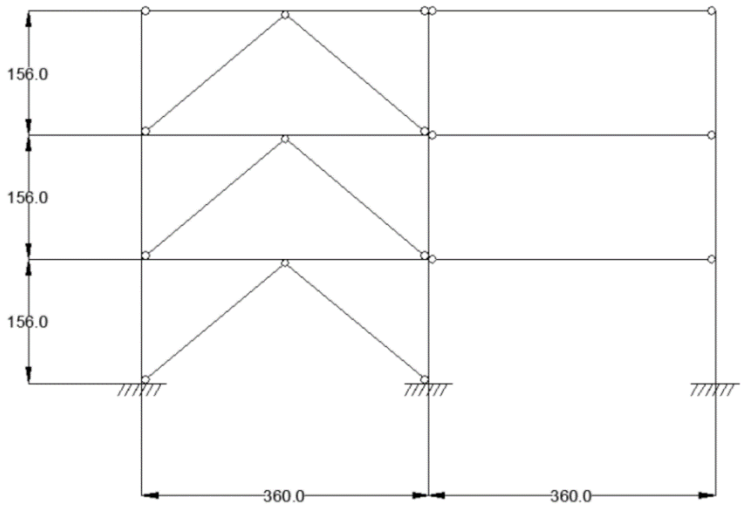

Figure 3.2 3-story chevron CBF with lean-on column (unit: inch)

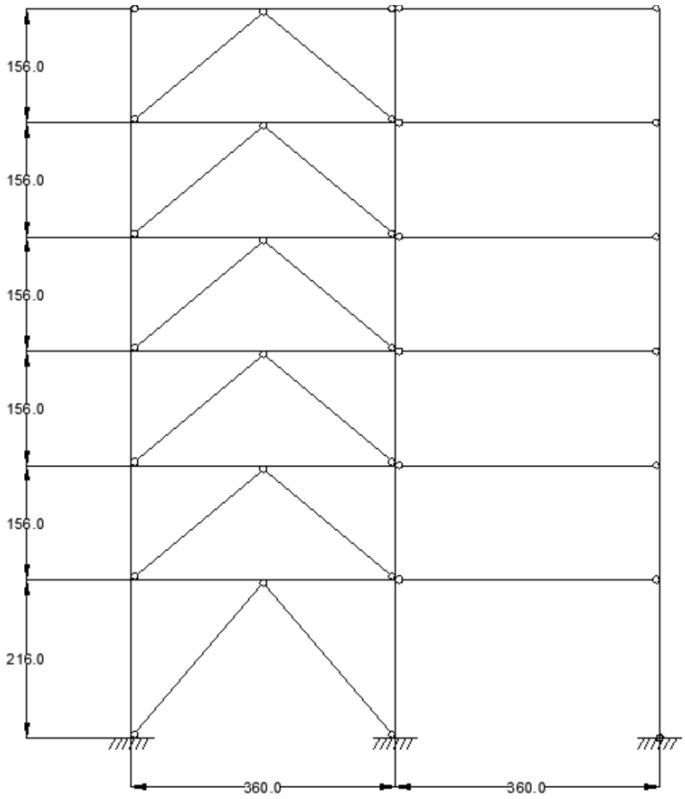

Figure 3.3 6-story chevron CBF with lean-on column (unit: inch)

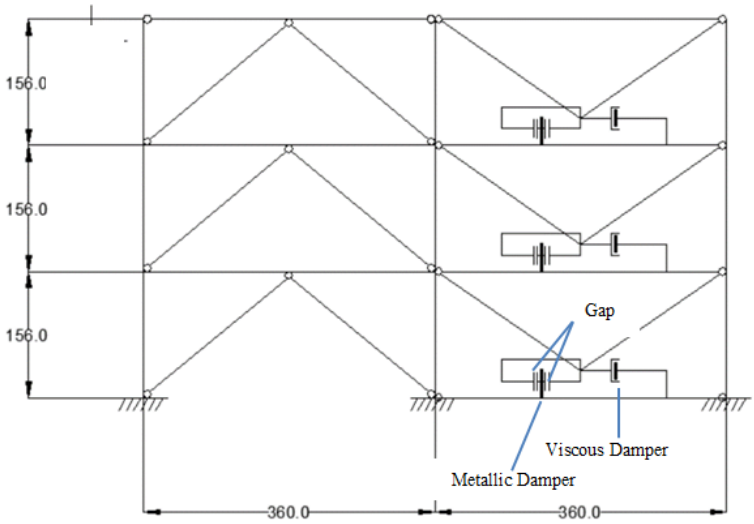

Figure 3.4 3-story chevron CBF with dual damper system

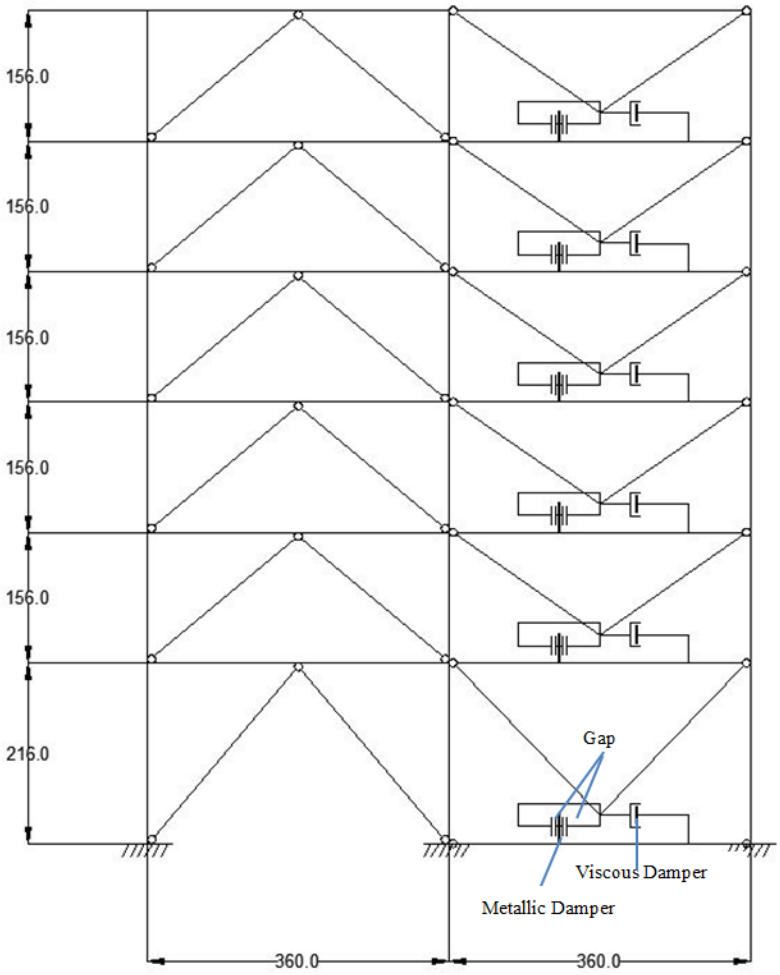

Figure 3.5 6-story chevron CBF with dual damper system

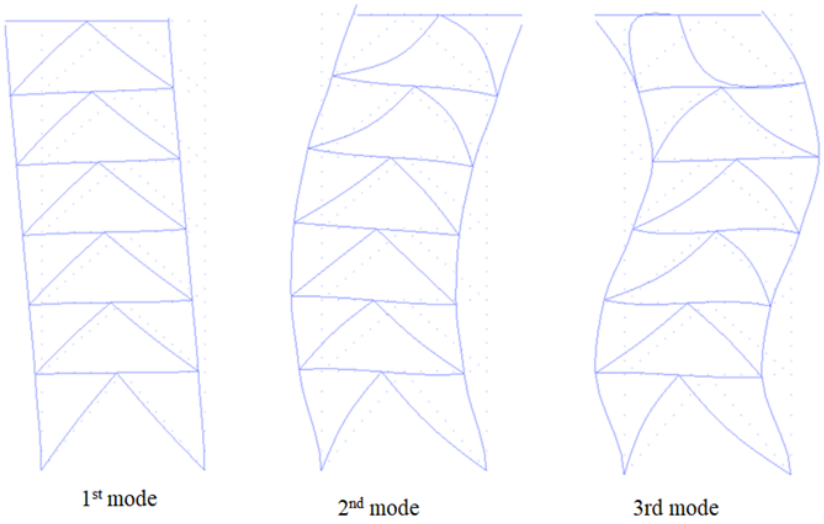

Figure 3.6 First three mode shapes of 6-story prototype CBF structure

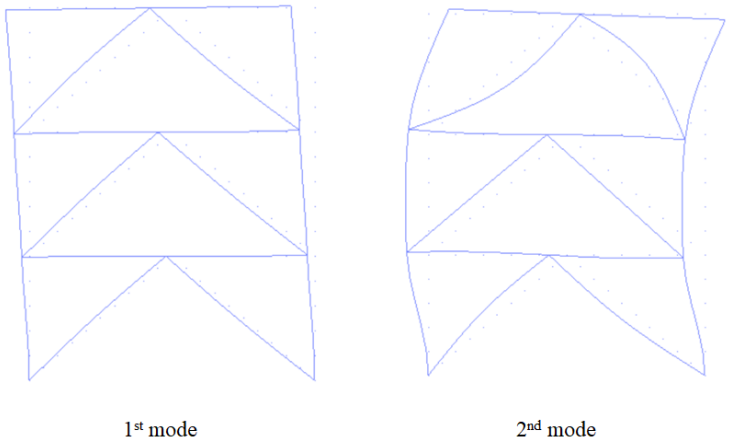

Figure 3.7 First two mode shapes of the 3-story prototype CBF structure

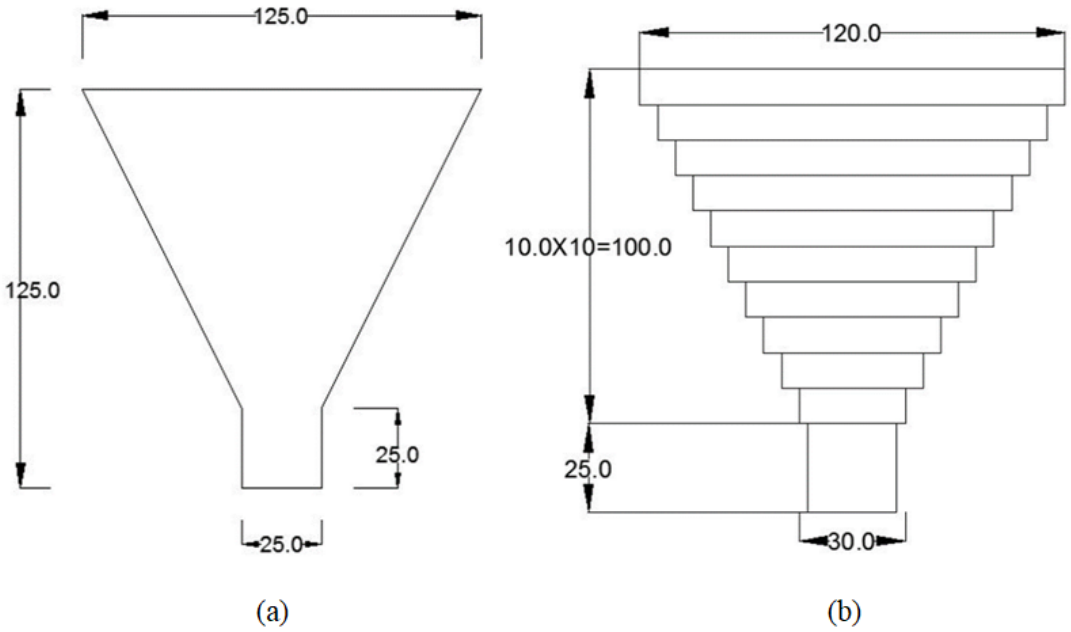

Figure 3.8 (a) Geometry of TPAD with tongue segment

(b) Geometry of Equivalent tapered-Beam model

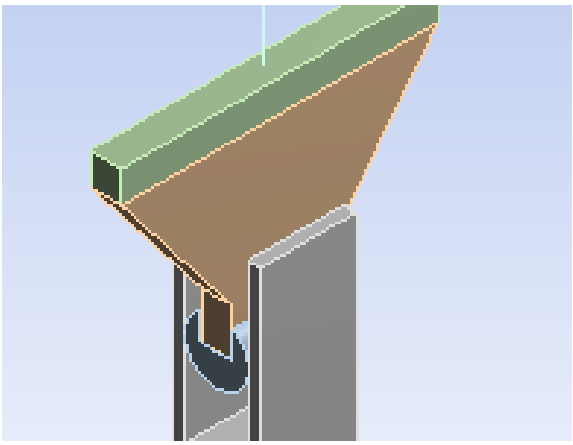

Figure 3.9 ANSYS model with solid elements for TPAD (Arshia) [15]

Figure 3.10 Actual schematic of TPAD devices [15]

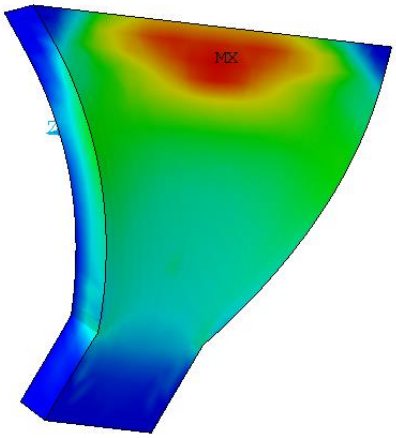

Figure 3.11 Strain contour of TPAD device (K. Arshia) [15]

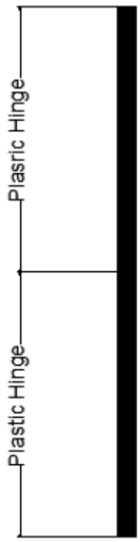

Figure 3.12 Plastic hinges region on individual *beamwithhinge* element

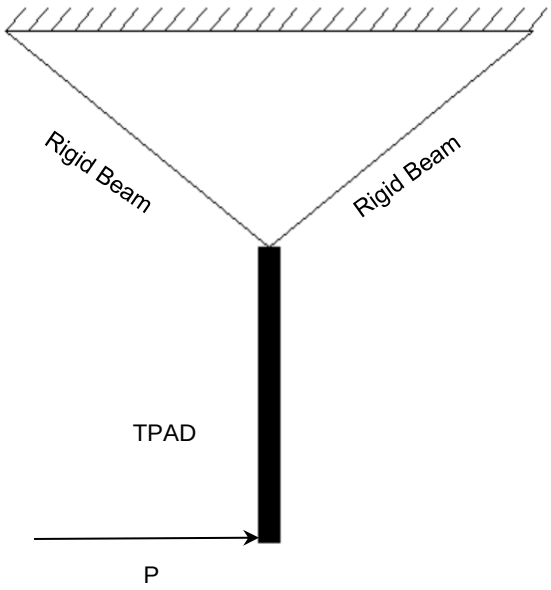

Figure 3.13 TPAD nonlinear static pushover numerical model

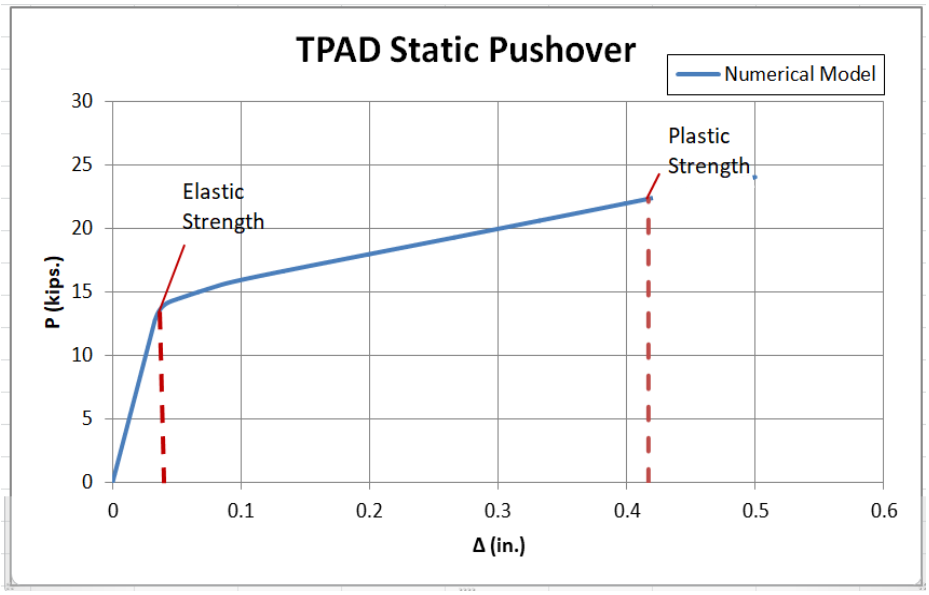

Figure 3.14 TPAD nonlinear static pushover P-Δ curve by Opensees

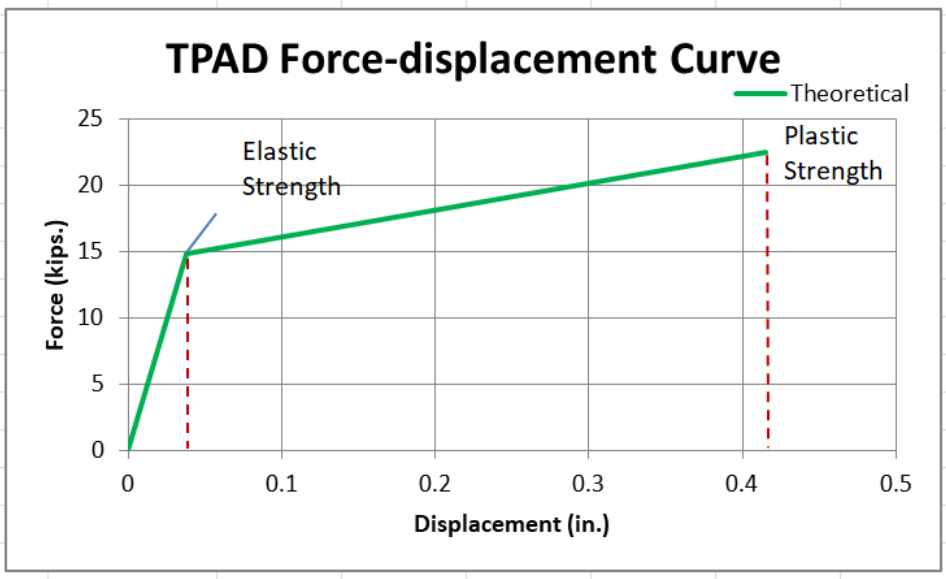

Figure 3.15 Theoretical TPAD force-displacement curve

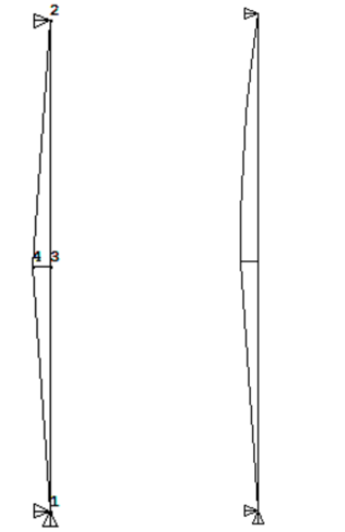

(a) Linear Perturbation Model

(b) Quadratic Perturbation Model

Figure 3.16 The perturbation shape of an individual brace element in CBF

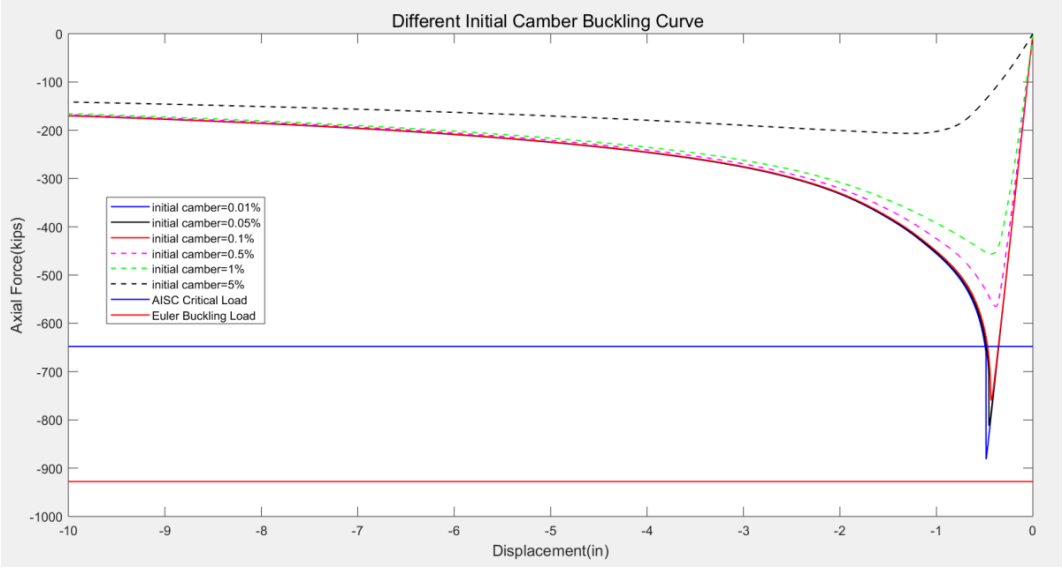

Figure 3.17 Compression buckling curve for braces with different initial camber

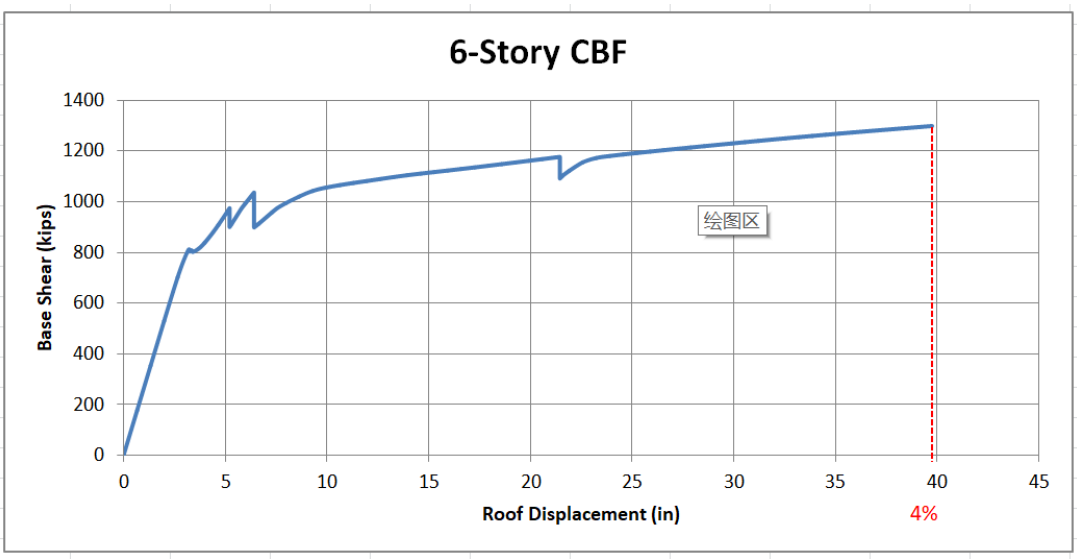

Figure 3.18 6-Story prototype CBF structure base shear-roof displacement curve

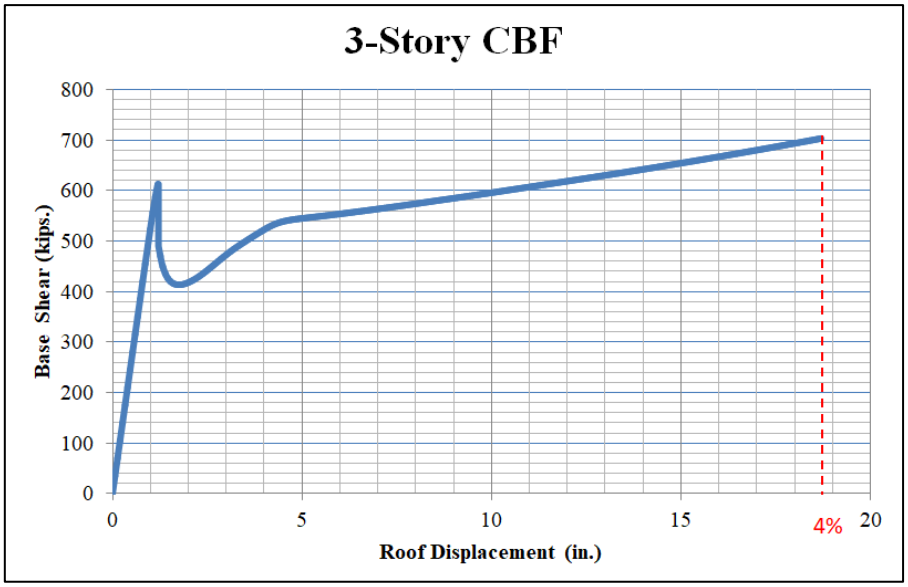

Figure 3.19 3-Story prototype CBF structure base shear-roof displacement Curve

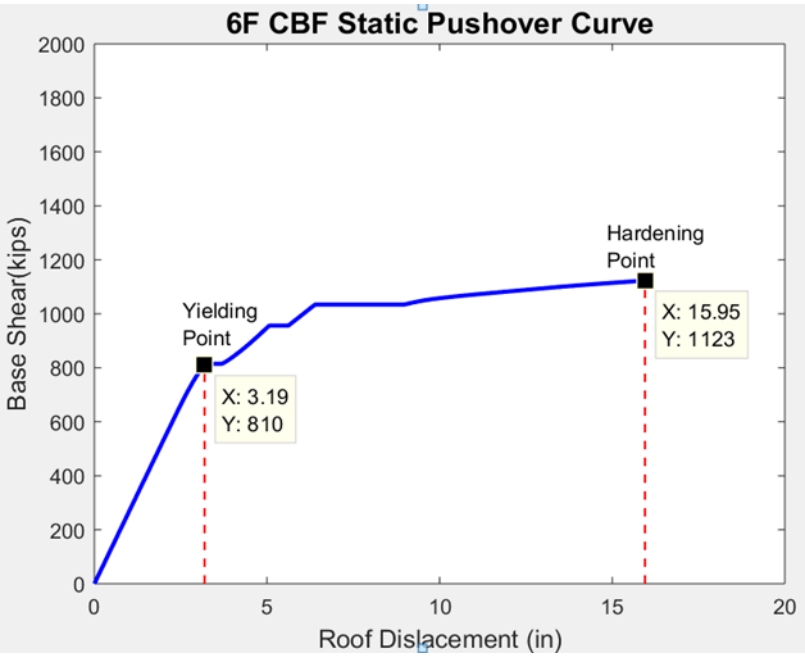

Figure 3.20 Original 6-Story CBF base shear-roof displacement curve for SPO2IDA

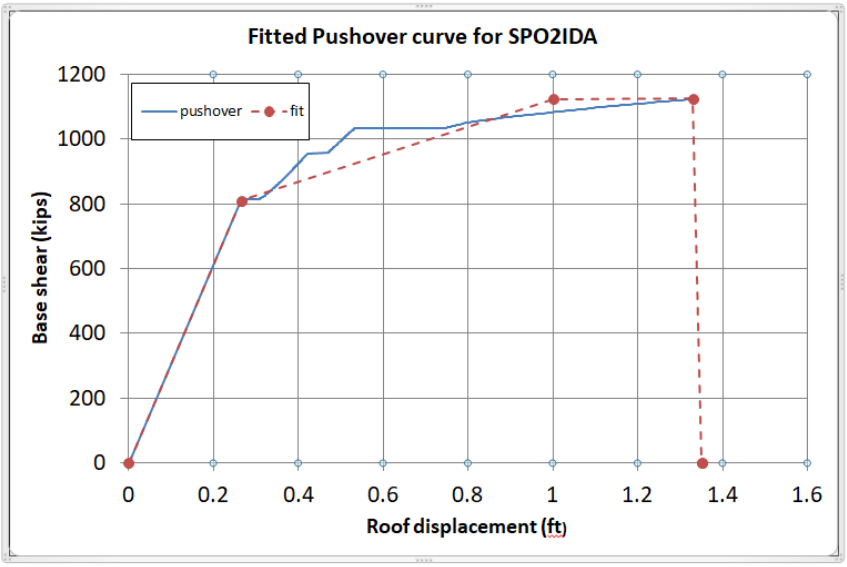

Figure 3.21 Fitted static pushover (SPO) curve for SPO2IDA

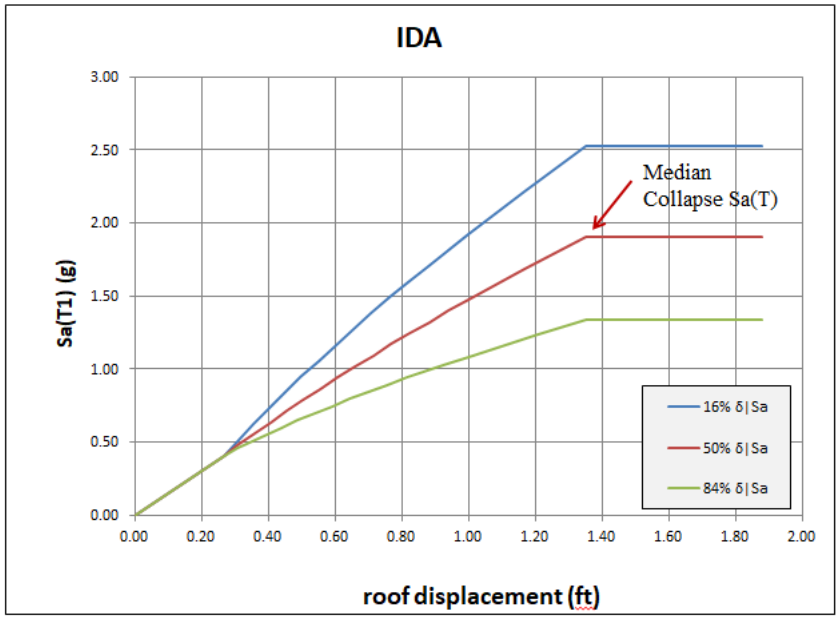

Figure 3.22 Simulated IDA SA-displacement curve for 6-story CBF

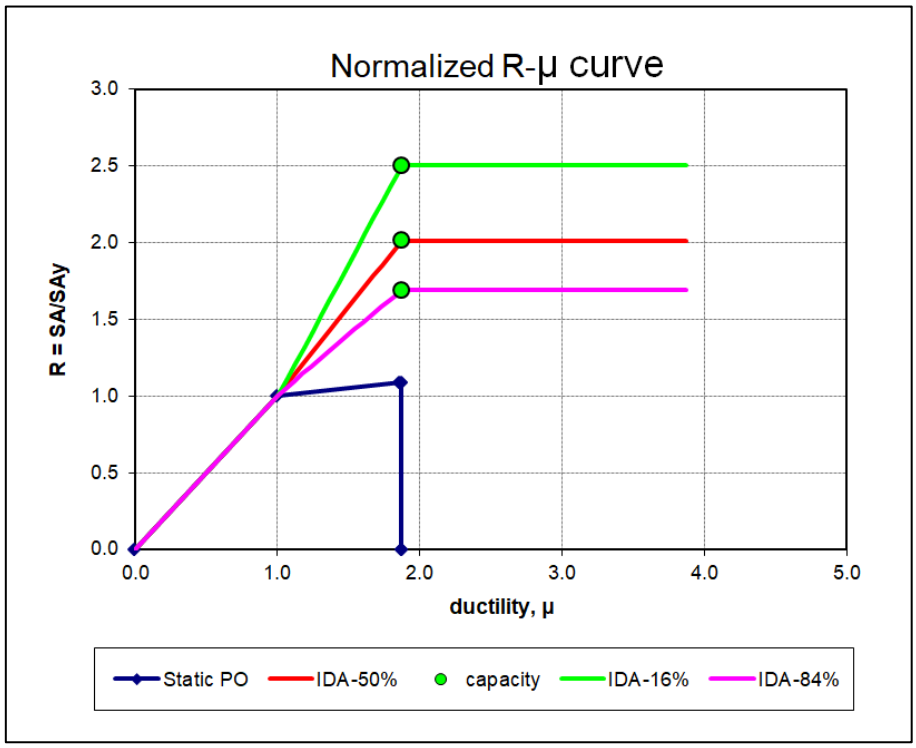

Figure 3.23 Normalized R-μ Curve for 6-story CBF

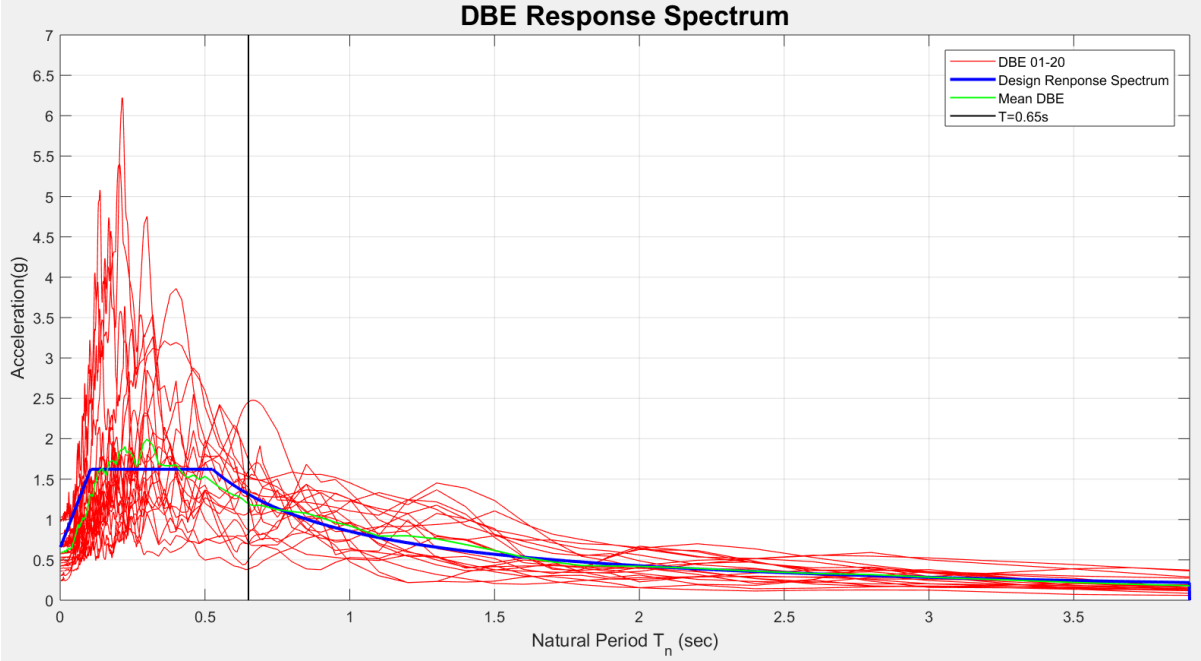

Figure 3.24 Response spectrum of the selected DBE ground motion (5% damping)

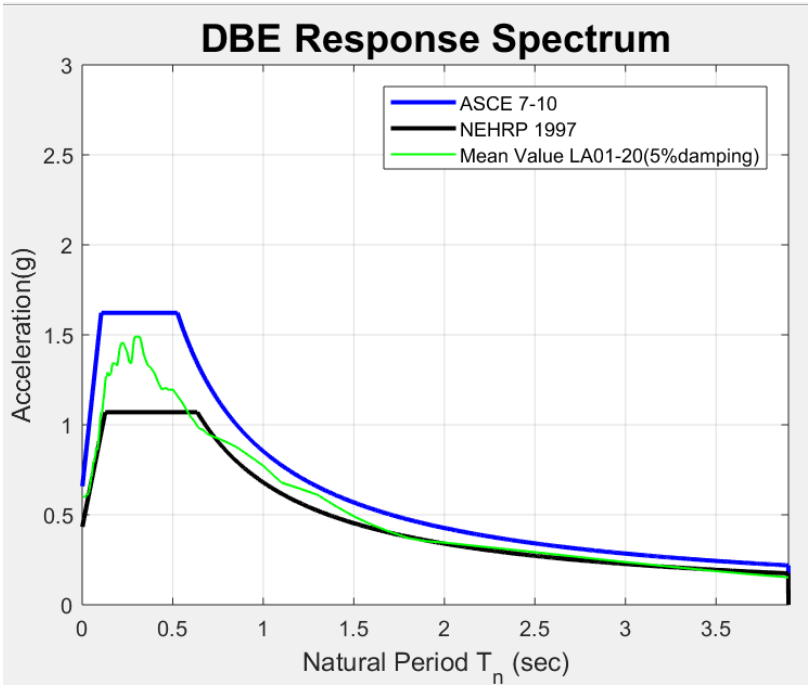

Figure 3.25 Different design spectrums (5% damping)

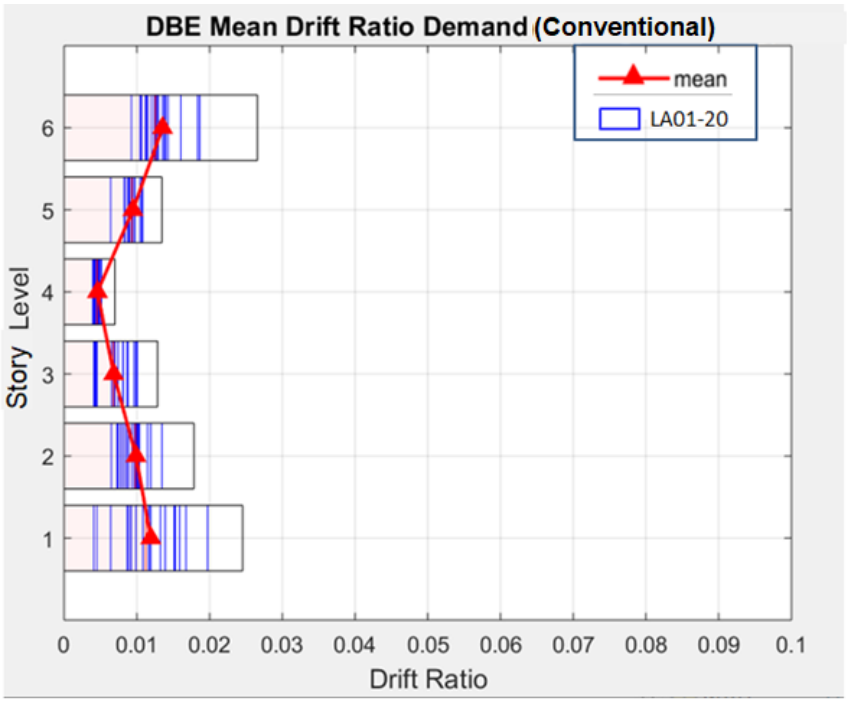

Figure 3.26 Conventional 6-story CBF drift ratio demand

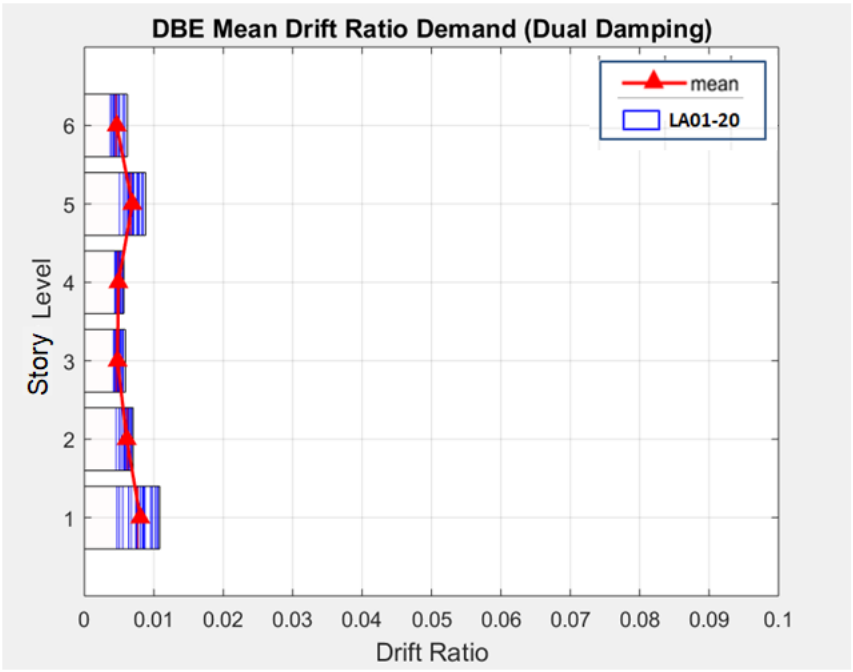

Figure 3.27 6-story CBF drift ratio demand with dual damping system

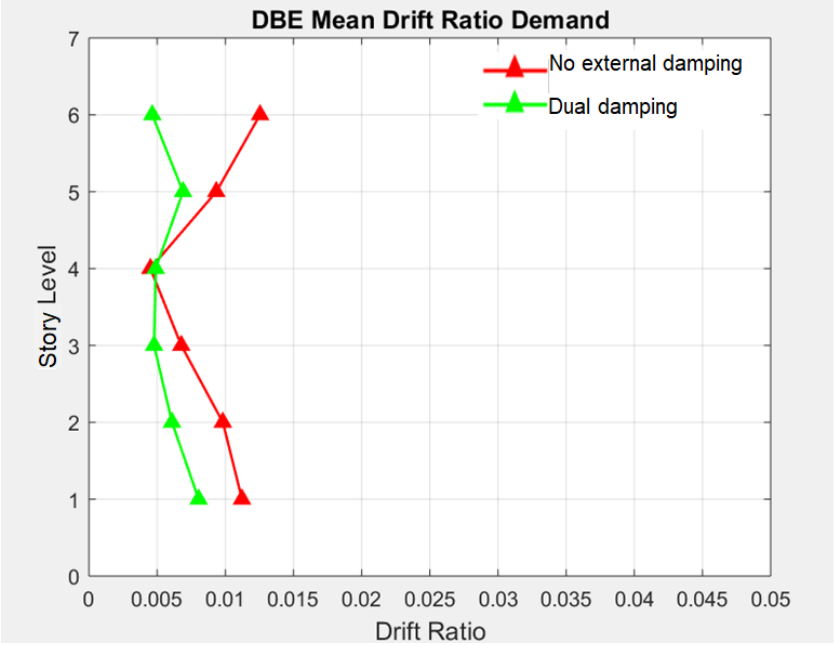

Figure 3.28 6-story CBF mean drift ratio demand comparison

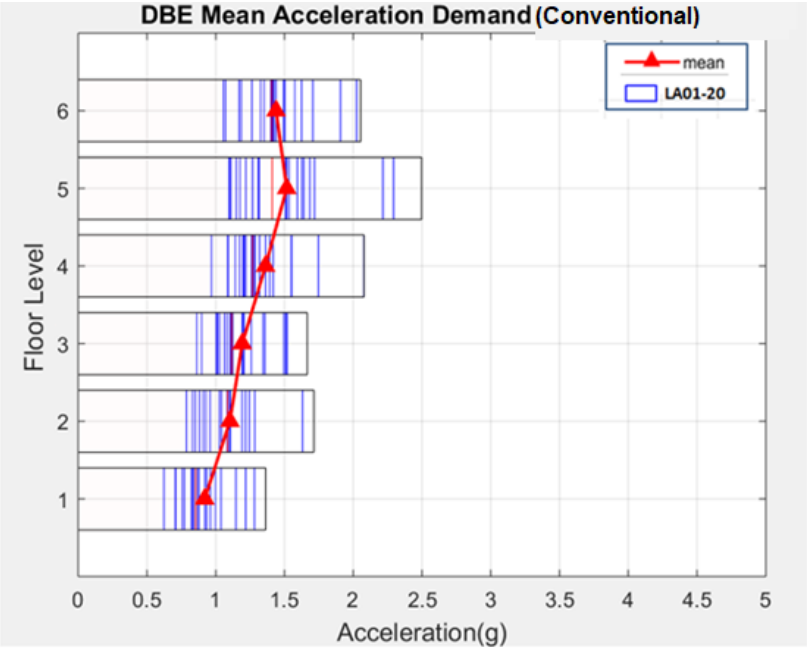

Figure 3.29 Conventional 6-story CBF acceleration demand*

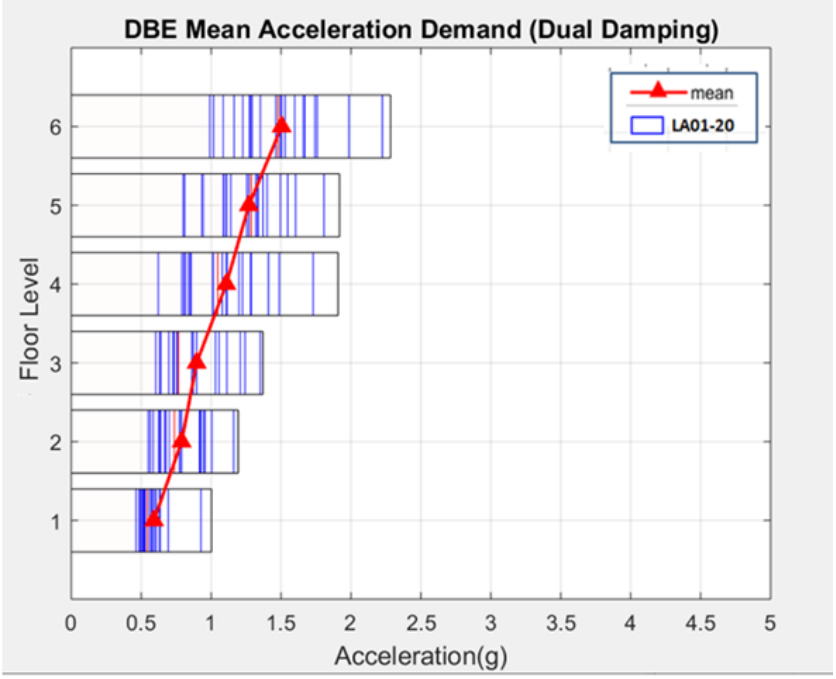

Figure 3.30 6-story CBF acceleration demand with dual damping*

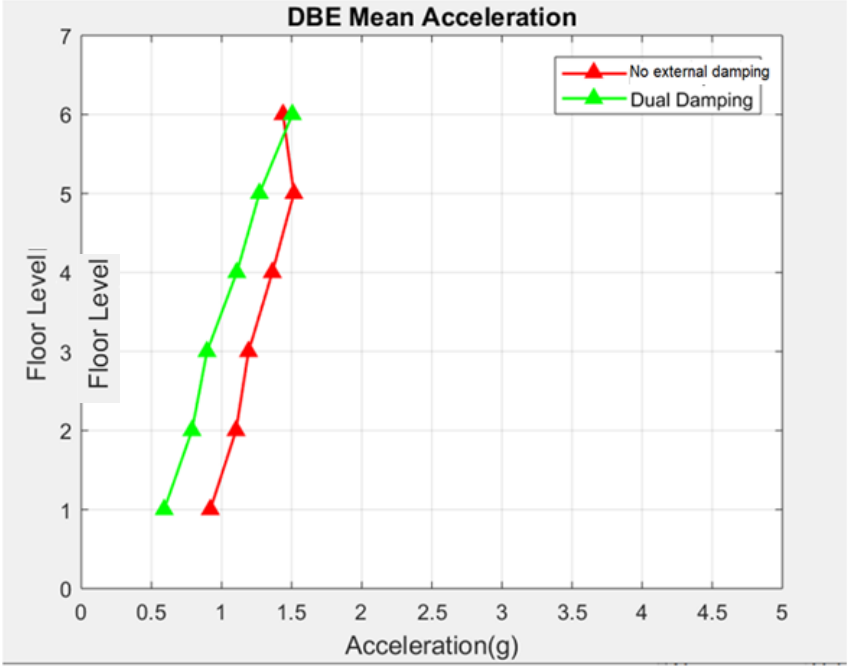

Figure 3.31 6-story CBF acceleration demand comparison*

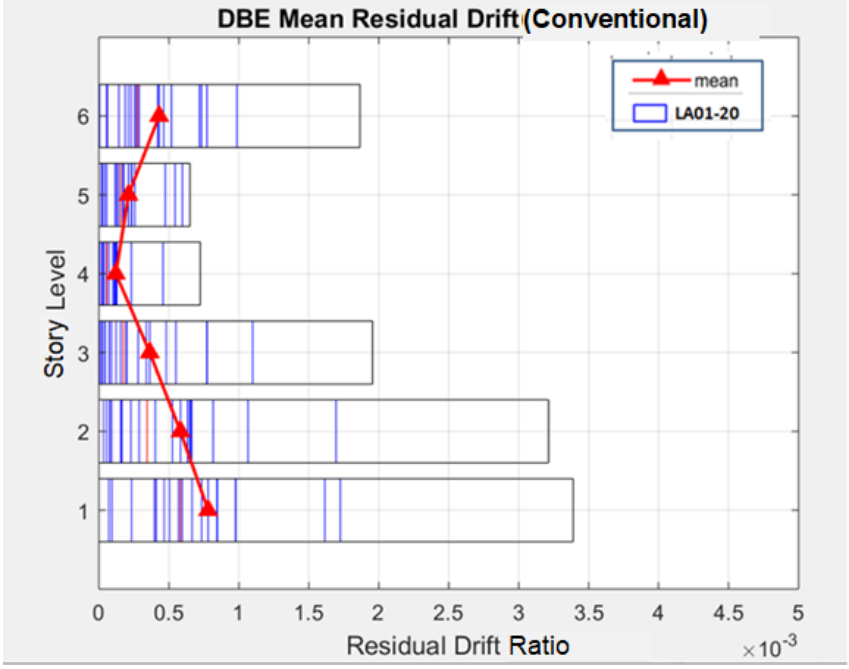

Figure 3.32 Conventional 6-story CBF residual drift demand

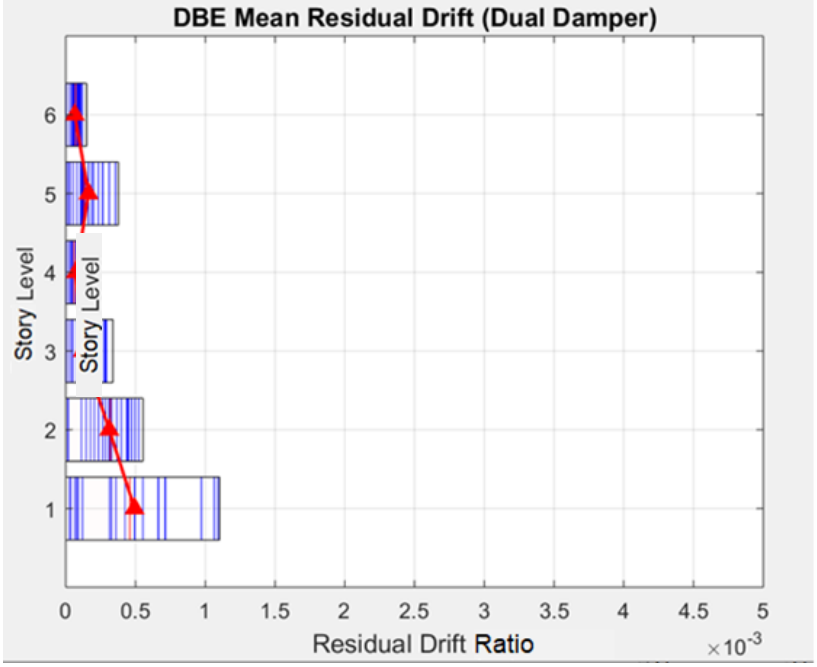

Figure 3.33 6-story CBF residual drift demand with dual damping

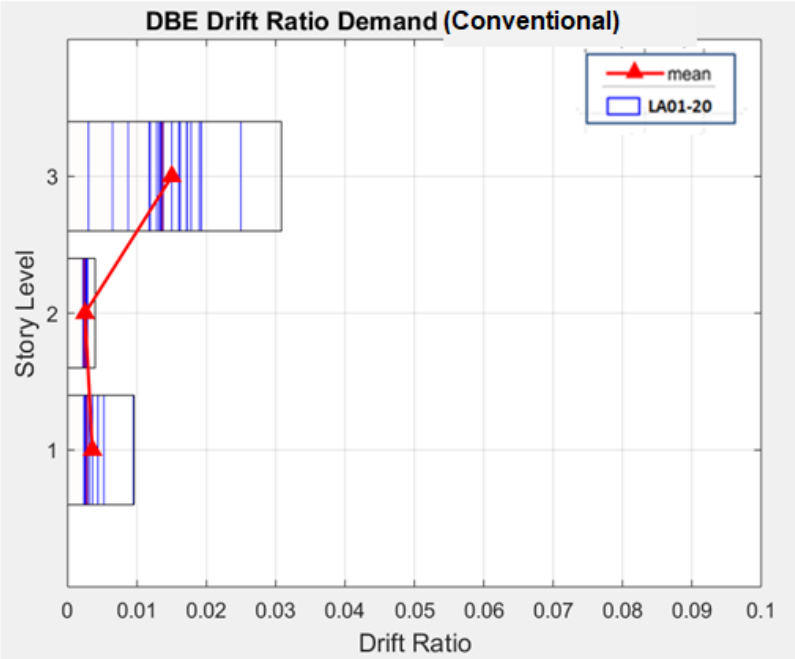

Figure 3.34 Conventional 3-story CBF drift demand only under DBE

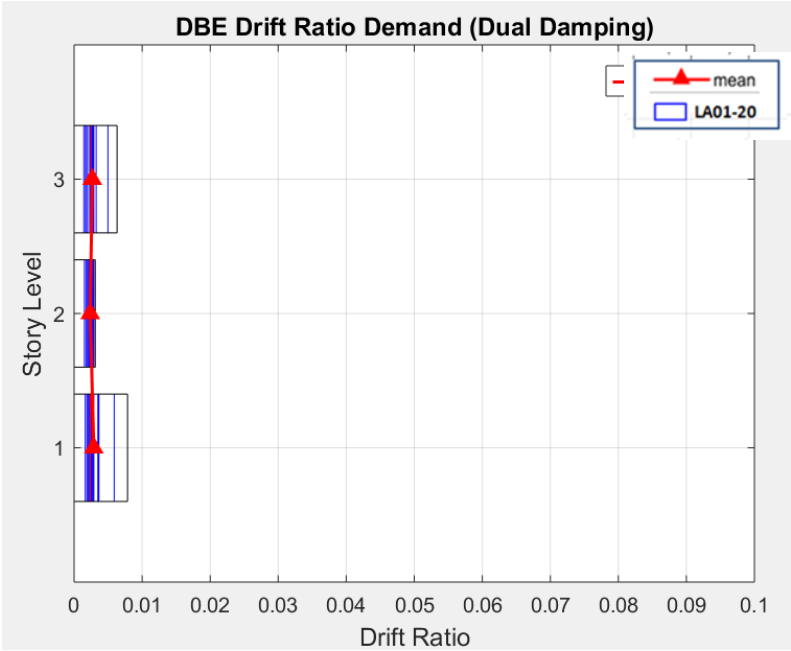

Figure 3.35 3-story CBF drift demand with dual damping under DBE

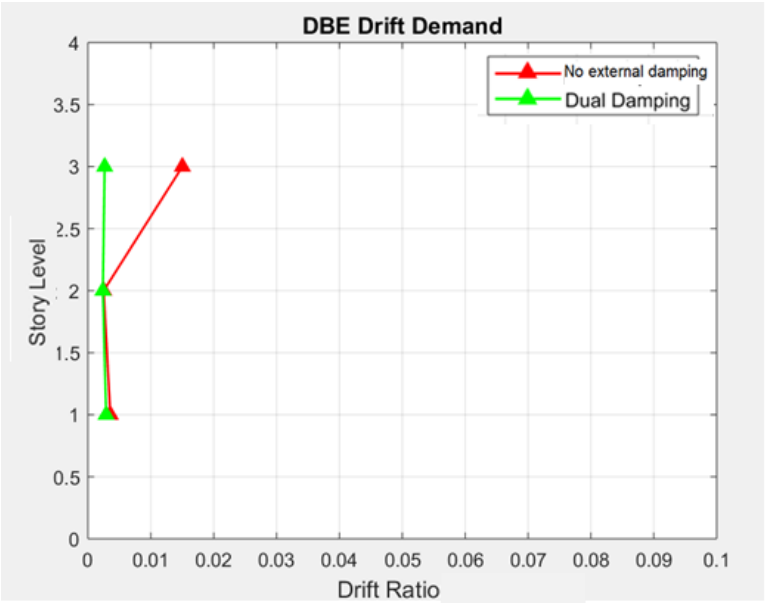

Figure 3.36 3-story CBF drift ratio demand comparison under DBE

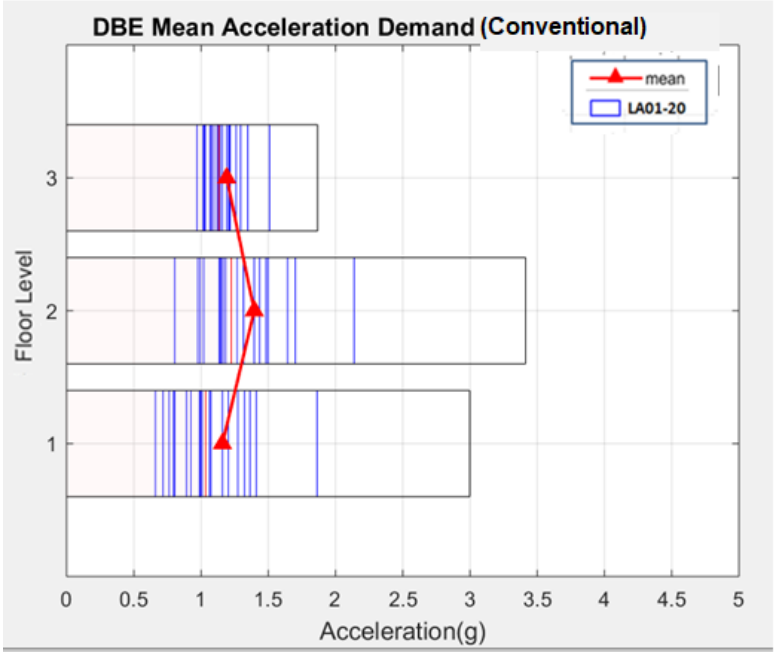

Figure 3.37 Conventional 3-story CBF acceleration demand under DBE*

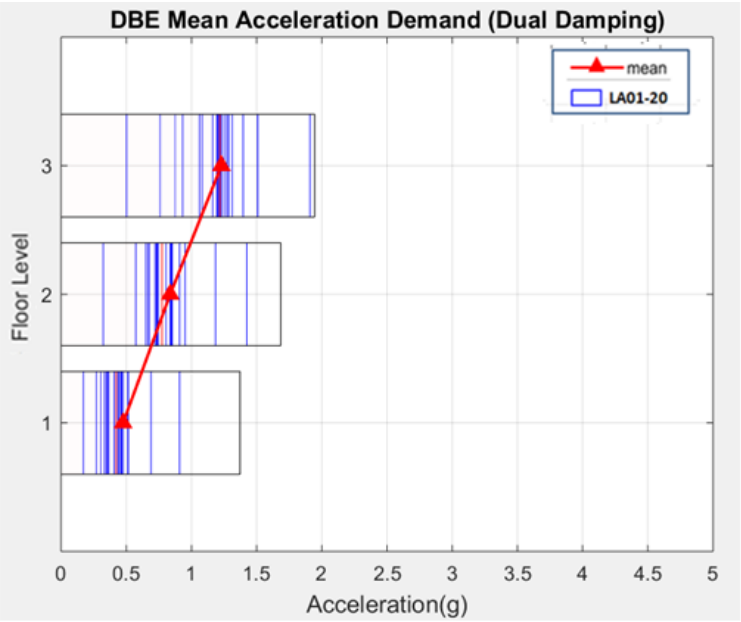

Figure 3.38 3-story CBF acceleration demand with dual damping under DBE*

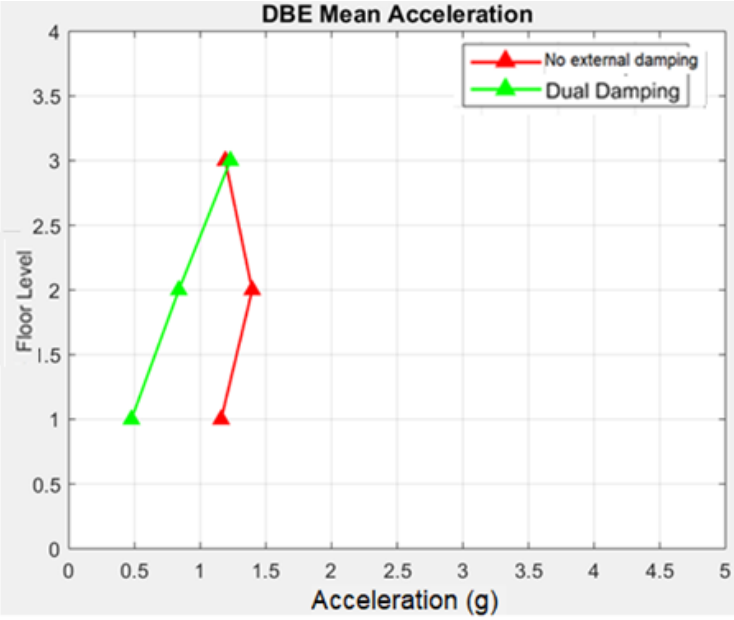

Figure 3.39 3-story CBF mean acceleration demand comparison under DBE*

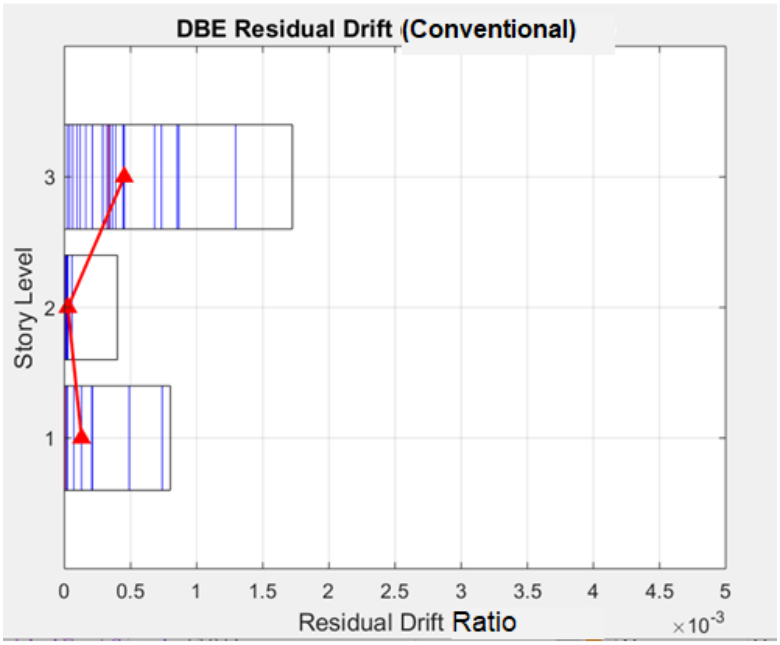

Figure 3.40 Conventional 3-story CBF residual drift under DBE

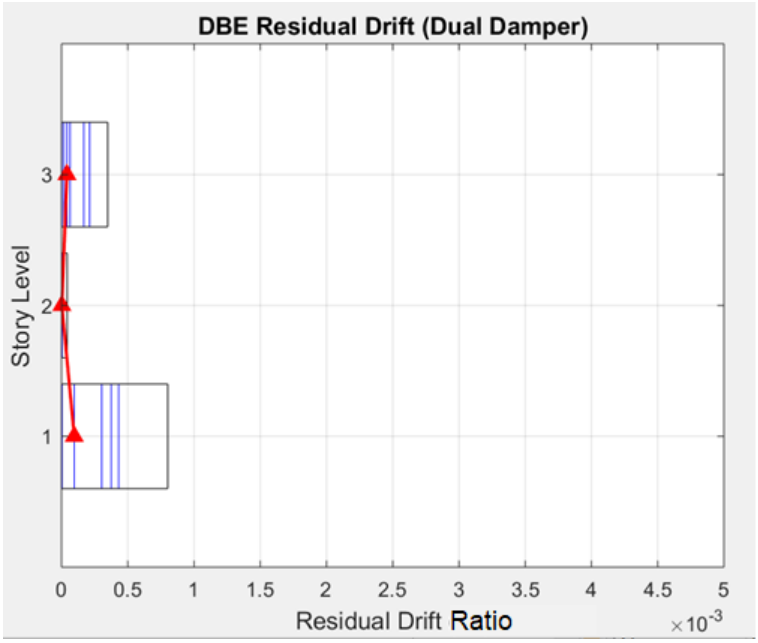

Figure 3.41 3-story CBF residual drift demand with dual damping under DBE

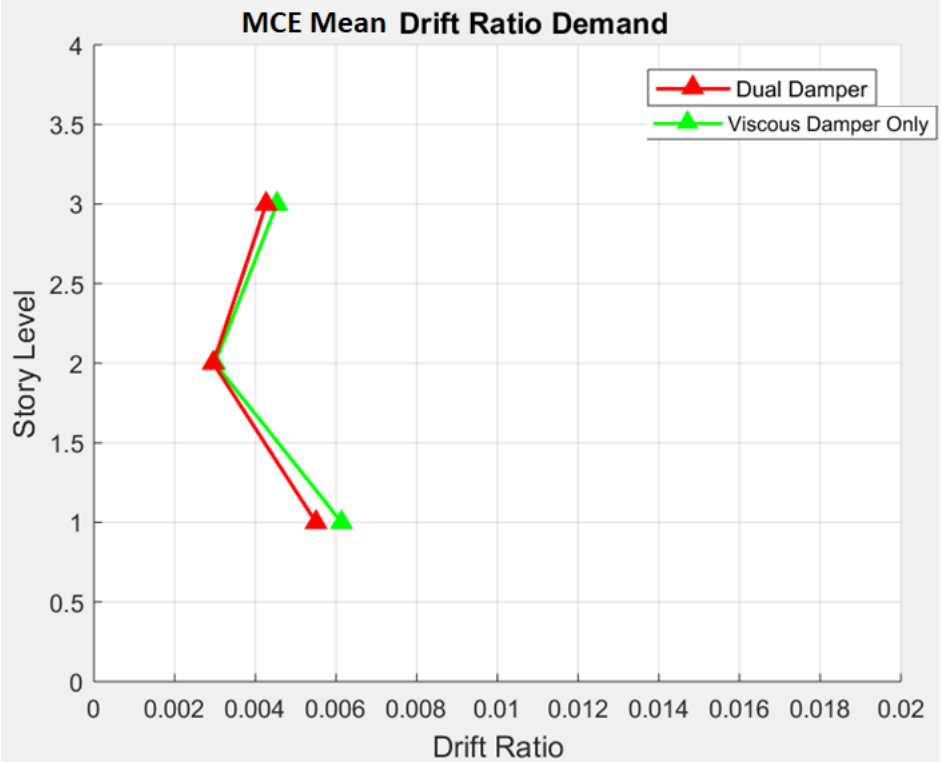

Figure 3.42 3-story CBF Mean Drift Demand comparison under MCE

*Floor numbers in the acceleration demand graphs refer to the top floor of each story, where the acceleration of ground floor is not shown.

Chapter 4 Seismic Resilience Assessment using PACT

PACT is a newly developed practical application tool of FEMA P-58 (2018) within the well-established performance-based earthquake engineering (PBEE) framework. Chapter 3 deals with hazard and structure analysis in which EDPs were obtained through nonlinear time history analysis under an ensemble of twenty earthquake ground motions scaled to DBE level at the building site, and the intensity-based assessment is considered as the approach for hazard analysis. This chapter presents the Damage State (DM) of the prototype structures' components and corresponding Decision Variables (DV) for steel CBF structures with and without dual action dampers. DVs are determined directly from DMs. DMs are defined for each component in the building based on different repair actions needed to restore the component to its original intact state. DMs are derived through Monte Carlo simulation from EDPs by large numbers of realizations. Figure 4.1 shows the procedure for each realization.

4.1 Background Information

The 3-story steel CBF and 6-story steel CBF buildings are both commercial office buildings located in metropolitan Los Angeles, CA. Losses can be divided into direct losses and indirect losses. Direct losses mainly refer to repair cost and repair time, and indirect losses include Casualties and Environment impact parameters.

Before applying the loss assessment, a rough estimation of total replacement cost is given by an online database. [27] The replacement cost employed in this study is the median value by simplified lump sum method based on building type, project location and the architectural layout of the building. The median total replacement cost for the 6-story office building is estimated to be about $12.59 million, so the estimated cost has been further scaled to $11.08 million to match the 2011 national averages in US dollars. The median value for the 3-story CBF building is taken as $4.86 million by a similar method. Other input parameters include maximum worker per square foot, which is taken as 0.002 using the population model (this is auto-generated by PACT, on a daily basis), as shown in Figure 4.2.

4.2 Resilience Assessment Procedure using PACT

Structural response inputs to the FEMA P-58 analysis procedure for the 3-story and 6-story CBF structures are calculated through nonlinear time history analysis in Opensees.

PACT assessment procedure basically includes the following steps:

(1) Input project and building information are shown in Figures 4.3(a) and 4.3(b). Identification information of the project, client and engineer are included. Region and date cost multipliers are taken as one so that all pecuniary cost is based on the Year 2011 national average. The same solver random seed value is used to ensure the results from each simulation execution to be the same. For the

building information tab, total replacement cost and time as well as building architecture layout are input.

(2) The second step is to set up the population mode. The default population model for commercial office building on a daily basis is shown in Figure 4.2. The default commercial office population model is then assigned to each floor and will be used for casualty estimation.

(3) Component fragility specifications included in the building model will be divided into three groups by the horizontal directions they apply to, as shown in Figure 4.3 (c). PACT model is then furnished by other required information such as quantity, corresponding population model and controlling EDP about each component entry in all directions. Quantity dispersion can be specified to deal with the uncertainties and each element in the same performance group is fragility uncorrelated, thereby the damage state and corresponding cost is not necessarily identical given the same EDP value.

(4) EDP values are from the nonlinear structural analysis in Chapter 3, including peak story drift ratio and floor acceleration based on selected DBE ground motion. (Figure 4.3 (d)) The study is based on the DBE intensity and employed 2,000 realizations for each building. Modelling dispersion is taken as 0.385 to account for the uncertainties in the numerical model. Damage state of the non-directional components are determined by the converted demand from each direction. PACT will automatically determine the non-directional demand parameters by multiplying the maximum value for the two input directions by a conversion factor which is taken as 1.2 in this study.

(5) PACT also considers irreparable conditions when spectral acceleration (SA) of the realization exceeds the median collapse SA or the residual drift exceeds the median repairable value and therefore repair cost will be totally alternated by replacement cost. This study considers 1% as median irreparable residual drift and assigns a dispersion factor of 0.3, as shown in Figure 4.3 (e). Residual drift demand is taken as the maximum value of residual drift from each story. It is taken as the average of story drift in the 30 seconds free vibration stage appended to the original ground motion record.

(6) Median Collapse SA is based on SPO2IDA tool in this study to be taken as 1.9g for the 6-story building. Four expected collapse modes with fatality and injury rate are estimated based on the results of nonlinear time-history analysis shown in Figure 4.3 (f).

The major results from the PACT assessment are in the following form: Repair time, Repair cost, Casualties (from collapse analysis), Unsafe placard, and Environmental impact.

Repair costs are estimated from the aggregation of performance groups of structure components and nonstructural components. Structure components in each building model include seismically rated brace elements in the prototype steel CBF structure. Architectural layouts for each building and the associated inventory of damageable nonstructural components are used for the aggregation.

Building components considered for the assessment are modeled from the commercial office model by FB&C Engineers Consulting Group, 2015[18], as shown in Table 4.1. Since the CBFs in this study satisfy the capacity design requirements for primary structure components, damages are assumed to be restricted to the brace elements.

The structural response inputs are then used in component-level fragility functions to calculate the damage predictions for all components in the building. The damage state controlling the structural response input to a given fragility function is considered to be either floor acceleration or story drift ratio demand, depending on the specific component. Component-level damage predictions are finally translated to component-level losses estimations by loss curves.

As aforementioned, the EDPs and collapse fragilities of the 3-story and 6-story CBF buildings were analyzed based on a 2-d one-braced-bay model with lean-on column. The planar model is acceptable for low-rise and medium rise building analysis since there is no significant 3D affect such as coupling or torsional irregularity in both structures. The lateral strength and stiffness in the two orthogonal directions are considered to be identical to each and thus only one direction will be considered in the model. A suite of twenty ground motion records were utilized to capture the variability in earthquake ground motion. The selected DBE level ground motions are recorded from stiff soil or rock sites (Class D) with moderate to large fault-rupture distances to the epicenter. EDPs are obtained for each ground motion case merely based on the DBE intensity measurement, and the side-sway dynamic instability is rarely observed throughout the time-history analysis. Large quantities of EDPs are generated by Monte-carlo simulation based on the nonlinear analysis results from the Opensees

model. In the 6-story CBF EDPs listed in Table 4.2, twenty sets of EDPs have been recorded while each set has seven individual variables. The probabilistic description of any two of critical EDPs in each set is assumed to be lognormal according to FEMA P-58. [28].

4.3 Fragility properties of TPAD Damper

Fragility parameters for the TPAD damper (i.e., metallic hysteretic damper with trapezoidal steel energy dissipation plates and a holder in each set) are shown in Figure 4.4. The damage state of the TPAD damper in this study can be classified into two states: 'None' or 'yielded'. The median demand for the damaged state is the steel energy dissipation plate's deformation at yielding point based on the TPAD damper's static pushover curve. Once plastic hinges appear along the steel energy dissipation plate, replacement of the TPAD damper would be required. The uncertainty dispersion recommended by PACT is taken as 0.45.

The repair cost and repair time consequence functions are shown in Figure 4.5.Imediate replacement is needed only for the TPAD damper and the no-replacement option is adopted for the viscous damper system because of the long stroke capacity of the viscous damper. The expected unit repair cost for one TPAD damper is estimated as $250 based on the material and geometric configuration of metallic plate, including the auxiliary parts such as holder and connecting bolts. A set of backup steel energy dissipation plates of the TPAD damper is usually provided in initial construction and placed next to the damper in the building and thus whenever a replacement occurs, the

total unit repair cost for the TPAD damper is assumed as $400, with deductions for large producing quantities as shown in Figure 4.5(a).

The time needed to replace one set of TPAD damper is experimentally confirmed as 30 minutes in a full scale structural test (Tong et al. 2019) [29]. A total number of 30 TPAD are thus expected to be replaced in one workday. So the unit repair time for this component is taken as 0.033 days. (Figure 4.5(b))

4.4 Observed DV Results and Comparison

DVs in this study refer to the total pecuniary and time cost associated with repair and replacement of structure and non-structural components to return the CBF structure back to its undamaged state after an earthquake. As illustrated in Figure 4.1, Repair costs are considered only if the structure is repairable. With the occurrence of collapse or the exceedance of allowable residual drift, the structure needs to be replaced and thereby the DV expectation for given intensity level refers to the total replacement cost of the structure. If no replacement of the structure is needed, the expected DV can be calculated by summing over all damageable component groups.

The repair time in this study mainly refers to the rational component of building down time according to Comerio's model (2006). The repair time calculation is based on the damage state categorized in FEMA P-58 performance group fragility function database. Detailed description of repair strategy necessary to return the component back to its pre-earthquake condition is specified thereby providing an insightful

estimation of the entire repair track for contractors. The contractor applies a direct downtime consequence function for DV calculation under this methodology. The irrational component of building down time planning allows owners and contractors to work together to figure out other contributing factors, such as damage inspections, assessments, consultations, as well as other business and technical interruptions, which will have to be performed on a case-by-case basis. This study assumes slow-track repair scheme where components are repaired serially for the repair time approximation. (Figure 4.10) This repair scheme restricts trades overlapping within or between floors. Details can be found in the Reiser's report. [30]

Repair cost and repair time of the archetype buildings are expressed in terms of the expected

loss at DBE level ground motion's intensity metric. The distribution of DVs by discretized points for each realization and a fitted lognormal CDF curve are shown in Figure 4.6 for the 6-story CBF with dual action dampers and Figure 4.8 for the 6-story CBF building without supplemental damper. Potential collapse is not included in these figures since EDP results directly obtained from finite element model indicate low probability of collapse. Unsafe Placard is plotted in Figure 4.7 and Figure 4.9 for 6-story CBF structure, where most of the post-earthquake immediate risk to safety comes from brace elements and suspended ceilings.

The calculated low (10^{th} percentile, P10), best estimate (50th percentile, P50), and high (90^{th} percentile, P90) values of repair cost and repair time for the 6-story CBF building under DBE level intensity are listed in Tables 4.3 and 4.4. The repair time and repair cost of 3-story CBF building are calculated by the same method and the

results are listed based on the same probabilistic description in Tables 4.5 and 4.6. Results of the repair cost estimation for each CBF building normalized by their replacement costs are summarized in Figures 4.12 and 4.13.

As shown in Figure 4.12, for the 6-story CBF without supplemental damper, expected repair cost of $3.15 million, equivalent to about 26.5% of the replacement cost, is predicted under the DBE intensity of averaged Sa (T). The expected repair time under serial repair scheme is 49 days. The identical structure with dual action dampers can reduce the expected repair cost to $1.75 million, equivalent to about 14.7% of the replacement cost on the same metric. The expected repair time is shortened to 26 days.

For the 3-story CBF building without supplemental damper, expected repair cost of $1.4 million, equivalent to about 28.43% of the replacement cost, is predicted under the DBE intensity of averaged Sa (T). The expected repair time under serial repair scheme is 23 days. The identical structure with dual action dampers have reduced expected repair cost of $ 0.45million, equivalent to about 9.26% of the replacement cost on the same metric. The expected repair time is shortened to 8 days.

DV assessment including potential collapse of the 6-story CBF building is also performed based on simplified IDA results shown in Figures 4.14 and 4.15. An expected maximum probability is given by the CBF curve for repair cost and repair time. It suggests the probability that the damage is repairable is about 84.8% and 15.2% of the total realizations should use replacement cost and time as DVs due to building collapse and large residual drift. Figure 4.15 shows the normalized repair cost on three different probability levels. The median repair cost and repair time for the 6-story

building are close to each other in both cases regardless replacement analysis is included or not. The potential risk of fatalities and injuries are provided by CDF plot.

4.5 Summary

The dual action damper can considerably reduce the expected median repair cost and repair time for both the 6-story and 3-story buildings under DBE intensity. The expected median repair cost for conventional 6-story CBF building is about 28.43% of the total replacement, applying the dual action dampers can reduce the median repair cost by about 44.44%. The repair time can be reduced by 46.94%. For the 3-story CBF building, median repair cost is about 28.81% of the total replacement of the original building. The total replacement can be reduced by 67.5% if dual action dampers are used. Soft story effect in the top story can be prevented by using dual action dampers.

Unsafe placard indicates immediate risk after the design-basis earthquake takes place. For conventional CBF building, there are high immediate risks in brace element and suspended ceilings, while unsafe placards also appear in partitions and exterior walls. If the building is equipped with dual action dampers the unsafe placard will be alleviated for all performance groups.

Table 4.1 Performance group for the commercial office Building

Structural Component Performance Groups						
Description	ID	Unit	Quantity(Assume identical in both directions)			Location
			Direction 1	Direction 2	Non-direction	

Structural Steel Braced Frame, Special Concentrically Braced Frame (CBF), Hollow structural section (HSS) (AISC minimum standard) , Chevron brace	B1033.031a	each bay	6 for 6-story CBF 4 for 3-story CBF	6 for 6-story CBF 4 for 3-story CBF	/	Floor 5&6
	B1033.031b	each bay	6 for 6-story CBF 4 for 3-story CBF	6 for 6-story CBF 4 for 3-story CBF	/	Floor 1-4
Cold-Formed Steel Stud Wall, 22 mil/31 mil steel sheathing, Stucco finish exterior	B1061.021b	each 100 ft^2 Wall Panel	53(Floor 1), 39(Floor 2-6)	53(Floor 1), 39(Floor 2-6)	/	All Stories
Nonstructural Component Performance Groups						
Exterior Wall						
Exterior Wall, Cold Formed Steel, Stud Wall, 22 Mil/31 Mil Steel Sheathing, Stucco Finish Exterior	B2011.021b	each 100 ft^2 Wall Panel	53(Floor 1), 39(Floor 2-6)	53(Floor 1), 39(Floor 2-6)	/	All Stories
Partition Wall						
GWB partition(steel studs, gypsum board both sides)	C1011.001a	Quantity is based upon 13'x100' Panels	6	6	/	All Stories
Floors and Roof						
Raised Access Floor, Seismically rated	C3027.002	each 100 ft^2 Wall Panel	/	/	20	All Floors
Roofing						
/						
Ceilings/Flooring						
Suspended Ceiling, SDC D/E: (Ip = 1.0) Vertical and lateral support for larger ceiling areas plus wider perimeter angle, Support: Vertical hanging wires only. Includes lighting fixtures in suspended ceiling.						
< 250 SF	C3032.003a	Costing for each 250 SF Unit	/	/	19.4	All Floors
250 – 1000 SF	C3032.003b	Costing	/	/	8.1	All

		for each 600 SF Unit				Floors
1000 – 2500 SF	C3032.003c	Costing for each 1800 SF Unit	/	/	2.7	All Floors
> 2500 SF	C3032.003d	Costing for each 2500 SF Unit	/	/	1.9	All Floors
Mechanical/Electrical						All Floors
Elevator, Traction, installed after 1975	D1014.011	Per elevator	/	/	2	All Floors
Cold Water Service, Cold or Hot Potable Pipe, Threaded Steel, diameter Φ ≤ 2.5",SDC D, E or F	D2021.023a	Based upon 1000 ft segments.	/	/	0.324	All Floors
	D2021.023b	Based upon 1000 ft segments.	/	/	0.324	All Floors
Hot Water Service, Cold or Hot Potable Pipe, Threaded Steel, diameter Φ ≤ 2.5",SDC D, E or F	D2022.013a,	Based upon 1000 ft segments.	/	/	1.6	All Floors
	D2022.013b	Based upon 1000 ft segments.	/	/	1.6	All Floors
Sanitary Waste Piping, Cast iron with bell and spigot couplings, SDC D, E or F	D2031.023a, D2031.023b	Each	/	/	1.2	All Floors
Chiller, Hard anchored or isolated, and restrained,350 to < 750 Ton, Simultaneously occurring AF(Anchorage failure) and ID(Internal damage)	D3031.013i	Based upon 1000 ft segments of duct	/	/	1	Roof
HVAC Ducting, galvanized Sheet Metal,< 6 SF in cross sectional area, SDC D, E or F	D3041.011c	Per unit	/	/	1.6	All Floors
Compressor, Isolated, not restrained, Small non-medical air supply, Simultaneously occurring AF and ID	D3032.012c	Per unit	/	/	1	Roof
Packaged Air Handling Unit, Hard anchored or isolated and restrained, 10000 to < 25000 CFM, Simultaneously occurring AF and ID	D3052.013i	Based upon 1000 ft segments.	/	/	4	Roof

Fire Sprinkler Water Piping – Horizontal Mains and Branches Old style Victaulic, thin-wall steel, SDC D, E or F	D4011.023a	per 100 units	/	/	4.3	All Floors
Fire Sprinkler Drop, Braced lay-in tile, Dropping into lay-in tile SOFT ceiling, SDC D, E, or F	D4011.053a	Per unit	/	/	1.95	All Floors
Motor Control Center, Hard anchored, Anchorage failure	D5012.013b	Per unit	/	/	6	Roof
Low Voltage Switchgear, Hard anchored, 750 to < 1200 Amp, Anchorage failure	D5012.023g	per unit and is based upon 1600 Amp.	/	/	1	All Floors
*TPAD	F1059.001a	Per unit	6 for 6-story CBF 4 for 3-story CBF	6 for 6-story CBF 4 for 3-story CBF	/	All Floors

Table 4.2 EDP input for 6-story CBF

Floor/Story	EQ1	EQ2	EQ3	EQ4	EQ5	EQ6	EQ7	EQ8	EQ9	EQ10	EQ11	EQ12	EQ13	EQ14	EQ15	EQ16	EQ17	EQ18	EQ19	EQ20
Floor 6-Roof (rad)	0.01122	0.01059...	0.01234...	0.02956...	0.01283...	0.01460...	0.01429...	0.01006...	0.01143...	0.01452...	0.010472	0.01861...	0.01592...	0.01293...	0.01149...	0.010757	0.01245...	0.01122...	0.01836...	0.01408...
Floor 5-6 (rad)	0.00940...	0.00935...	0.00861...	0.01306...	0.00905...	0.01039...	0.00991...	0.00862...	0.00829...	0.00824...	0.00620...	0.01038...	0.01061...	0.00929...	0.00904...	0.00899...	0.00951...	0.00905...	0.01042...	0.01059...
Floor 4-5 (rad)	0.00960...	0.00802...	0.01342...	0.00443...	0.00431...	0.00799...	0.00981...	0.00460...	0.00869...	0.00474...	0.00469...	0.00700...	0.00415...	0.00806...	0.00765...	0.00460...	0.00995...	0.00880...	0.00562...	0.00411...
Floor 3-4 (rad)	0.00460...	0.00461...	0.00520...	0.00444...	0.00412...	0.00460...	0.00554...	0.00401...	0.00442...	0.00425...	0.00404...	0.00487...	0.00426...	0.00462...	0.00453...	0.00420...	0.00719...	0.00479...	0.00425...	0.00404...
Floor 2-3 (rad)	0.00963...	0.00801...	0.01889...	0.00853...	0.00946...	0.01076...	0.00991...	0.01113	0.01195...	0.01261...	0.01013...	0.00732...	0.00652...	0.01027...	0.00869...	0.01019...	0.01359...	0.00890...	0.00728...	0.00784...
Floor 1-2 (rad)	0.00447...	0.00903...	0.02564...	0.00834...	0.01180...	0.01728...	0.011133	0.01646...	0.01384...	0.02129...	0.012485	0.00863...	0.00406...	0.01321...	0.00936...	0.016282	0.01539...	0.00644...	0.00918...	0.01009...
Roof (g)	1.18565...	1.16954...	1.32664...	1.90661...	1.05620...	1.35170...	1.62423...	1.50487...	1.05525...	1.42387...	1.57497...	2.05388...	1.49257...	1.41475...	1.07211...	1.17057...	1.26226...	1.40105...	2.02506...	1.70618...
Floor 6 (g)	1.30896...	1.53292...	1.64179...	2.21552...	1.09541...	1.68360...	1.17624...	1.31631...	1.26713...	1.50688...	1.59385...	2.49679...	1.15031...	1.10484...	1.21887...	1.10869...	1.26828...	1.62589...	2.29360...	1.71840...
Floor 5 (g)	1.02930...	1.10489...	1.20715...	1.35879...	0.89747...	1.19685...	1.00719...	1.12425...	0.86208...	1.25900...	1.06364...	1.51993...	1.01415...	1.34422...	1.08266...	1.00434...	1.10878...	1.51007...	1.49557...	1.66561...
Floor 4 (g)	1.28615...	1.54910...	1.22055...	2.07629...	1.09148...	1.41732...	1.20908...	1.14284...	1.08656...	1.19794...	1.27600...	2.07834...	0.96851...	1.39190...	1.25982...	1.20259...	1.17432...	1.55262...	1.74625...	1.31904...
Floor 3 (g)	1.08981...	0.92858...	0.90887...	1.19098...	0.83091...	1.10605...	1.19144...	1.28321...	1.02665...	1.10216...	1.21614...	1.63070...	0.95950...	1.04197...	0.88265...	1.08266...	0.78740...	0.85180...	1.24400...	1.71368...
Floor 2 (g)	0.82489...	0.86650...	0.99799...	0.93510...	0.84038...	0.96086...	0.71030...	1.03786...	0.75538...	0.87762...	1.14642...	1.36298...	0.77213...	0.83733...	0.82595...	0.82392...	0.70660...	0.62335...	1.28153...	1.21756...
Floor 1 (g)	0.43492...	0.49959...	0.62208...	1.04308...	0.50270...	0.58733...	0.51099...	0.67823...	0.45562...	0.62429...	0.82156...	0.95810...	0.49274...	0.38714...	0.47211...	0.44411...	0.63460...	0.59404...	1.12697...	0.88436...

Table 4.3 Repair cost of 6-story CBF under DBE

Repair Cost (thousand dollars)		
	Conventional 6-story CBF	6-story CBF with Dual Damper System
10% probability smaller than	1150	500
50% probability smaller than	3150	1750
84.8% probability smaller than	4500	2900

Note: Collapse analysis is not included.

Table 4.4 Repair time of 6-story CBF under DBE

Repair Time(days)		
	Conventional 6-story CBF	6-Chevron CBF with Dual Damper System
10% probability smaller than	30	15
50% probability smaller than	49	26
84.8% probability smaller than	79	46

Note: Collapse analysis is not included.

Table 4.5 Repair cost of 3-story CBF under DBE

Repair Cost (thousand dollars)		
	Conventional 3-story CBF	3-story CBF with Dual Damper System
10% probability smaller than	600	90
50% probability smaller than	1400	450
84.8% probability smaller than	3400	1200

Note: Collapse analysis is not included.

Table 4.6 Repair time of 3-story CBF under DBE

Repair Time(days)		
	Conventional 3-story CBF	3-story CBF with Dual Damper System
10% probability smaller than	8	0
50% probability smaller than	23	8
84.8% probability smaller than	55	19

Note: Collapse analysis is not included.

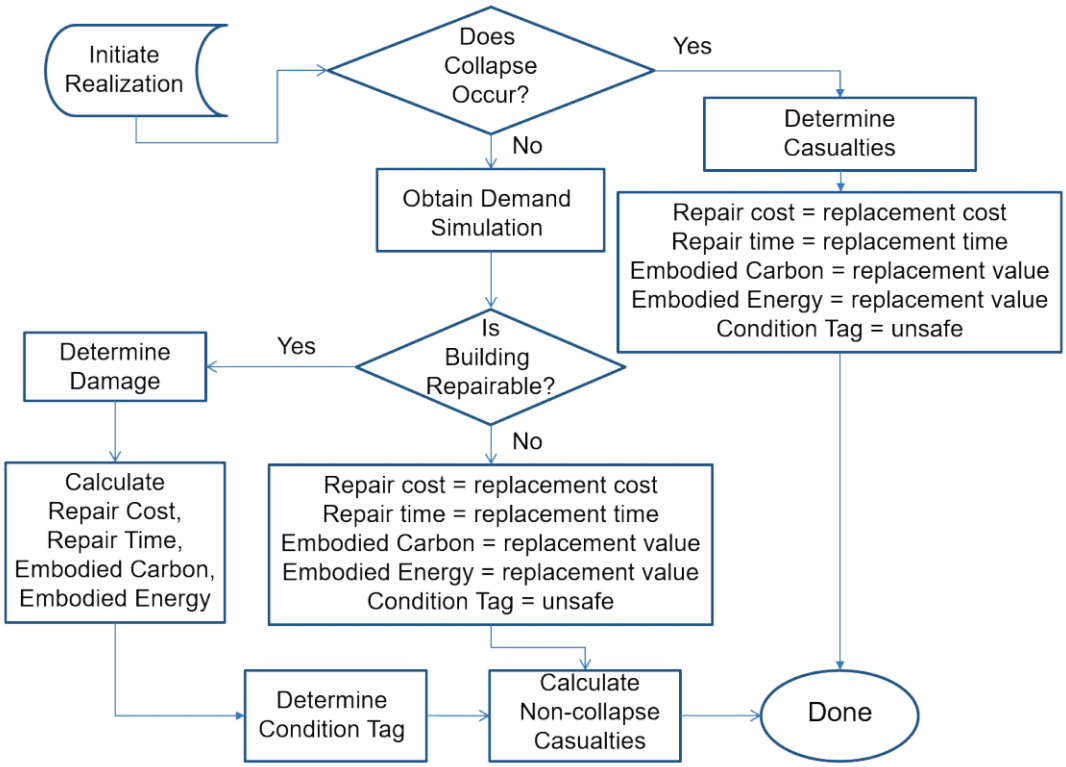

Figure 4.1 Flowchart for assessing a performance outcome in each realization (FEMA P-58, Volume 2)

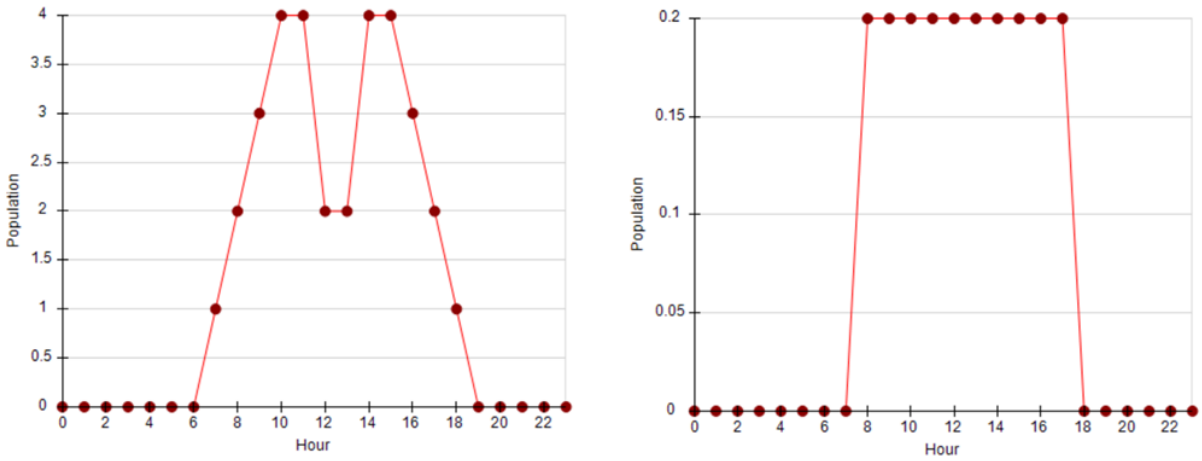

(a)Weekdays (b) Weekends

Figure 4.2 Population Model on daily basis (PACT)

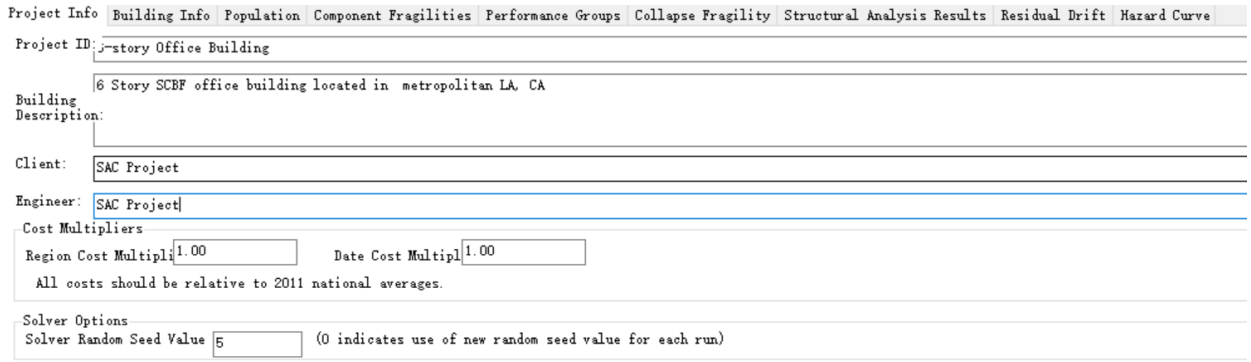

(a) Project information (PACT)

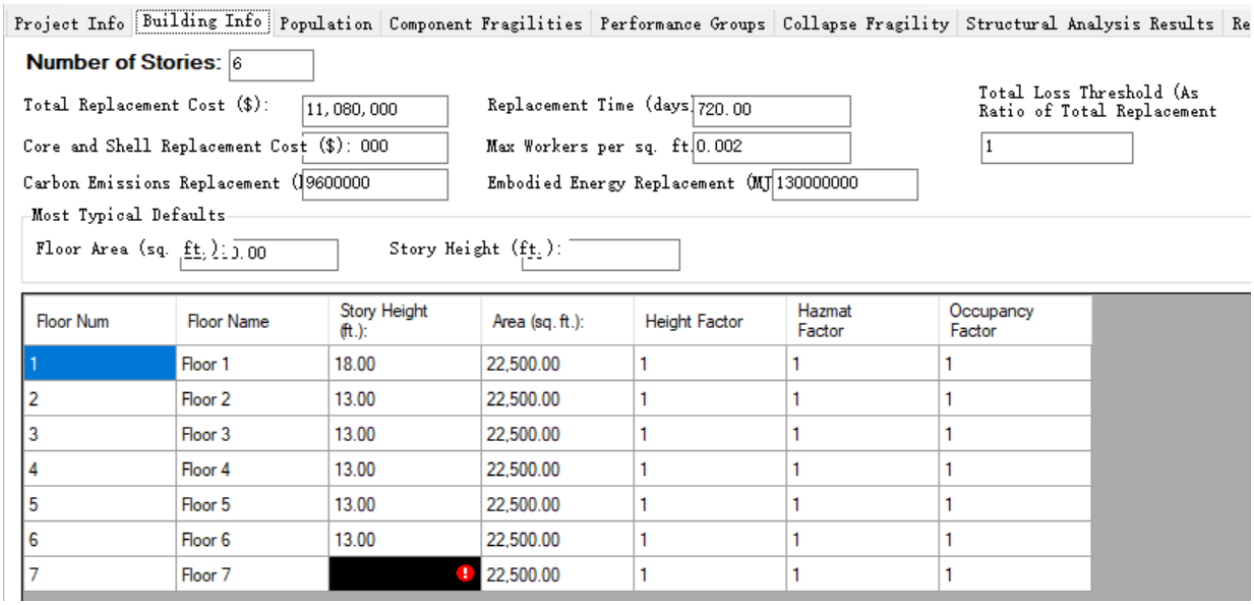

(b) Building information (PACT)

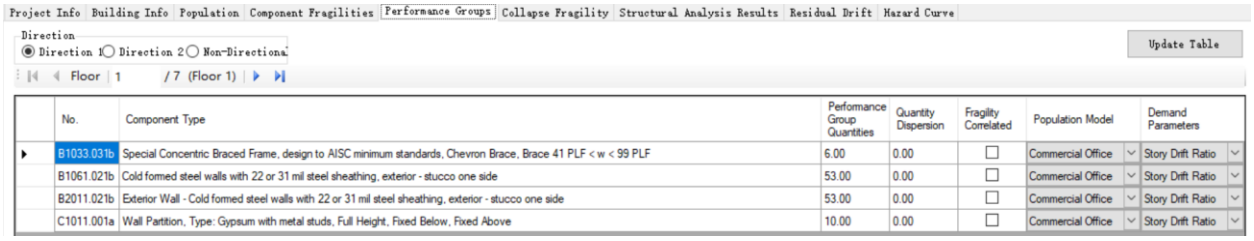

(c) Performance Group and Component Fragilities (PACT)

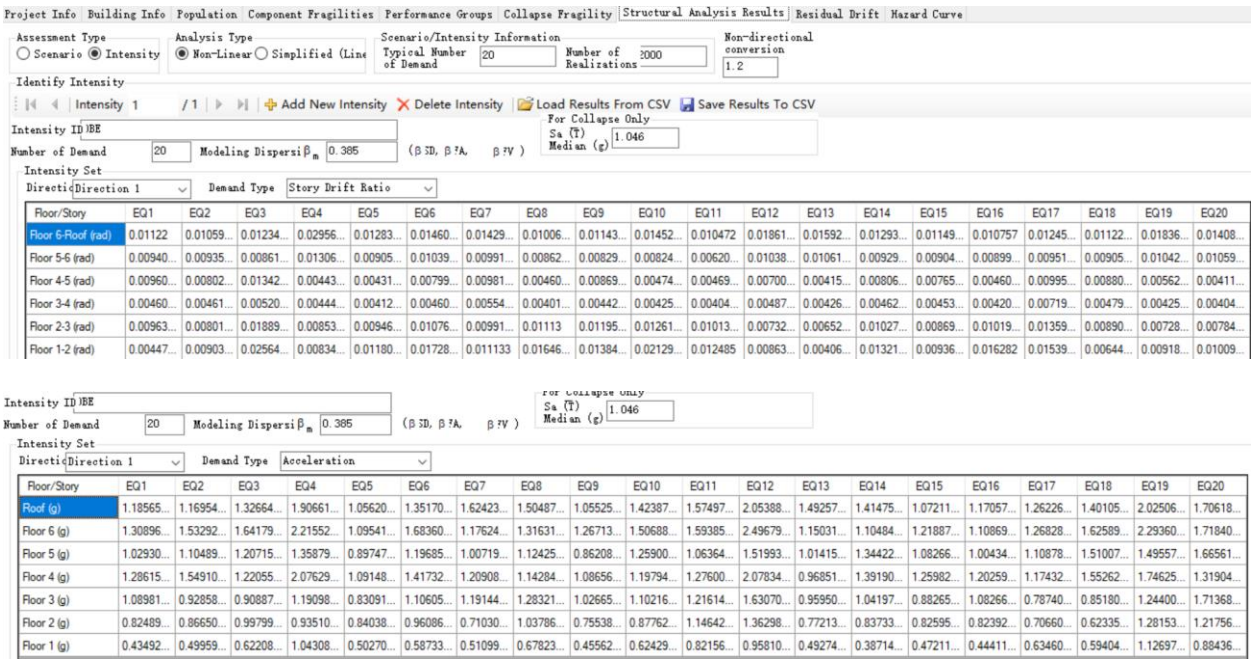

(d) Structural analysis results (PACT)

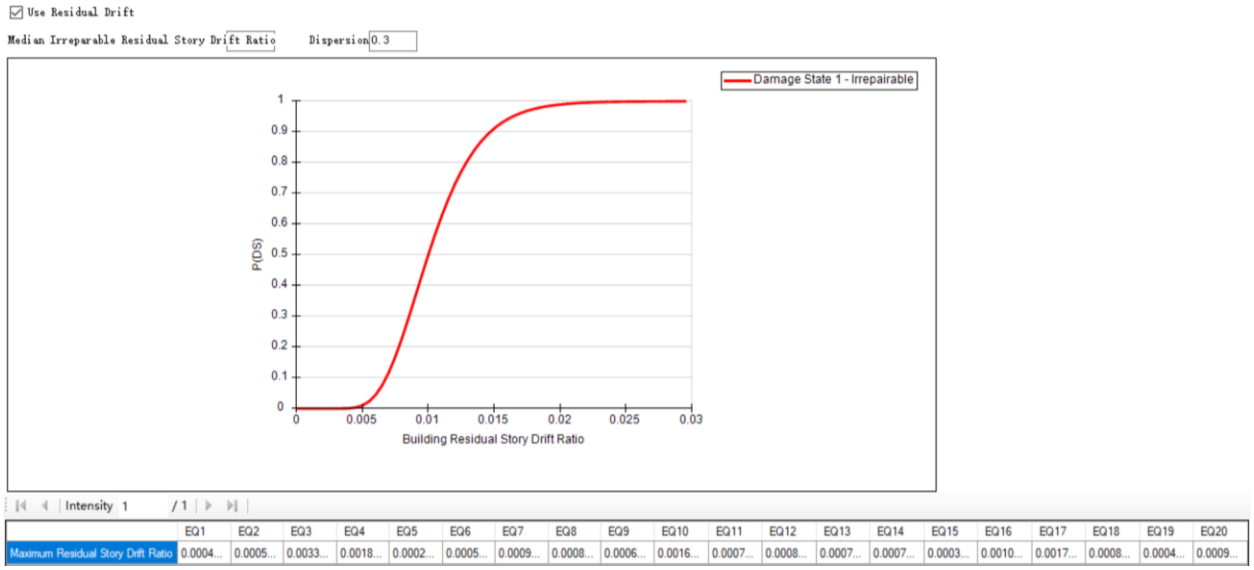

(e) Residual drift fragility (PACT)

☐ Include Potential Collapse in Assessment

Collapse Fragility Median: 1.9 Dispersion: 0.6
In terms of Sa (T)

Number of Potential Collapse M 4

Mutually Exclusive Probability of Mode Given Collapse

Mode 1	Mode 2	Mode 3	Mode 4
0.2	0.2	0.4	0.2

Fraction of Floor Subject to Collapse Debris

Floor	Mode 1	Mode 2	Mode 3	Mode 4
Floor 6 (6)	1	0.3	0.4	0.3
Floor 5 (5)	1	0.1	0.2	0.3
Floor 4 (4)	1	0.1	0.1	0.3
Floor 3 (3)	1	0.1	0.1	0.3
Floor 2 (2)	1	0.2	0.2	0.3
Floor 1 (1)	1	0.6	0.4	0.3

Collapse Consequences

Mode 1 / 4

Floor	Fatality Rate Mean	Fatality Rate COV	Injury Rate Mean	Injury Rate COV
Floor 6 (6)	0.9	0	0.1	0
Floor 5 (5)	0.9	0	0.1	0
Floor 4 (4)	0.9	0	0.1	0
Floor 3 (3)	0.9	0	0.1	0
Floor 2 (2)	0.9	0	0.1	0
Floor 1 (1)	0.9	0	0.1	0

(f)Collapse fragility and casualty estimation model

Figure 4.3 Building model and analysis results import (PACT)

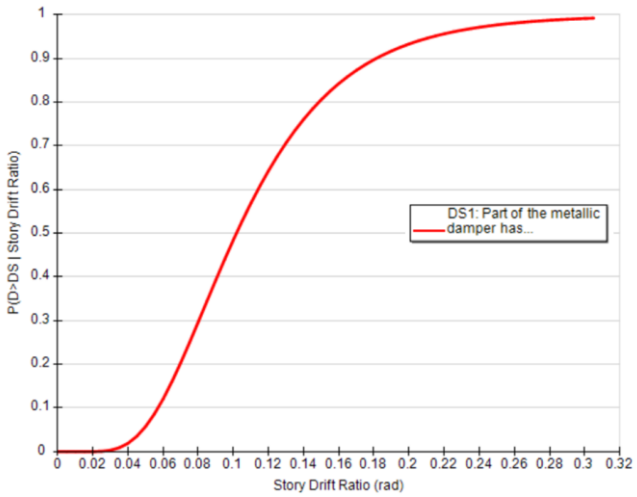

Figure 4.4 Damage states fragility CDF curve for TPAD system (PACT)

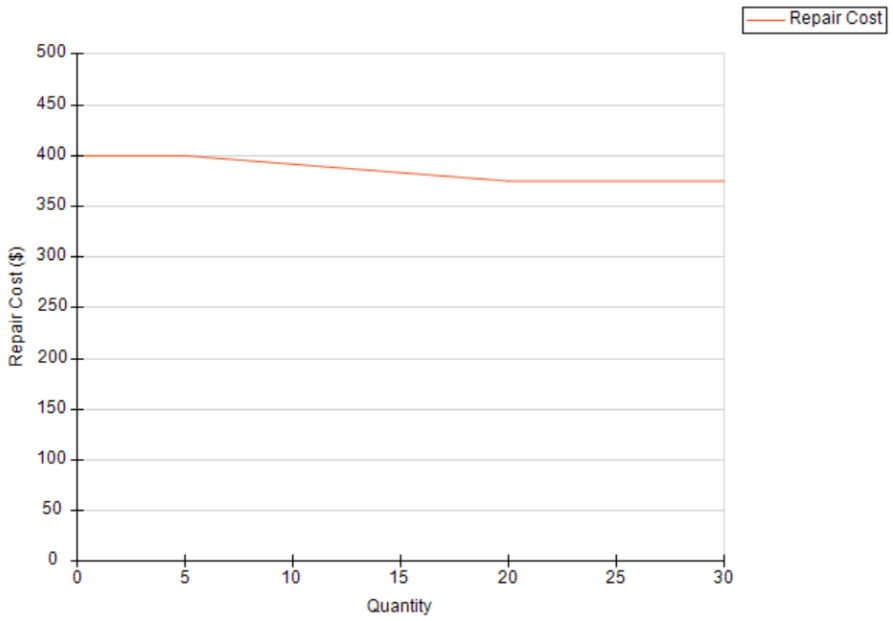

(a) TPAD repair cost consequence (PACT)

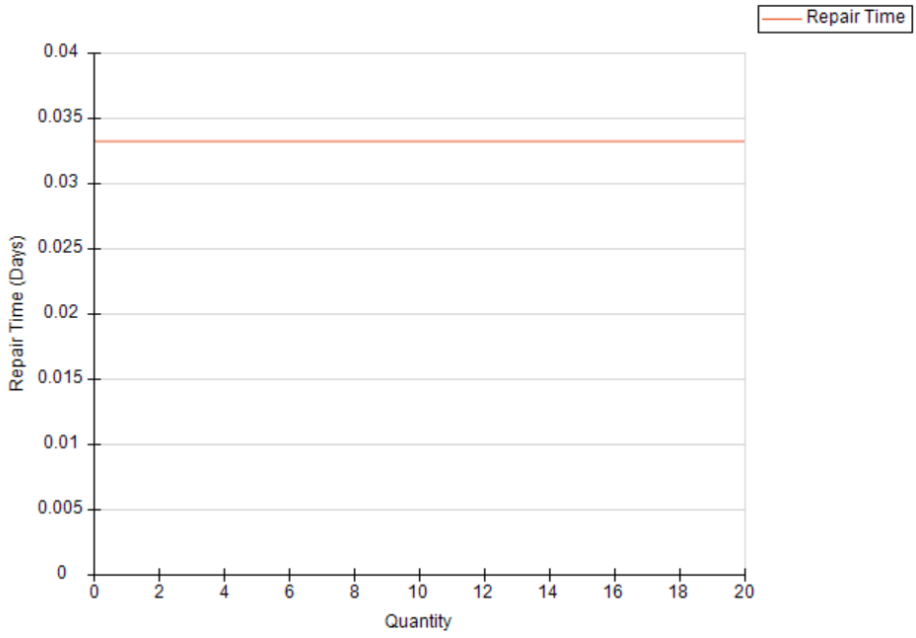

(b) TPAD repair time consequence (PACT)

Figure 4.5 TPAD fragilities (PACT)

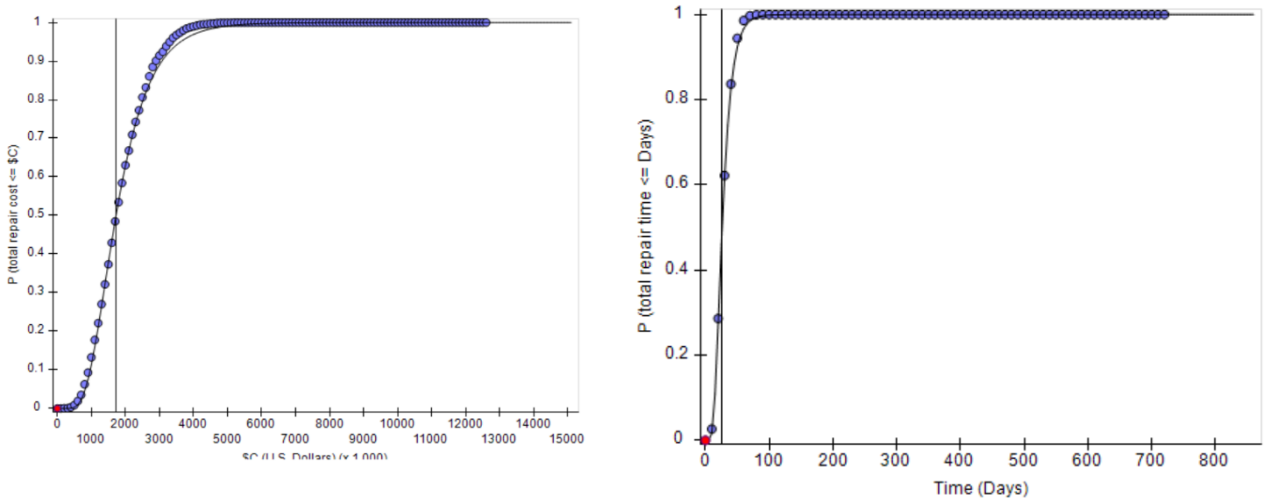

(a) Repair Cost (b) Repair time

Note: No potential collapse considered.

Figure 4.6 DV CDF of the 6-story CBF with dual dampers under DBE

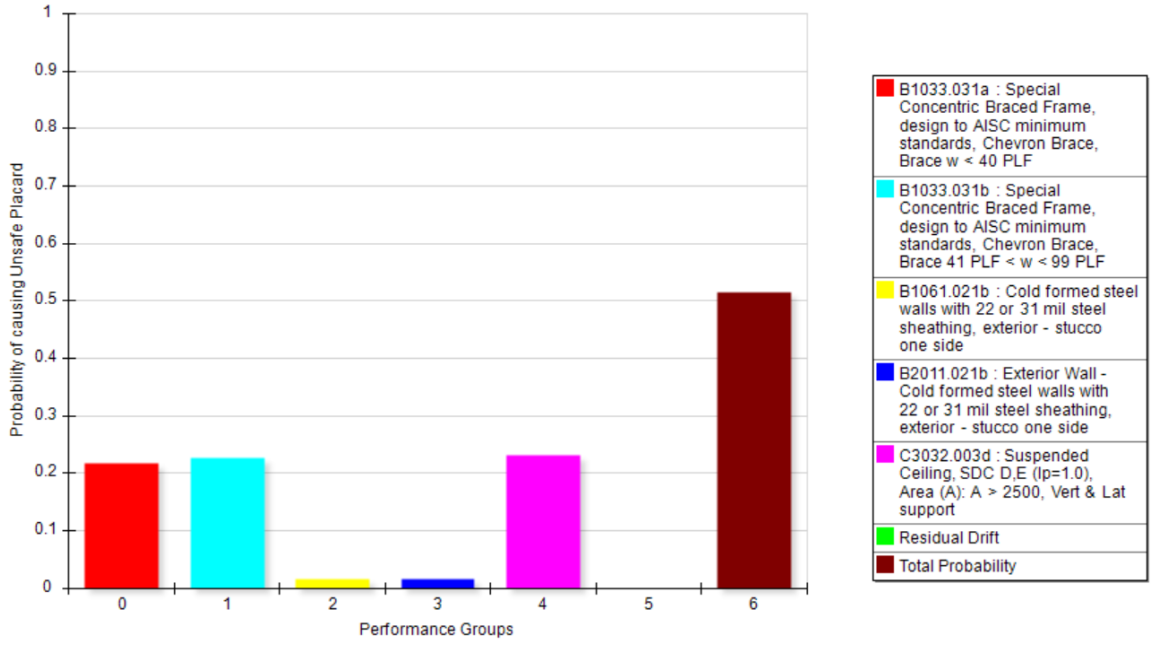

Note: No potential collapse considered.

Figure 4.7 Unsafe placard of 6-story CBF with dual dampers under DBE

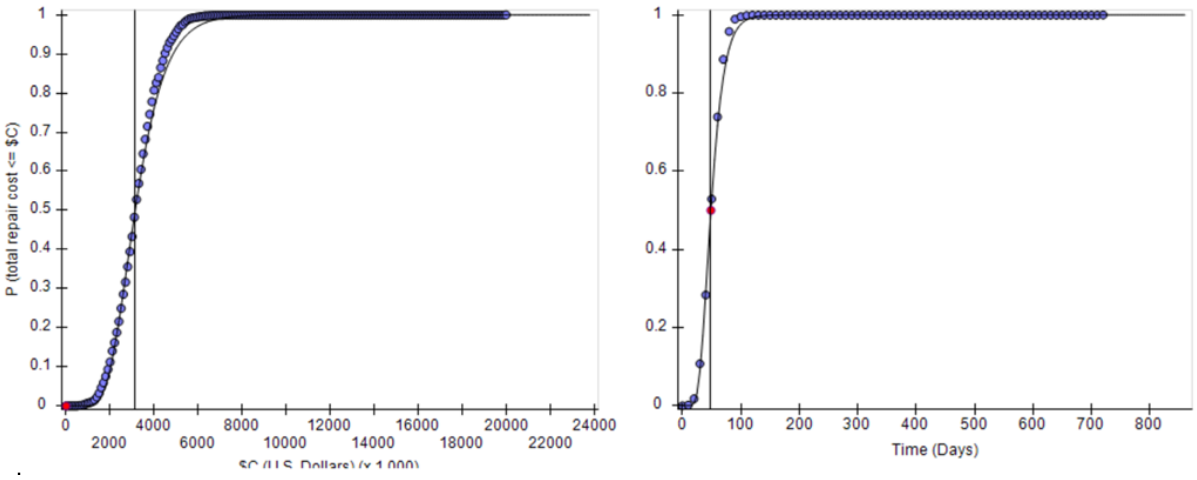

(a) Repair Cost (b) Repair time

Note: No potential collapse considered.

Figure 4.8 Decision Variable CDF of the conventional 6-story CBF under DBE

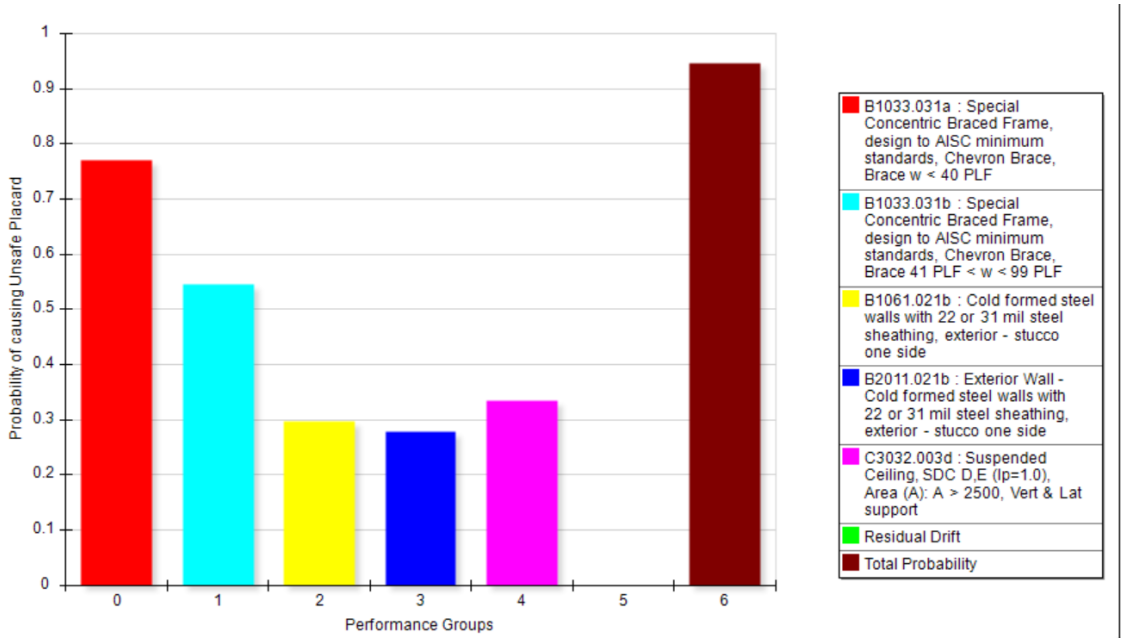

Note: No potential collapse considered.

Figure 4.9 Unsafe placard of 6-story conventional CBF only under DBE

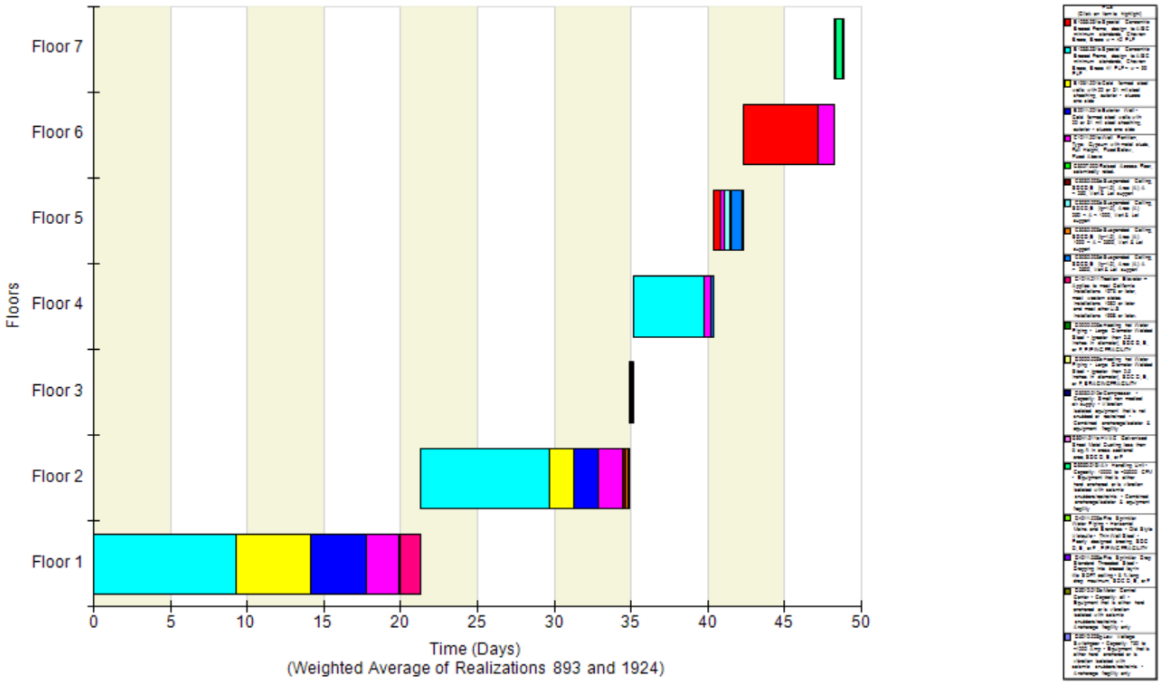

Figure 4.10 Median repair time realizations for 6-story CBF based on serial repair scheme

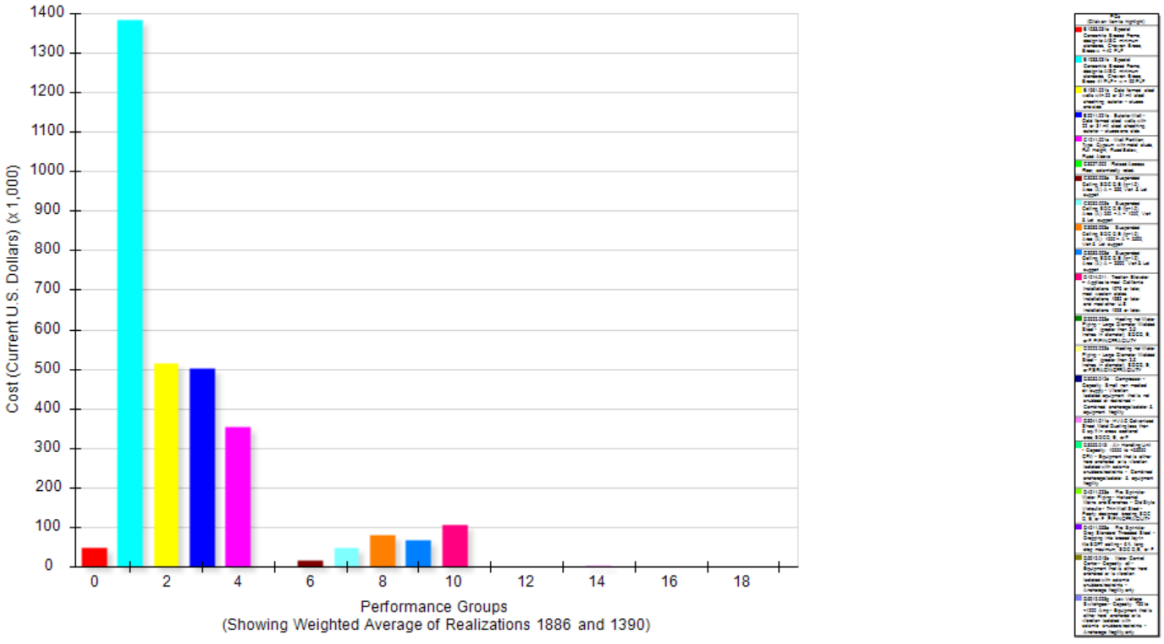

Figure 4.11 Median repair cost realizations for 6-story CBF by discretized performance group

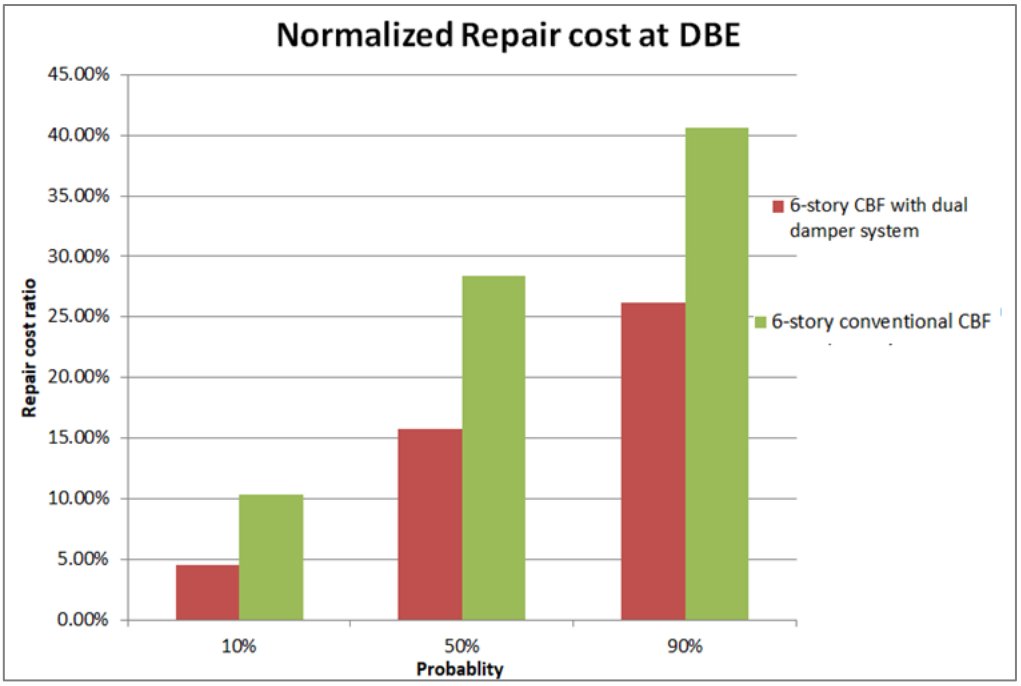

Note: No potential collapse considered.

Normalized Repair Cost (NRC) = (repair cost at given probability level/total replacement cost)*100%

Figure 4.12 6-story CBF normalized repair cost at DBE

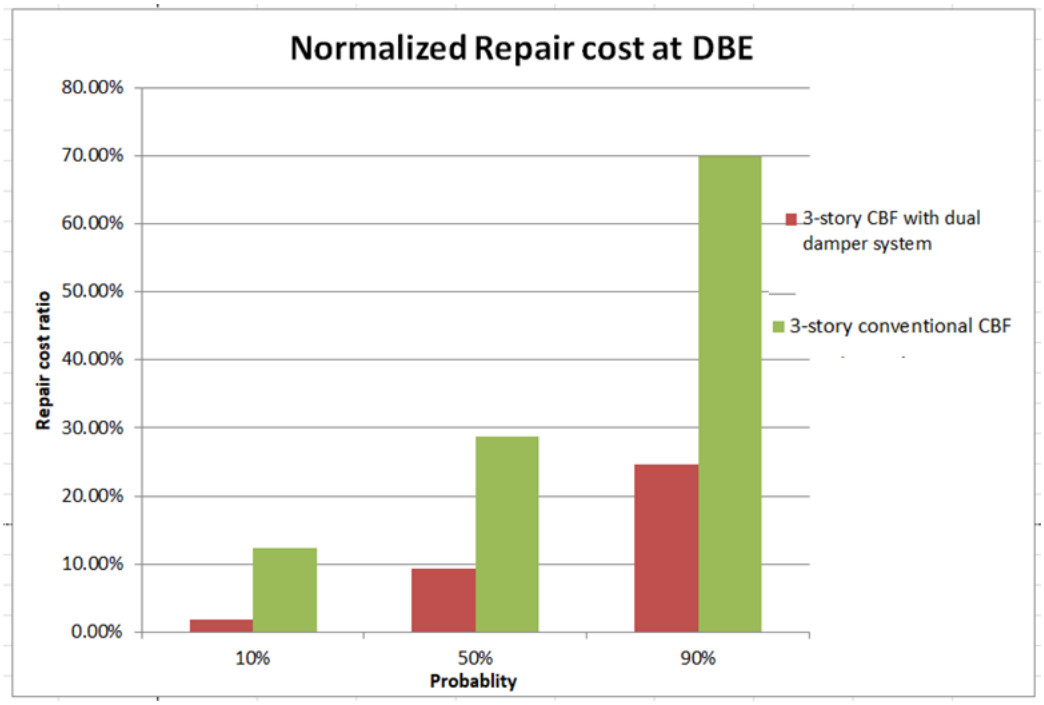

Note: No potential collapse considered.

Figure 4.13 3-story CBF normalized repair cost at DBE

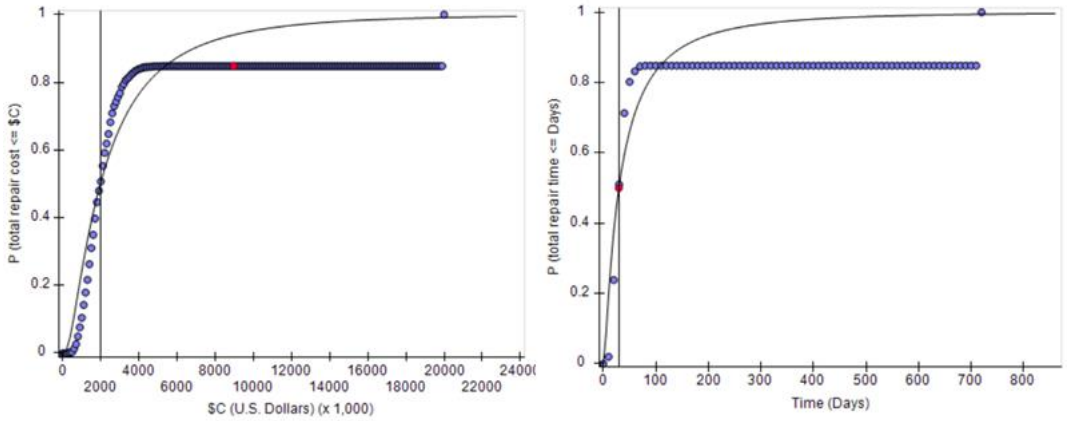

(a) Repair Cost (b) Repair time

Note: Potential collapse considered.

Figure 4.14 Decision Variable CDF of the 6-story CBF with dual under DBE

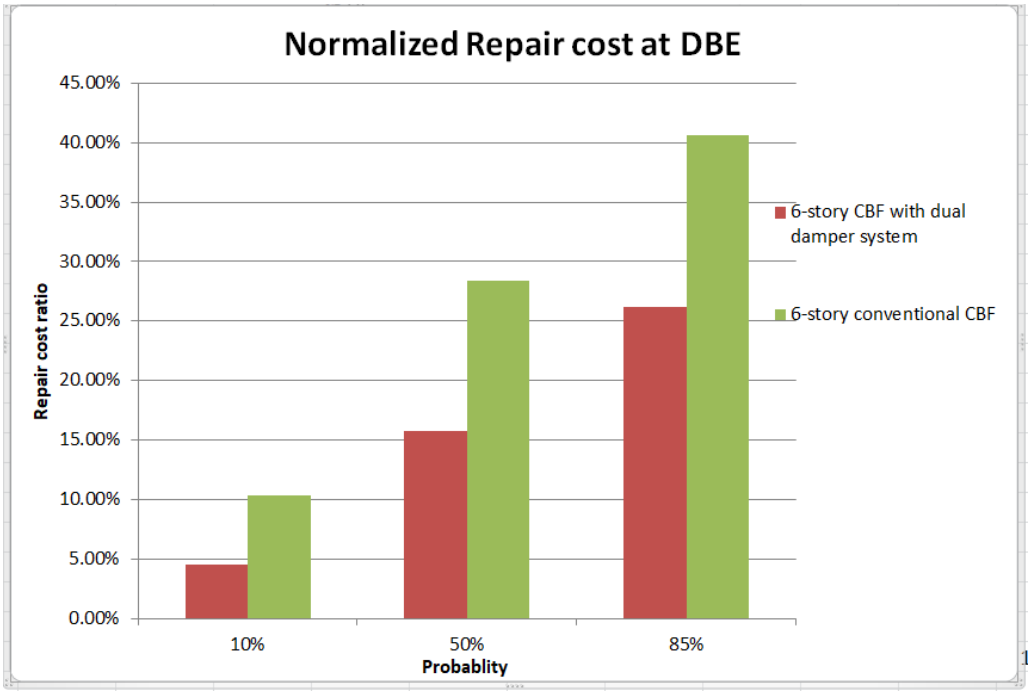

Note: Potential collapse included.

Figure 4.15 6-story CBF normalized repair cost at DBE

Chapter 5 Conclusions

5.1 Research Summary and Findings

In this study, two steel concentrically braced frame (CBF) buildings including a 3-story building and a 6-story building originally designed for the SAC project in 1997 are adopted as prototype buildings with and without supplemental dual action dampers (viscous damper + steel hysteretic damper) for seismic resilience quantification. Their seismic performance under design basis earthquake (DBE) is investigated through nonlinear finite element simulation study in a general structural analysis software - Opensees. Both nonlinear static and nonlinear time history analysis were conducted to obtain the structures' response under seismic excitation, which was subsequently used as input parameters for seismic resilience assessment.

The performance of the prototype buildings under DBE was evaluated using PACT, a software tool newly developed as the application for FEMA P-58 (2018). Monte Carlo simulations based on large quantities of realizations were carried out by the software using the nonlinear time history analysis results. Five major decision variables (DV) adopted by PACT include repair cost, repair time, casualties, unsafe placard and environmental impact. DVs are obtained by aggregations of performance groups consisting of structure components and non-structural components. All DVs from each realization are represented as binned points and the lognormal cumulative distribution function (CDF) curve has been used to fit the distribution where the expected cost is taken as the median point and the dispersion indicates the degree of variance. The DV

results are also presented for individual performance groups or separate floors in the building, where the performance-controlling components' fragility can be highlighted.

This study also performs analytical analysis and finite element analysis of newly developed dual metallic hysteretic and viscous dampers (hereafter referred to as dual action damper), and the promising use of this dual action damper to mitigate the seismic response of conventional CBF building with regard to the cost and risk reduction.

A summary of the research findings made in this study are listed as follows,

- For the 6-story CBF building under DBE excitation, large inter-story drift is found in the first and roof story. Acceleration is generally higher at upper floors than at the lowest floor. For the 3-story CBF building, large story drift was observed at the roof floor. There is a high risk of partial or entire collapse associated with excessive story drift and 'soft story' caused excessive story drift would increase the risk of economic loss and injuries. The risk of collapse of the CBF building is low under DBE, but there is a potential risk of excessive story drift concentrated to the roof story of the 3-story CBF building and ground story of the 6-story CBF building. Residual drift obtained from the nonlinear time history analysis indicate that replacement risk due to irreparable plastic deformation is relatively low under DBE intensity. The time history analysis results suggest high probability of necessary repair on the components of the building instead of replacement of the entire structure.

- The newly developed dual action dampers are proved to be helpful in enhancing the resilience of CBF buildings. Installing dual action damper can considerably mitigate the seismic response of the prototype CBF buildings such as inter-story drift ratio, floor acceleration and residual drift. It can also reduce the total unsafe placard of the entire building, thus implicating less immediate risks from damaged braces, partitions and ceilings after given level of earthquake. The metallic hysteretic damper (also called TPAD damper due to its trapezoidal steel energy dissipation plate) works as a backup energy dissipation device and is activated only when the story drift ratio exceeds 1% to further mitigate the dynamic response of CBF structure under large magnitude of earthquake excitations. For frequent earthquake with lower magnitude but more frequent, seismic energy dissipation mostly relies on the viscous damper which does not need immediate replacement because of its long operating stroke. This study also found that for the 3-story CBF building, all engineering parameter demands (EDP) can also be reduced even under maximum considerable earthquake (MCE) excitation. The performance group of dual action dampers has been developed based on the lognormal fragility function with a median damage EDP based on analytical calculation, and repair cost and time consequence functions are determined for the component. The replacement of TPAD damper has been proved to be economical and less time-consuming for post-earthquake retrofit of CBF building.
- PACT provides a useful tool for performance-based seismic design (PBSD) by giving an estimated prediction of risk of life, occupancy, and economic loss for

future earthquakes. It takes into account uncertainties from different aspects for each level as specified in the PBEE framework. PACT can provide a useful insight of building performance under series intensities of hazard. However, PACT power can be further expanded by including modules for seismic response mitigation devices such as the proposed dual action dampers, which it currently lacks. Empowered by including full spectrum of seismic force resisting systems and supplemental dampers, it would allow owners and engineers to set expected performance goal under different risk level by specifying each structural as well as non-structural component in the building.

5.2 Future Studies

Potential future studies along the line of this research can be summarized as below:

- As mentioned in Chapter 3, the structural median collapse spectrum acceleration (SA) is based on simplified IDA results, from linear regression of static pushover curve in finite element model. Equivalent lateral load pattern is based on the first vibration mode and only the most critical engineering demand parameter (EDP) values are given by the simplified method. Future collapse analysis can be performed based on IDA results from the selected ground motion records with different scaling factors to find the SA point at the ultimate strength of CBF structure. More intensity levels of earthquake in addition to DBE can be taken into account.

- Ultimate strength and deformation of the structure is estimated based on limited number of available large scale structural test data. Failure mode such as brace fracture under cyclic loading is not considered in the numerical model of this study. Low cycle fatigue damage model can be introduced in future study.
- The parameters of dual action damper such as viscous damper and TPAD damper are not optimized. Further study can be done to optimize the properties of dual action dampers for the CBF buildings.

References

[1] Sabelli, Rafael, Roeder, Charles W., and Hajjar, Jerome F. (2013). “Seismic design of steel special concentrically braced frame systems: A guide for practicing engineers,” NEHRP Seismic Design Technical Brief No. 8, produced by the NEHRP Consultants Joint Venture, a partnership of the Applied Technology Council and the Consortium of Universities for Research in Earthquake Engineering, for the National Institute of Standards and Technology, Gaithersburg, MD, NIST GCR 13-917-24.

[2] American institute of steel construction (AISC) (2010), “Seismic Provisions for Structural Steel Building”, AISC standard ANSI/AISC 341-16, Chicago, Illinois.

[3] Federal Emergency Manage Agency (FEMA), United States Geologic Survey (USGS), and the Pacific Disaster Center (PDC) (2017), “Hazus Estimated Annualized Earthquake Losses for the United States”, Technical Report FEMA P-366.

[4] American Society of Civil Engineers (ASCE) (2017), “Seismic evaluation and retrofit of existing buildings”, ASCE standard ASCE/SEI 41-17, Reston, Virginia.

[5] Federal Emergency Manage Agency (FEMA) (2018), “Seismic Performance Assessment of Buildings Volume 1-Methodology”, Second Edition, FEMA P-58-1, Washington D.C., Dec. 2018.

[6] Mazzoni, S., McKenna, F., Scott, M.H., and Fenves, G.L. (2009). "The Open System for Earthquake Engineering Simulation (OpenSEES) User Command-Language Manual." ,Version 2.5.0,Pacific Earthquake Eng. Research Center, Univ. Calif., Berkeley, CA, (http://opensees.berkeley.edu).

[7] T. T. Soong and G. F. Dargush (1997). “Passive Energy Dissipation Systems in Structural Engineering”, Wiley, Chichester, England.

[8] T. T. Soong And B. F. Spencer,. “Active, Semi-Active and Hybrid Control of Structures”, JR2, 12 WCEE, 2000.

[9] Alehashem SMS, Keyhani A, and Pourmohammad H. “Behavior and performance of
structures equipped with ADAS & TADAS dampers (a comparison with conventional structures)”. The 14th World Conference on Earthquake Engineering, Beijing, China, 2008.

[10] Moghaddasi, Mehdi & Namazi, Ali. (2016). “Assessment of Performance of TADAS Dampers for the Seismic Rehabilitation of Buildings”, International Journal of Applied Engineering Research, 11. 10516-10523.

[11] R.K.Mohammadi, A.Nasri and A.Ghaffary. “TADAS Dampers in very large deformations, International Journal of Steel Structures”, 2016, 10.1007/S13296-017-6011-y.

[12] Z. Li, G.Shu and Z. Huang. “Development and cyclic testing of an innovative shear-bending combined metallic damper”, Journal of Constructional Steel Research, 2019, 10.1016/ j.jcsr.2019. 03.008.

[13] A. Ghaffary and R. K .Mohammadi. “Framework for virtual hybrid simulation of TADAS frames using opensees and abaqus”, Journal of Vibration and Control 2018; 10.1177/ 107754631 6679029

[14] H. S. Dareini, B. H. Hashemi. “Use of Dual Systems in TADAS Dampers to Improve Seismic Behavior of Buildings in Different Levels”, The Twelfth East Asia-Pacific Conference on Structural Engineering and Construction 2011; 1877–7058

[15] Keivan, A. Nonlinear Seismic Performance of Self-centering Eccentrically Braced Frame Structures with Replaceable Hysteric Damper, Doctoral Dissertation, Department of Civil and Environmental Engineering, University of Maryland, College Park, Maryland, USA, 2018.

[16] Keith A. Porter. “An Overview of PEER’s Performance-Based Earthquake Engineering Methodology”, Ninth International Conference on Applications of Statistics and Probability in Civil Engineering (ICASP9) July 6-9, 2003, San Francisco.

[17] Jack Moehle and G.G. Deierlein. A Framework Methodology for Performance-Based Earthquake Engineering, 13th World Conference on Earthquake Engineering Vancouver, B.C., Canada, 2004. Paper No. 679.

[18] FB&C Engineers Consulting Group. Sample Seismic Risk Assessment Full Detailed Report. 162 Folsom Street San Francisco, CA, 2015.

[19] G. M. Del Gobbo, M. S. Williams, Anthony Blakeborough. Seismic Performance Assessment of a Conventional Multi-story Building. Int. J Disaster Risk Sci. (2017) 8:237–245.

[20] C. Del Vecchio, M. Di Ludovico, S. Pampanin, A. Prota. Actual versus predicted repair costs: case studies on RC buildings damaged by L’Aquila earthquake, 16th World Conference on Earthquake Engineering, 16WCEE 2017 Santiago Chile, January 9th to 13th 2017, Paper N° 2754 Registration Code: S-P1465537252

[21] Dong, Y., and Frangopol, D. M. (2016). Performance-based seismic assessment of conventional and base-isolated steel buildings including environmental impact and resilience. *Earthquake Engng Struct. Dyn.*, 45: 739– 756. doi: 10.1002/eqe.2682.

[22] Rafael Sabelli, (2001). "Research on Improving the Design and Analysis of Earthquake-Resistant Steel-Braced Frames", The 2000 NEHRP Professional Fellowship Report, October 2001.

[23] Patxi Uriz and Stephen A. Mahin, "Toward Earthquake-Resistant Design of Concentrically Braced Steel-Frame Structures", PEER Report 2008/08, Pacific Earthquake Engineering Research Center, College of Engineering, University of California, Berkeley,November 2008.

[24] Heng Liu and Yunfeng Zhang (2019), "Deep Learning based Brace Damage Detection for Concentrically Braced Frame Structures under Seismic Loadings", Dept. of Civil & Environmental Engineering, University of Maryland, College Park.

[25] Beamwithhinge element, online Opensees wiki manual, https://opensees.berkeley.edu/ wiki/index.php/Beam_With_Hinges_Element

[26] Cameron R. Bradley, Larry A. Fahnestock, Eric M. Hines and Joshua G. Sizemore. (2017). "Full-Scale Cyclic Testing of Low-Ductility Concentrically Braced Frames", ASCE Journal of Structural Engineering, 10.1061/(ASCE)ST.1943-541X.0001760.

[27] Buildingjournal Online construction estimating tool, 03 November 2019, 9:00 p.m., https://www.buildingjournal.com/construction-estimating.html

[28] Federal Emergency Manage Agency (FEMA) (2018), "Seismic Performance Assessment of Buildings Volume 2-Implementation Guide", Second Edition, FEMA P-58-2, Washington D.C., Dec. 2018.

[29] Tong, L, **Zhang, Y**, Zhou X, Keivan A, Li R. (2019). "Experimental and analytical investigation of D-type self-centering steel eccentrically braced frames with replaceable hysteretic damper," ASCE J Structural Engrg, 145(1): 04018229.

[30] Judith Mitrani-Reiser (2008), "Risk Management Products Team Downtime Model", FEMA P-58/BD-3.7.7, Department of Civil Engineering, Johns Hopkins University, Baltimore, Maryland.